Development of understanding in hydro-climate services in India to inform food and water security

Final Report
June 2018

Amanda J. Robinson

Julian R. Thompson

Mohammed Rahman

Nathan J. Rickards

Cédric L.R. Laizé

Helen Houghton-Carr

Adam Griffin

Lisa Stewart

Giuseppe Formetta

Michael C. Acreman

T. Thomas

Manish Nema

Prabhash Mishra

Shikha Gaur

Pushpendra Agarwal

Yatveer Singh

Sharad Jain

Chingka Kalai

Arpita Mondal

Table of Contents

1. Introduction

This project aims to improve understanding of hydro-climate services in India in order to inform food and water security. It involves collaboration between UCL and the Centre for Ecology and Hydrology (CEH) in the UK and the National Institute of Hydrology (NIH), Roorkee and Indian Institute of Technology (IIT), Bombay in India. This report is structured around the three main themes of the project: catchment hydrological modelling, assessment of environmental flows under climate change, and a feasibility study to assess the potential of developing guidance for India similar to that of the Flood Estimation Handbook for the UK.

The Upper Narmada in Central India provides the focus of the hydrological modelling (Chapter 2) and environmental flow assessments (Chapter 3). Two initial models of the Narmada were previously developed as part of the NERC funded project "Building joint India-UK capacity, capability, research and innovation in the environment". A MIKE SHE model of the Upper Narmada was developed at UCL in collaboration with CEH and NIH. An earlier GWAVA model was also enhanced and then applied to the Narmada by CEH and NIH. Both of these models have undergone significant improvements as part of the current project. The two calibrated / validated models are forced with a consistent set of climate change scenarios developed as part of the project and adopting a newly established bias correction approach. Subsequent results from the two models are compared before they are employed to assess the potential for ecological risk of change using the Ecological Risk due to Flow Alteration (ERFA) screening method.

The foci of the flood frequency estimation research (Chapter 4) are the Godavari and Krishna river basins. A pilot study investigates the feasibility of developing spatially consistent flood frequency estimates using an index flood approach. The work includes development of a web application designed to demonstrate how stakeholders and practitioners in the region could make use of the results of this part of the project.

2. Catchment hydrological modelling

A.J. Green, J.R. Thompson, M.M. Rahman, N.J. Rickards, T. Thomas, M. Nema, P. Mishra, S. Gaur, P. Agarwal, Y. Singh, S. Jain

2.1. Hydrological modelling of the Upper Narmada Basin

The Narmada River is located in central and western India and is the largest western flowing river of peninsula India (Government of India Ministry of Water Resources, 2014). The basin largely falls within the State of Madhya Pradesh, but also covers parts of Gujarat, Maharashtra and Chhattisgarh (Figure 2.1). With a population of over 16 million (Government of India Ministry of Water Resources, 2014) and a drainage area of 98,796 km^2 (India-WRIS, 2015), the Narmada is an example of a river basin facing numerous management challenges. In particular, there are multiple on-going and planned dam and irrigation development projects for the basin (Government of India Ministry of Water Resources, 2014). At the same time, it is vital that environmental flow requirements (the flow needs of the river ecosystem; Richter *et al.*, 1997; Acreman and Dunbar, 2004) continue to be met, in order to sustain the economically, socially and ecologically important ecosystem services provided by the river.

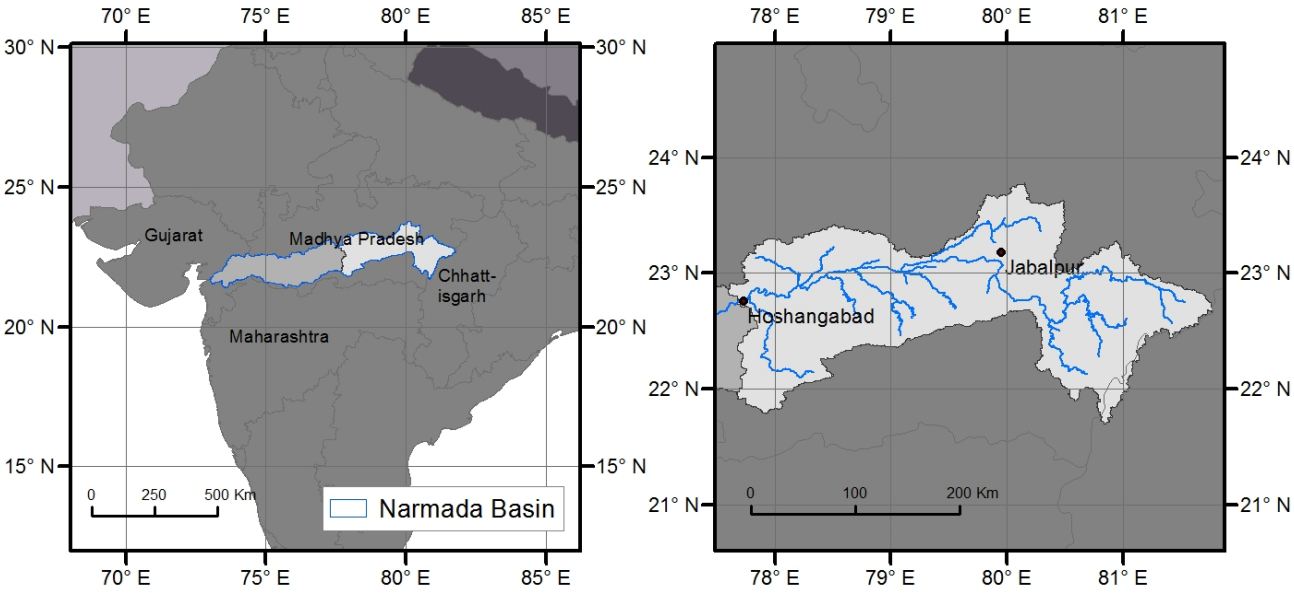

Figure 2.1. The Narmada Basin (left) and the Upper Narmada Basin (right).

This project improved upon an existing MIKE SHE hydrological model of the Upper Narmada Basin that was developed for a previous NERC funded project ("Building joint India-UK capacity, capability, research and innovation in the environment"). The Upper Narmada Basin down to Hoshangabad lies within the states of Madhya Pradesh and Chhattisgarh and has a catchment area of 44,725 km^2. Section 2.2 describes the development/improvement of a

MIKE SHE model of the Upper Narmada. The development of climate scenario data is described in Section 2.3. Results, including projected changes in climate and river discharge, are presented in Section 2.4. Sections 2.5–2.9 replicate this approach for a second hydrological model developed for the same area. Section 2.5 describes the GWAVA water resources model whilst Section 2.6 outlines the enhancement of a GWAVA model of the Upper Narmada that, like the MIKE SHE model, was originally configured and applied as part of the earlier NERC project. Calibration of the GWAVA model is described in Section 2.7 with Section 2.8 outlining the approach used to simulate the same climate change scenarios as those investigated using MIKE SHE. Finally Section 2.9 describes the calibration / validation results from the GWAVA model and the impact on river flow and water resources associated with the climate change scenarios. Section 2.10 briefly compares the results of the two models.

2.2. Development/improvement of a MIKE SHE model of the Upper Narmada Basin

MIKE SHE is a comprehensive, deterministic, distributed modelling system, capable of simulating the major processes of the land phase of the hydrological cycle (Graham and Butts, 2005). It has a modular structure and although it was originally designed as physically-based model code, many modules now offer a range of process descriptions, some of which are conceptual and semi-distributed. These are particularly applicable for large basins such as the Narmada where the focus is the simulation of river flow and where detailed data required for more physically-based approaches, such as spatially and vertically discretized hydrogeological characterisation, are not available (Andersen *et al.*, 2001; Stisen *et al.*, 2008; Refsgaard *et al.*, 2010).

Table 2.1 summarises the set-up of the initial MIKE SHE model of the Narmada. The model grid size was set to 2000 m × 2000 m in order to retain a balance between representing catchment characteristics and efficient computation time (Vázquez *et al.*, 2002; Thompson *et al.*, 2013). The model time-step is 24 hours. Overland flow is calculated using a finite-difference approach to solve the two-dimensional Saint–Venant equations (Graham and Butts, 2005). The two-layer water balance method was employed for the unsaturated zone. For modelling the saturated zone, the conceptual, semi-distributed, linear reservoir method was selected. Advantages of this method include lower data requirements and reduced computation time compared to physically based solutions (Andersen *et al.*, 2001; Stisen *et al.*, 2008; Thompson *et al.*, 2013; 2014a; 2014b). This method requires the model domain to be

divided into groundwater sub-catchments. This was based on topography and the locations of gauging stations.

Table 2.1. Summary of set-up of pre-existing MIKE SHE model of the Upper Narmada.

Model component	Key inputs	Data sources/ derivation
Model domain	Catchment extent – the basin area upstream of Hoshangabad	ESRI polygon shapefile provided by NIH.
Topography	Topography	Extracted from SRTM (Shuttle Radar Topography Mission) DEM (digital elevation model).
Land use/ vegetation	Land use distribution	Raster provided by NIH. There are five land cover classes: Forest, Shrub, Water bodies, Bare soil and Agriculture.
	Leaf Area Indexes	Based on Kite (2001) and Jain *et al.* (1992).
	Root depths	Based on DHI (2009) vegetation properties file, previous modelling experience (e.g. Thompson *et al.*, 2013) and the literature.
Overland flow: modelled using the 2D finite-difference method	Manning's M for overland flow resistance	Spatially distributed according to land cover. Values based on Vieux (2004).
Unsaturated zone: modelled using the two-layer water balance method	Soil classes	The spatial distribution of six soil classes was specified using a 1 km × 1 km grid based on a georectified and digitised version of a Government of India Survey of India soil map, provided by NIH.
	Soil hydraulic properties	Values for the different soil classes derived from the literature (Clapp and Hornberger, 1978; Norman and Dixon, 1995).
Saturated zone: modelled using the conceptual, linear reservoir method	Spatial distribution of groundwater sub-catchments	The basin was divided into groundwater sub-catchments based on topography and the locations of the five calibration gauging stations.
Catchment meteorology: Precipitation and evapo-transpiration modules.	Precipitation	0.25° × 0.25° gridded daily precipitation obtained from the IMD (India Meteorological Department) / NCC (National Climate Centre) High Spatial Resolution (0.25° × 0.25°) Long Period (1901–2013) Daily Gridded Rainfall Data Set Over India (Pai *et al.*, 2014).
	Potential evapotranspiration (PET)	Calculated using the Hargreaves method using IMD/NCC high resolution (1° × 1°) gridded daily temperature data (Srivastava *et al.*, 2009).
MIKE 11 one-dimensional hydraulic model for simulating channel flow	Plan of the main river channels	ESRI polygon shapefile provided by NIH.
	Synthetic cross-sections	Based on channel width measurements taken from satellite imagery in Google Earth and the literature (Rajaguru *et al.*, 1995; Payasi, 2015).
	Manning's n for bed resistance	Representative value based on the literature (Chow, 1959) and previous modelling experience.

Within each sub-catchment, the saturated zone is represented by a shallow interflow reservoir, and two baseflow reservoirs to simulate faster and slower baseflow storage. Exchanges between reservoirs, and ultimately the MIKE 11 hydraulic model, are controlled by time constants (DHI-WE, 2009). The two time constants (interflow and percolation) for each

interflow reservoir and the baseflow time constant for each baseflow reservoir were varied during model calibration. In the earlier MIKE SHE model of the Upper Narmada, the domain was divided into five groundwater sub-catchments, whereas the current model was improved by dividing the basin into seven groundwater sub-catchments, as shown in Figure 2.2.

Daily gridded precipitation data for the Upper Narmada were derived from the IMD (India Meteorological Department) / NCC (National Climate Centre) High Spatial Resolution (0.25° × 0.25°) Long Period (1901–2013) Daily Gridded Rainfall Data Set Over India (Pai *et al.*, 2014).

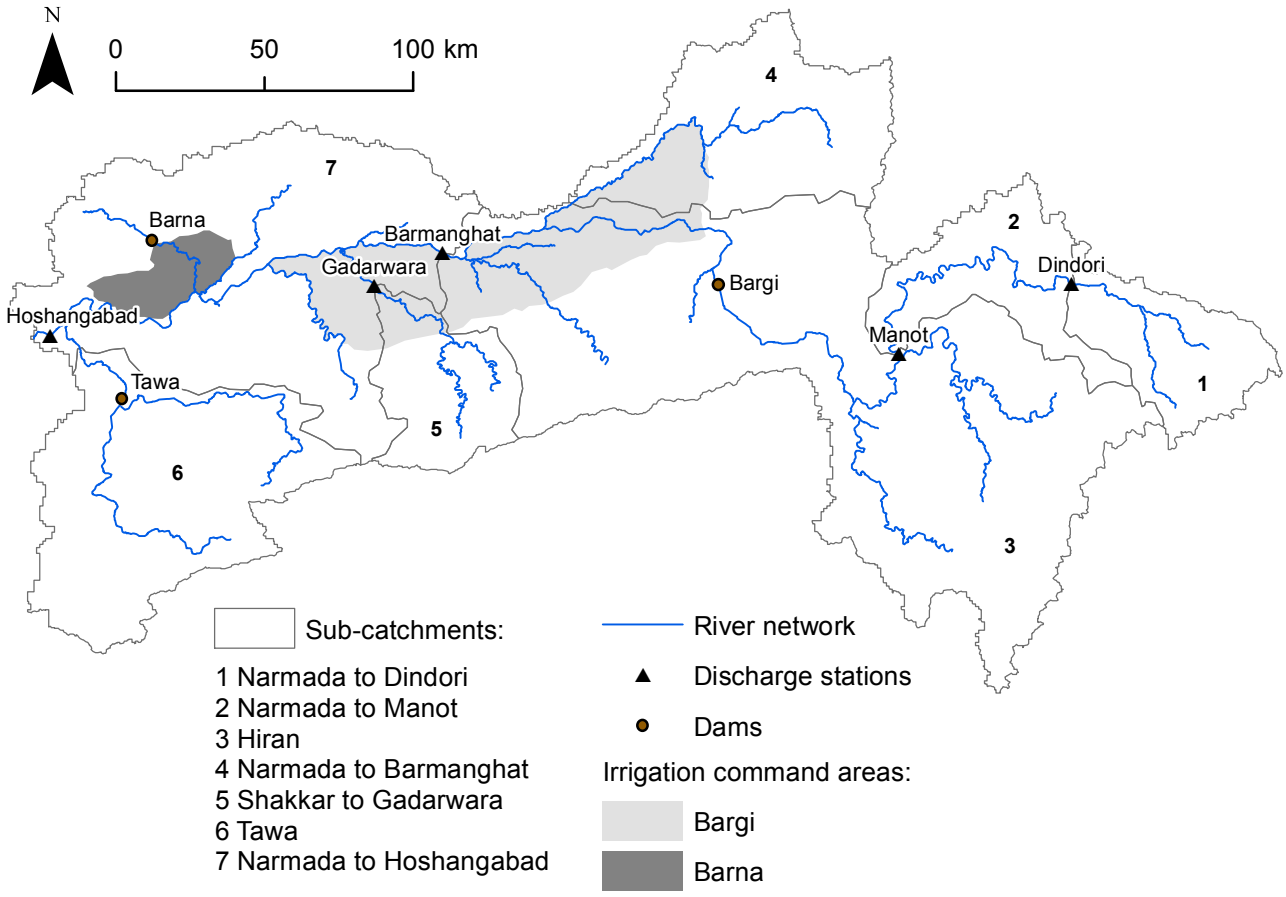

Figure 2.2. Sub-catchment distribution and river discharge gauging station locations.

A precipitation lapse rate was applied over the spatial extent of sub-catchments 1, 2 and 4, which are upstream sub-catchments located at higher elevations. The lapse rates were subject to calibration. For calculation of daily gridded potential evapotranspiration (PET), IMD/NCC high resolution (1° × 1°) gridded daily temperature data (Srivastava *et al.*, 2009) were used. The spatial distribution of precipitation and PET inputs are show in Figure 2.3. PET was calculated using the Hargreaves method, the approach recommended by the FAO where there are insufficient data to calculate Penman-Monetith (Allen *et al.*, 1998). Parameters for the

equation were obtained from ECALTOOL, a computer program that provides location specific calibrated values for the CH and EH parameters of the Hargreaves equation (Patel *et al.*, 2014). These values vary through the year on a seasonal basis. For the earlier MIKE SHE model, the CH and EH parameters were subject to further calibration to improve model performance. However, within the improved model, the CH and EH parameters were taken directly from the ECALTOOL, as this was deemed a more robust approach.

For the simulation of channel flow, MIKE SHE is dynamically coupled to MIKE 11 (Havnø *et al.*, 1995), a one-dimensional hydraulic model. A plan of the main river network was digitised in MIKE 11. For the generation of synthetic cross-sections, channel width measurements were taken from satellite imagery in Google Earth. A generalised cross-section profile and a relationship between channel width and maximum channel depth were based on limited data available from NIH (a single cross-section for the river channel at Hoshangabad) and the literature (Rajaguru *et al.*, 1995; Payasi, 2015). Cross-sections were specified as depths relative to the bank, with bank elevations taken from the SRTM DEM (digital elevation model).

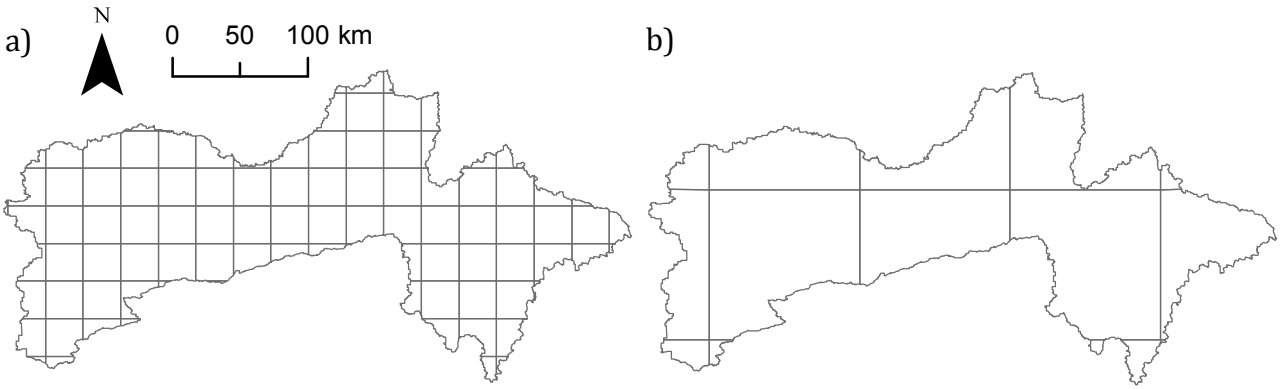

Figure 2.3. Spatial distribution of a) precipitation inputs and b) PET inputs.

Irrigation was included within the model over two command areas: Bargi (1570 km^2) and Barna (579 km^2). The locations of the command areas (see Figure 2.2) were based on a figure from Government of India Ministry of Water Resources (2014) that was georectified and digitised in ArcGIS. Data on the location of the cultivated command area (land actually irrigated) within the gross command area (the overall region containing irrigated land) were not available. However, the acreages of the command areas included in the MIKE SHE model were made to match those reported on the India-WRIS (Water Resources Information System) website (India-WRIS, 2013a, b) and in Government of India Ministry of Water Resources (2014). Irrigation water for the Bargi and Barna command areas was specified as

being abstracted from the river sections at the locations of Bargi reservoir and Barna reservoir, respectively. During model calibration, an evapotranspiration crop coefficient (Kc) of 1.2 was added over the command areas for the months of May–September. This means that the PET over these areas is multiplied by 1.2 in these months. Crop coefficients are commonly employed to adjust potential evapotranspiration estimates specifically for cropland, and a Kc of 1.2 is within the range of normal Kc values according to Allen *et al.* (1998).

A key improvement that was made to the model for the current study is that that the three largest dams (with the largest reservoirs) in the Upper Narmada Basin, (Bargi, Barna and Tawa, see Figure 2.2) were incorporated within the model. Figure 2.4 demonstrates that there are multiple dams in the upper basin. However, the reservoir area and capacity of the Bargi, Tawa and Barna Dams is considerably greater than that of the other dams, with Bargi having the largest reservoir. Table 2.2 summarises some key characteristics of the three dams.

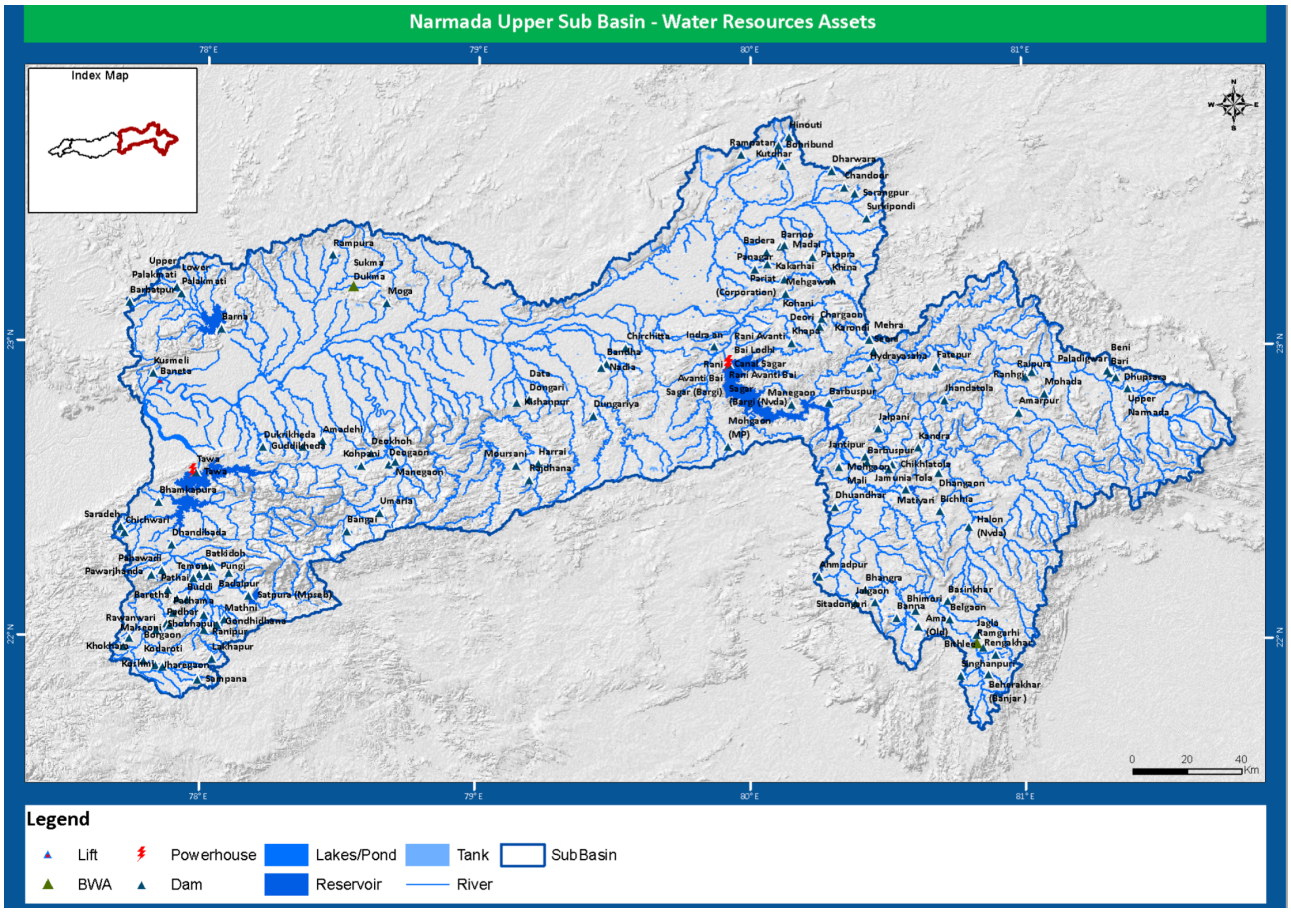

Figure 2.4. Dams and other water resource assets in the Upper Narmada Basin. Source: Government of India Ministry of Water Resources (2014).

Dam implementation within the model required representation of the reservoir dimensions within the MIKE 11 model. Cross-sections were established using a combination of width measurements acquired using Google Earth and information from the literature. Limited availability of information on dam regulation, as well as the highly variable regulation on a day-to-day basis, necessitated that the dam operation rules within the model are highly simplified compared to the actual dam operation. Model testing investigated the number of spillway gates to be included within each dam, since for all three dams, only a small number of the gates are open the majority of the time. The optimal gate level for each dam through the year was also tested. Table 2.3 summarises the implementation of the dams within the model, including the sources of information used for guidance.

Table 2.2. Characteristics of the three largest dams in the Upper Narmada Basin. Source of information: Government of India Ministry of Water Resources (2014).

Dam	River	Year of completion	Gross storage capacity (MCM)
Bargi	Narmada	1988	3924.8
Barna	Bargi	1977	539
Tawa	Tawa	1978	2312

Table 2.3. Summary of dam implementation within the MIKE 11 model

Dam	Summary of dam operation within MIKE 11	Sources used in dam and reservoir implementation
Bargi	Modelled as a control structure with 5 radial gates. The actual dam has 21 radial gates, but many of these are closed for much of the year. Gate width: 13.71 m. Gate sill level: 407.5 m. Gate opening temporally constant, with a vertical opening of 20 cm. Overflow/spill level: 425.7 m.	Goel *et al.* (2000)
Barna	Modelled as a control structure with 3 radial gates. The actual dam has 8 radial gates, but many of these are closed for much of the year. Gate width: 12.2 m. Gate sill level: 341.7 m. Gate closed September–July, with a vertical opening of 30 cm in August. Overflow/spill level: 348.55 m.	National Institute of Hydrology (1997)
Tawa	Modelled as an overflow structure with 10 gates, where spill over the dam only occurs when the reservoir water level reaches the gate level (i.e. top of the overflow gate). The gate level varies on a monthly basis according to the recommended upper rule curve for the dam from National Institute of Hydrology (1997). The actual dam has 13 radial gates, but all of these are closed for much of the year.	National Institute of Hydrology (1997)

Irrigation associated with Tawa Dam is not simulated explicitly within the model because much of the command area served by the dam is outside of the model domain, further downstream. Irrigation abstractions from Tawa Reservoir were instead accounted for by applying two hydrodynamic boundaries with negative flows, one representing the Right Bank

Canal and one representing the Left Bank Canal. Abstractions vary on a monthly basis and were based on abstraction values in a report on the operation policy of the dam (National Institute of Hydrology, 1997). The values used are summarised in Table 2.4

Table 2.4. Target monthly demands from Tawa Reservoir based on National Institute of Hydrology (1997).

Month	Irrigation demand Left Bank Canal (10^6 m^3)	Irrigation demand Left Bank Canal – rate (m^3 s^{-1})	Irrigation demand Right Bank Canal (10^6 m^3)	Irrigation demand Right Bank Canal – rate (m^3 s^{-1})
Jan	224.658	83.88	60.825	22.71
Feb	153.528	62.90	39.419	16.15
Mar	143.669	53.64	33.485	12.50
Apr	57.045	22.01	0.000	0.00
May	79.581	29.71	0.000	0.00
Jun	205.643	79.34	38.148	14.72
Jul	88.737	33.13	26.704	9.97
Aug	84.511	31.55	25.432	9.50
Sep	219.024	84.50	59.129	22.81
Oct	252.829	94.40	45.566	17.01
Nov	216.912	83.69	58.493	22.57
Dec	169.726	63.37	44.294	16.54

To summarise, the following improvements were made to the MIKE SHE model of the Upper Narmada as part of the current project:

- Division of the model domain into eight groundwater sub-catchments, instead of five.
- For the calculation of PET, the CH and EH parameters of the Hargreaves equation were obtained directly from ECALTOOL (Patel *et al.*, 2014).
- The representation of irrigation within the model was adjusted.
- Abstractions from Tawa Reservoir for irrigation are now represented.
- The three largest dams in the Upper Narmada Basin (Bargi, Barna and Tawa) were incorporated within the model, albeit with simplified operation strategies.

Whilst incorporating the above improvements, the model was iteratively re-calibrated using the period 2002–2008 (the same period employed in the calibration of the original model). Calibration was undertaken against discharge records from five gauging stations and the calibration parameters were the time constants of the saturated zone's interflow and baseflow linear reservoirs and the precipitation lapse rates over selected sub-catchments (see below). The implementation of dams and their associated reservoirs (e.g. number of gates included and gate levels) were also subject to sensitivity analysis/calibration. Model

performance at each discharge station was evaluated both qualitatively, through visual comparison of observed and simulated discharge, and quantitatively, using model performance statistics. The indicators used were the Nash–Sutcliffe coefficient (NSE; Nash and Sutcliffe, 1970), the Pearson correlation coefficient (r) and the percentage deviation in simulated mean flow from the observed mean flow (Dv; Henriksen *et al.*, 2003). NSE can vary between -1 and 1, whilst r can vary between 0 and 1; in both cases, the closer the value to 1, the better the model performance according to that criteria. In the case of Dv, the closer the value to 0, the better. Model performance according to the NSE and Dv values was classified using the scheme of Henriksen *et al.* (2008). Model validation was subsequently undertaken for the period 2009 to May 2013 (again repeating the approach used for the earlier model) using the same stations and performance criteria.

To provide baseline simulated discharge for a 30 year period, the MIKE SHE model was driven with IMD / NCC based precipitation and PET for the period 1971–2000. A secondary validation was undertaken using observed and simulated river discharge records for the Hoshangabad station for the period September 1972 – December 2000. Data were unavailable for the other gauing stations used in model calibration.

2.3. Simulation of climate change

Daily climate scenarios for precipitation and temperature (minimum and maximum) were generated for the RCP4.5 scenario for 17 GCMs for the time slice 2031–2060. The GCMs for which scenario data were generated are summarised in Table 2.5. The derivation of climate change scenarios followed the approach described by Rahman (2016). Data were first obtained from the NASA Earth Exchange (NEX) Global Daily Downscaled Projections (GDDP) dataset[1], which provides GCM projections from Coupled Model Intercomparison Project Phase 5 (CMIP5) (Taylor *et al.*, 2012) that have been downscaled to a spatial resolution of 0.25° × 0.25° using the Bias-Correction Spatial Disaggregation (BCSD) method (Thrasher *et al.*, 2012).

BCSD uses a statistical, quantile mapping bias correction approach. Using cumulative distribution functions (CDFs), it compares historical GCM outputs to climate observations over a common period. It then uses this information to adjust (bias correct) historical and future GCM outputs, whilst preserving climate trends (Thrasher *et al.*, 2012). The algorithm

[1] Acknowledgment: Climate scenarios used were derived from the NEX-GDDP dataset, prepared by the Climate

also uses spatial detail from the observational data to inform the interpolation of GCM outputs to a higher spatial resolution (Thrasher *et al.*, 2013). For application to the Narmada MIKE SHE model, the NEX-GDDP data were spatially averaged to match the grid of the IMD / NCC precipitation and temperature data. An additional stage of bias correction was subsequently undertaken using a similar quantile mapping technique to that used by the BCSD method. This time, the GCM bias for the historical period of 1971–2000 was assessed in relation to the IMD / NCC data and this information was used to correct the future GCM projections. The daily temperature data were employed to calculate Hargreaves PET, with daily minimum temperature and daily maximum temperature being averaged to provide mean temperature.

Table 2.5. GCMs used in this investigation.

Model no.	Model name	Institution	Group name	Group no.	No. of models
1	ACCESS1-0	Commonwealth Scientific and Industrial Research Organisation (CSIRO) and Bureau of Meteorology (BOM), Australia	ACCESS1-0	1	1
2	CanESM2	Canadian Centre for Climate Modelling and Analysis	CanESM2	2	1
3	CSIRO-Mk3.6.0	Commonwealth Scientific & Industrial Research Organisation in collaboration with Queensland Climate Change Centre of Excellence	CSIRO-Mk3.6.0	3	1
4	CNRM-CM5	Centre National de Recherches Météorol-ogiques/ Centre Européen de Recherche et de Formation Avancée en Calcul Scientifique	European	4	3
5	MPI-ESM-LR	Max-Planck-Institut für Meteorologie (Max Planck Institute for Meteorology)			
6	MPI-ESM-MR				
7	GFDL-CM3	NOAA Geophysical Fluid Dynamics Laboratory	GFDL	5	2
8	GFDL-ESM2M				
9	IPSL-CM5A-LR	Institut Pierre-Simon Laplace	IPSL	6	2
10	IPSL-CM5A-MR				
11	MIROC5	Atmosphere and Ocean Research Institute (The University of Tokyo), National Institute for Environmental Studies, and Japan Agency for Marine-Earth Science and Technology	MIROC	7	3
12	MIROC-ESM				
13	MIROC-ESM-CHEM				
14	bcc-csm1-1	Beijing Climate Center, China Meteorological Administration	NCAR	8	4
15	BNU-ESM	College of Global Change and Earth System Science, Beijing Normal University			
16	CCSM4	National Center for Atmospheric Research			
17	CESM1-BGC	Community Earth System Model Contributors			

To provide baseline simulated discharge for a 30 year period, the MIKE SHE model was driven with IMD / NCC based precipitation and PET for 1971–2000. The model was then driven with the NEX-GDDP based RCP4.5 scenario data for 17 GCMs for the period 2031–2060.

2.4. Results

2.4.1. Model calibration and validation

Table 2.6 summarises the optimised values of the calibration parameters. Precipitation lapse rates were employed over sub-catchments 1, 2 and 4, following initial model runs that displayed consistent underestimation of discharge at gauging stations downstream of these sub-catchments (Dindori, Manot and Gadarwara, respectively). Furthermore, these are three upstream sub-catchments that are located at higher elevations and exhibit relatively large ranges in elevation. Rain gauge networks in mountainous regions often display a bias towards stations being located at lower elevations, which can lead to systematic underestimation of precipitation (e.g. Frei and Schär, 1998; Frei *et al.*, 2003). Precipitation lapse rates can be employed to try and address this issue (e.g. Immerzeel *et al.*, 2012b; Wijesekara *et al.*, 2012; Li *et al.*, 2016). The final lapse rate values are within the range of those previously reported in mountainous regions (e.g. Immerzeel *et al.*, 2012a; 2012b).

Table 2.6. Final calibration parameter values.

Sub-catchment number	**1**	**2**	**3**	**4**	**5**	**6**	**7**
Sub-catchment name	**Din**	**Man**	**Hiran**	**Barm**	**Gad**	**Tawa**	**Hosh**
Precipitation lapse rate (%/100 m)	5	5			6		
Interflow time constant for interflow reservoir	4	6	6	6	4	14	6
Percolation time constant for interflow reservoir	4	14	14	14	4	14	14
Time constant for baseflow reservoir 1 (days)	35	35	35	35	65	65	65
Time constant for baseflow reservoir 2 (days)	300	200	300	1500	120	350	350

Model performance statistics for the calibration period are provided in Table 2.7. As indicated, a shorter period of 2001–2006 was employed at Manot, due to data availability. Observed and simulated mean monthly, monthly and daily discharges are presented in *Figures 2.5, 2.6* and *2.7*, respectively. The annual river regime is represented fairly well by the model, as are monthly discharges, with good sequencing of the annual monsoon flood pulse

achieved at all gauging stations. Mean discharges are also well represented by the model for the calibration period, with Dv classed as "very good" to "excellent" at all stations.

Table 2.7. Model performance statistics for the calibration and validation periods (validation shaded). Model performance indicators are taken from Henriksen et al. (2008).

Station	Period	Dv	Daily NSE	Daily r	Monthly NSE	Monthly r
Dindori (a)	Cal: 01/02–12/08	-3.06 *****	0.40 **	0.64	0.84 ****	0.92
	Val: 01/09–05/13	7.54 ****	0.56 ***	0.79	0.81 ****	0.93
Manot (b)	Cal: 01/02–12/06	-4.42 *****	0.53 ***	0.73	0.94 *****	0.97
Barmanghat (c)	Cal: 01/02–12/08	-2.29 *****	0.72 ****	0.85	0.94 *****	0.97
	Val: 01/09–05/10, 06/11–05/13	7.57 ****	0.70 ****	0.84	0.89 *****	0.95
Gadarwara (d)	Cal: 01/02–12/08	-1.61 *****	0.35 **	0.59	0.64 ***	0.80
	Val: 01/09–05/10, 06/12–05/13	-19.54 ***	0.75 ****	0.88	0.86 *****	0.97
Hoshangabad	Cal: 01/02–12/08	-3.77 *****	0.76 ****	0.87	0.93 *****	0.97
(e)	Val: 01/09–05/13	14.20 ***	0.77 ****	0.88	0.89 *****	0.96
	Val: 09/72–12/00	2.72 *****	0.77 ****	0.90	0.93 *****	0.97

Performance indicator	Excellent *****	Very good ****	Fair ***	Poor **	Very poor *
Dv	< 5%	5–10%	10–20%	20–40%	>40%
NSE	>0.85	0.65–0.85	0.50–0.65	0.20–0.50	<0.20

Model performance at a daily resolution is notably weaker compared to at a monthly resolution, as demonstrated in Figure 2.7 and Table 2.7. Using monthly discharges, NSE values for the calibration period are classed as "fair" to "excellent" and r values of 0.80 and above are achieved. In comparison, at a daily resolution, NSE is classed as "poor" (two stations) to "very good" (two stations) and r values range between 0.59 and 0.87.

This weaker performance at a daily resolution may partly be related to the quality and spatial resolution of the gridded precipitation and PET data. It may also relate to the operation of dams within the Upper Narmada Basin. Only the three largest dams are represented within the MIKE SHE/MIKE 11 model, whereas there are numerous smaller dams that are not included within the model (see Figure 2.4) and for which detailed information regarding their design and operation are lacking. These dams are likely to have impacted flows at a daily resolution. Furthermore, the operation of the three dams that are included within the MIKE SHE/MIKE 11 model (Bargi, Tawa and Barna) is highly simplified, with dam gate levels within

the model being either temporally consistent, or varying on a monthly basis. In contrast, operation of the dam gates can, in reality, vary on a daily basis.

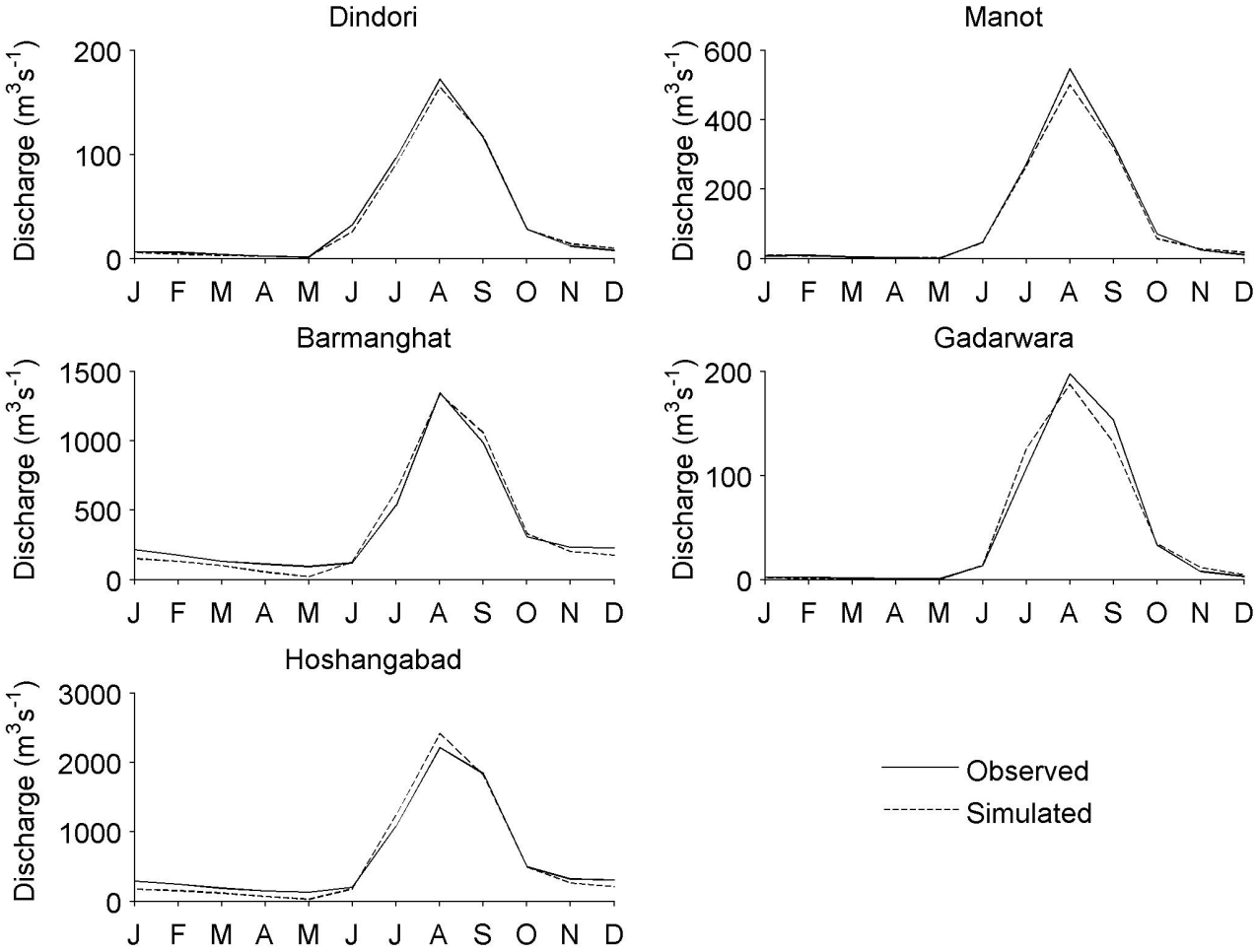

Figure 2.5. Observed and simulated river regimes for the calibration period (2002–2008).

The primary/main model validation was undertaken using the period 2009 to May 2013. However, observed discharge records were unavailable for the gauging station at Manot, and data were only available for three and a half years for the Barmanghat station and two and a half years at Gadarwara, as indicated in Table 2.7 and demonstrated visually in Figure 2.7. As for the calibration period, good sequencing of the annual monsoon flood pulse is achieved at all fours stations for the validation period (Figure 2.7). Furthermore, daily r is close to 0.8 or higher and monthly r is over 0.9 at all of the gauging stations, representing a strong positive correlation between observed discharges and those simulated by the MIKE SHE/MIKE 11 model.

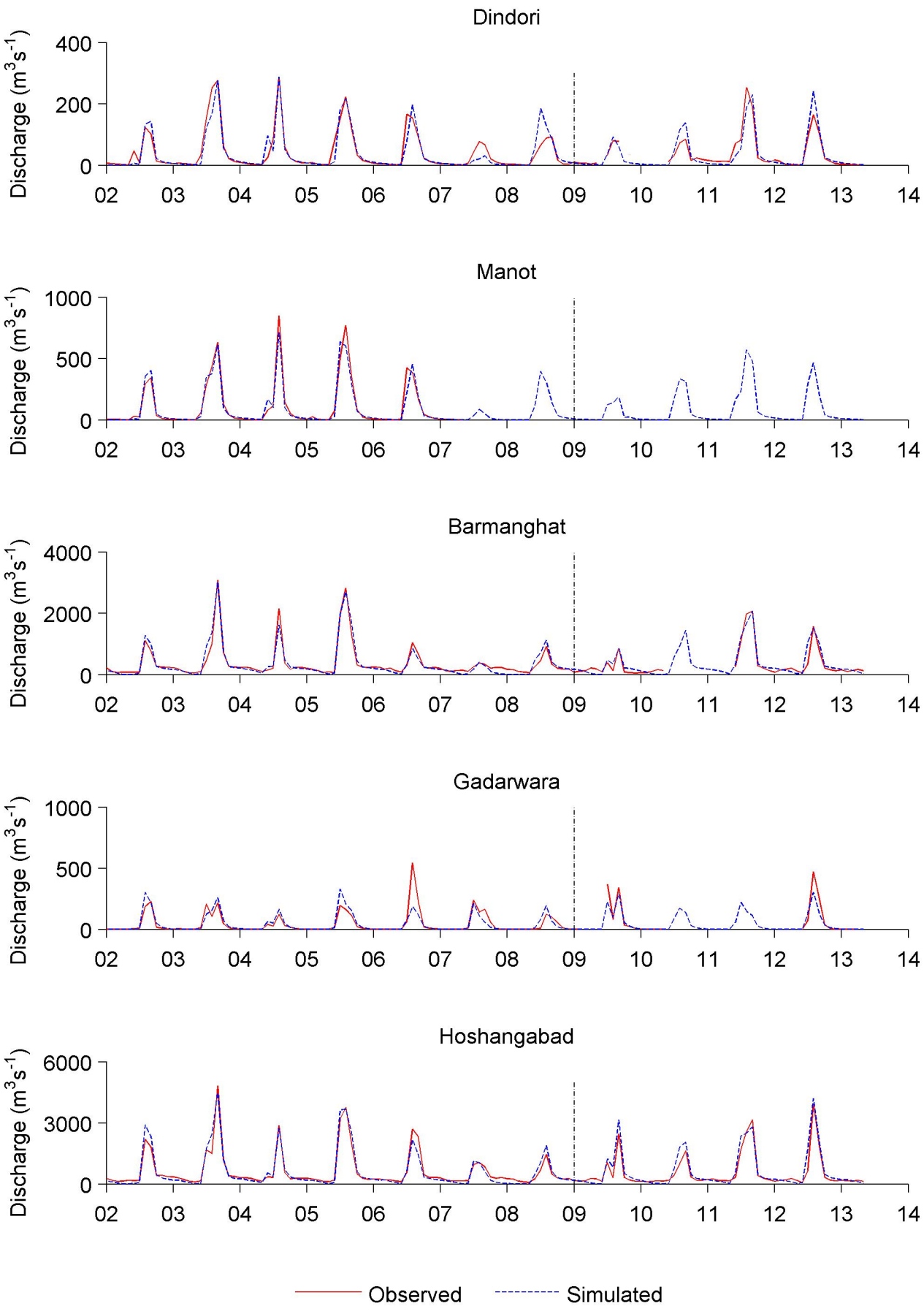

Figure 2.6. Observed and simulated monthly mean discharge for the calibration and validation periods (separated by dashed line).

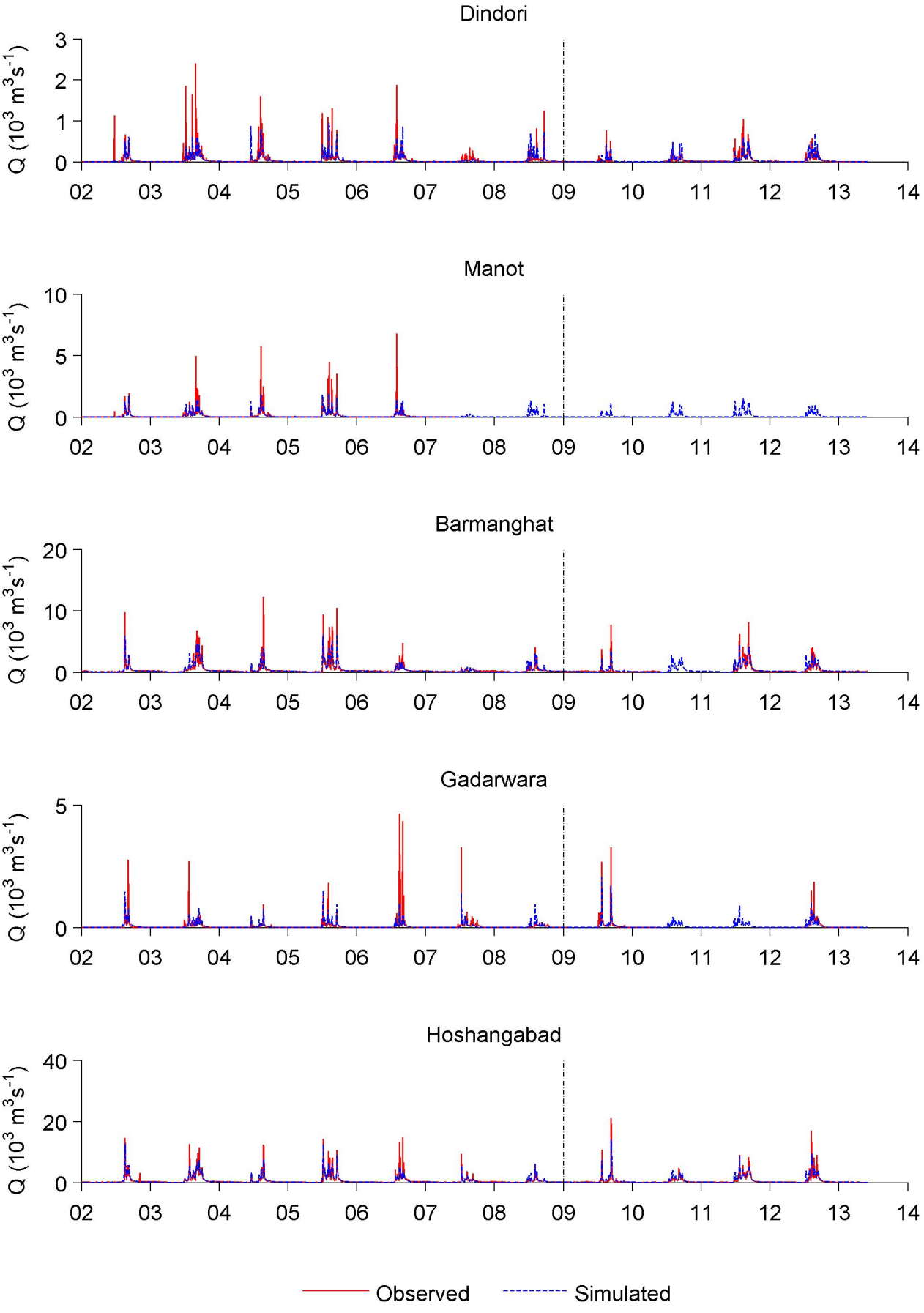

Figure 2.7. Observed and simulated daily discharge for the calibration and validation periods (separated by dashed line).

At Dindori and Barmanghat, overestimation of mean discharge for the validation period results in Dv being classed as "very good" rather than "excellent". However, at Dindori, the daily NSE value indicates an improvement in model performance compared to the calibration period, whilst monthly NSE continues to be classed as "very good" and "excellent" at Dindori and Barmanghat, respectively, despite a small reduction. At Gadarwara, although mean discharge shows greater underestimation for the validation period (a more negative Dv), NSE and r indicate an overall improvement in model performance at this station, at both a daily and monthly resolution. Finally, at Hoshangabad, Dv displays an increase, leading to its classification falling from "very good" to "fair". Despite this, performance at a daily resolution according to NSE remains "very good", and the monthly NSE value remains "excellent". Figure 2.8 demonstrates that although river regimes for the validation period match the observed less closely than during the calibration period, there is still a reasonable fit.

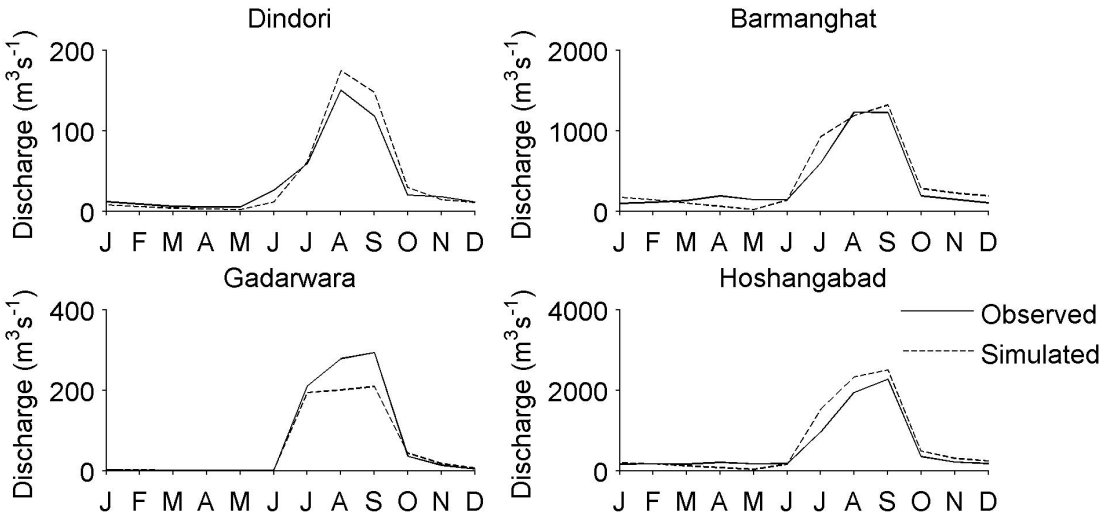

Figure 2.8. Observed and simulated river regimes for the validation period (2009–May 2013, but shorter for some stations).

For the secondary validation at Hoshangabad for the period 1972–2000, model performance is "very good" at a daily resolution according to NSE and "excellent" according to Dv and monthly NSE. Figure 2.9 presents observed and simulated river regimes, monthly mean discharge and daily discharge over this period. It demonstrates that model performance is generally good over this period, although performance is again weaker at a daily resolution compared to a monthly resolution, with underestimation of peak daily discharges. Figure 2.9*b* illustrates the impact of Bargi Dam on flows at Hoshangabad. In the model, the three dams are included throughout the simulation. However, Bargi Dam was not completed until 1988, with the reservoir being filled to capacity in 1990. Consequently, prior to 1990, simulated baseline

flows are higher than those observed, and there is a greater tendency towards underestimation of peak monthly discharges.

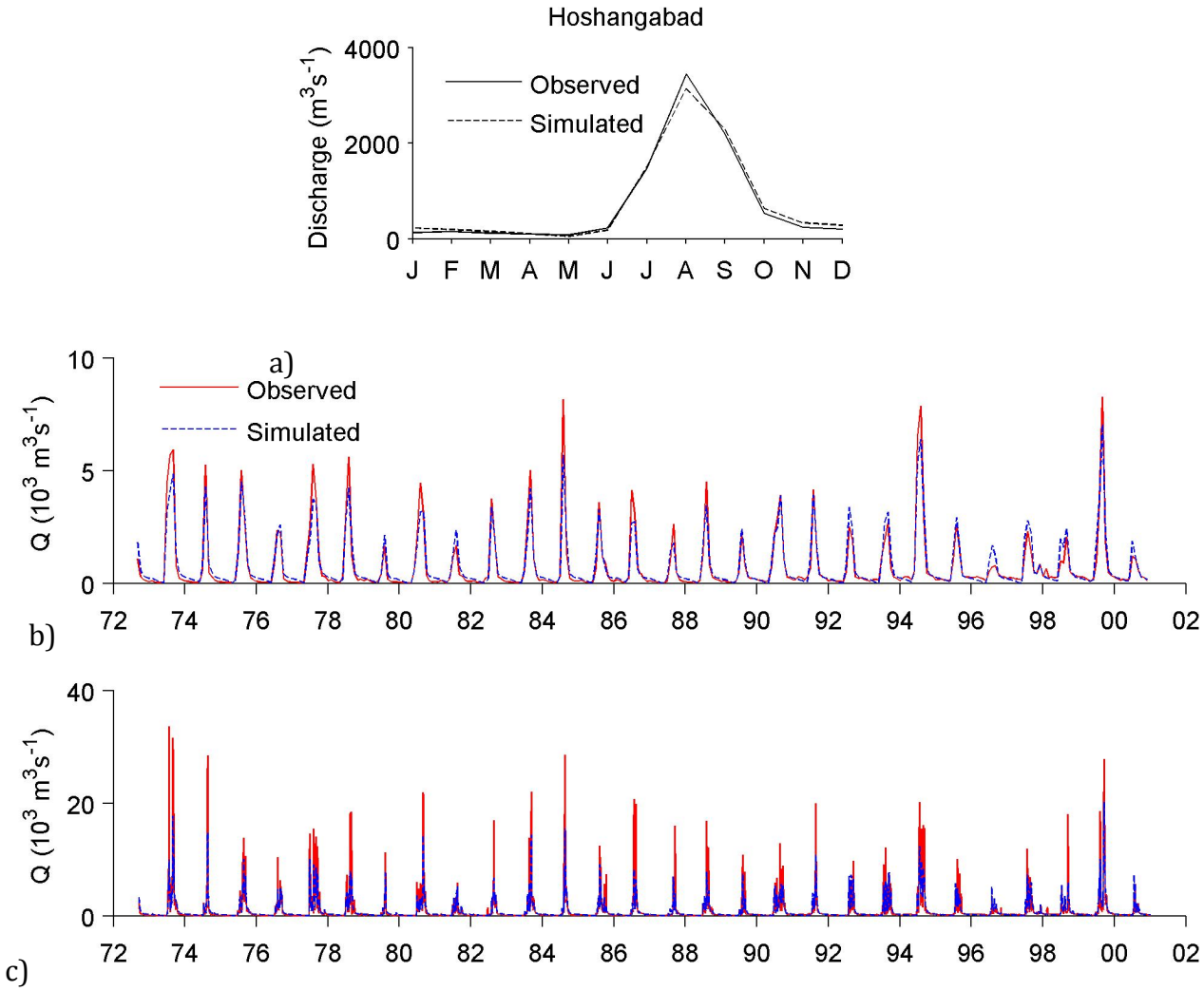

Figure 2.9. Observed and simulated: a) river regimes, b) monthly mean discharge and c) daily discharge at Hoshangabad, for the secondary validation period (1972–2000).

Overall, performance of the model is considered appropriate to allow use of the model in further investigations, including climate change scenario simulation (e.g. Thompson *et al.*, 2013) and the assessment of the impacts of climate change upon environmental flows (e.g. Thompson *et al.*, 2014b), particularly as comparisons between baseline and scenario discharges will be made at a temporal resolution lower than daily, such as monthly or annual.

2.4.2. Scenario climate

Projected changes in climate are assessed relative to the observed baseline datasets for the period 1971–2000. The spatial distribution of baseline mean annual precipitation values and

changes in mean annual precipitation under the RCP4.5 scenario (2031–2060 time slice) are presented in Figure 2.10. For each GCM, the boxplots in Figure 2.11 summarise the variability in projected change in mean annual precipitation across the 98 grid cells.

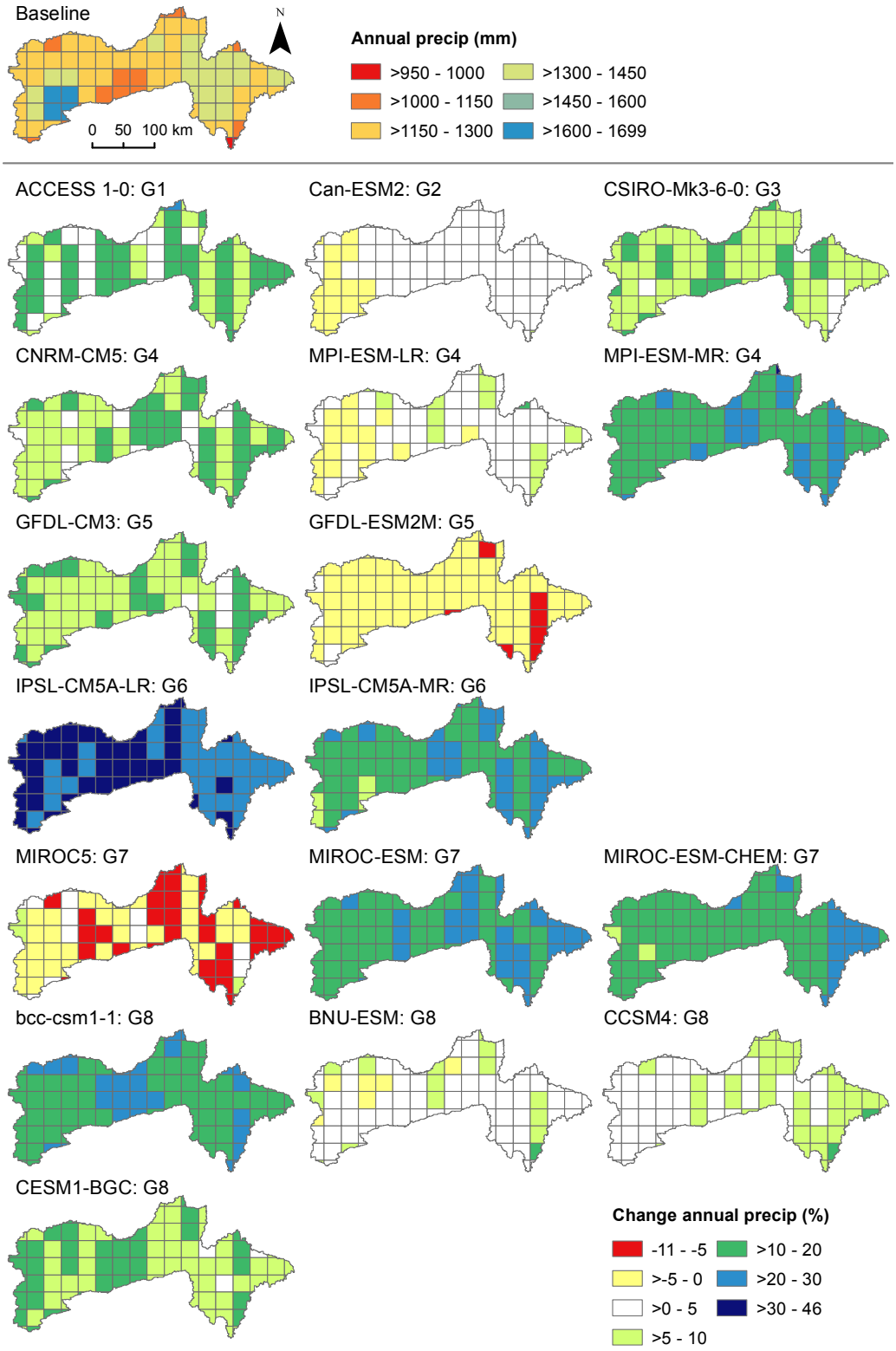

Figure 2.10. Baseline mean annual precipitation (top) and changes (%) in mean annual precipitation. (Gn represents the GCM group number.)

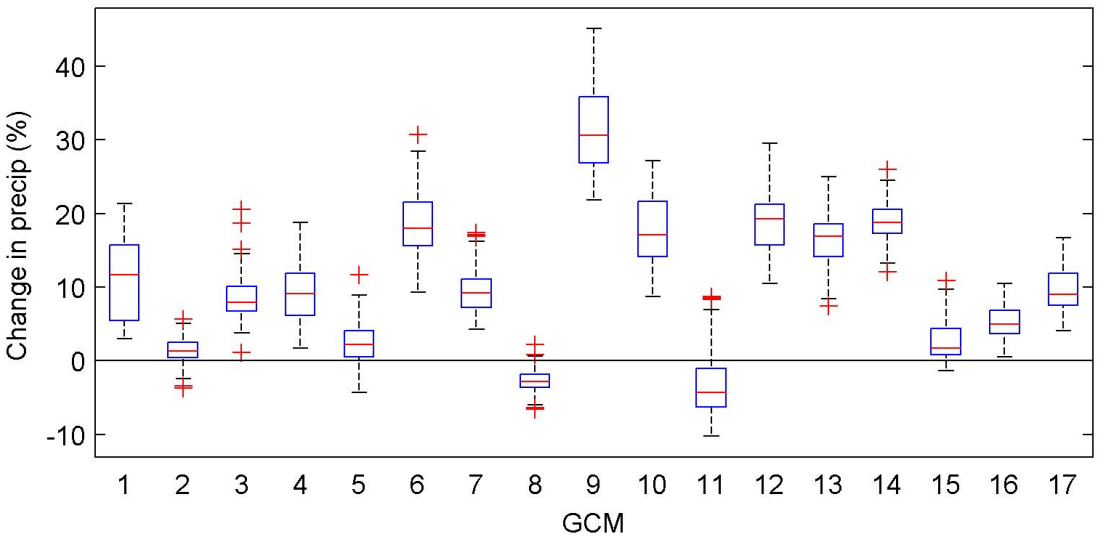

Figure 2.11. Boxplots (one per GCM) summarising change in mean annual precipitation across the 98 grid cells in the Upper Narmada Basin. The boxplots show the median, 25th and 75th quartiles, and range of the data. Any value that lies more than 1.5 times the interquartile range below the 25th quartile or above the 75th quartile is plotted as an outlier (+).

These figures demonstrate that the majority of GCMs project increases in mean annual precipitation across most of the basin. 12 GCMs project increases for all grid cells, three project increases for >75% of grid cells and only two GCMs (GCM 8: GFDL-ESM2M and GCM 11: MIROC5) project reductions for >75% of grid cells. Amongst the GCMs that project increases for most of the basin, the magnitude of change varies considerably between GCMs. For example, whilst some GCMs project increases of no more than 10%, with the middle 50% of change values falling between 0–5%, others project increases of >10% for the majority of grid cells, with the middle 50% of change values falling between 15–25%. GCM 9 (IPSL-CM5A-LR) displays the largest increases, with the middle 50% falling between +25 and +35%. The GCMs tend not to show a clear or consistent spatial pattern of change across the catchment.

For each GCM, Figure 2.12 summarises the variability in projected change in mean annual PET across the 14 grid cells used to distribute PET. Projected changes in annual PET display much less variability between GCMs compared to precipitation. With the exception of a single GCM (GCM 13: MIROC-ESM-CHEM), all GCMs project increases in annual PET for all grid cells, with changes varying between +1% and +6% and individual GCMs showing a range of up to 1% across the grid cells. The remaining GCM, MIROC-ESM-CHEM, projects only minor reductions of up to -0.3% for six grid cells, and small increases of up to 1.6% for the remaining eight grid cells.

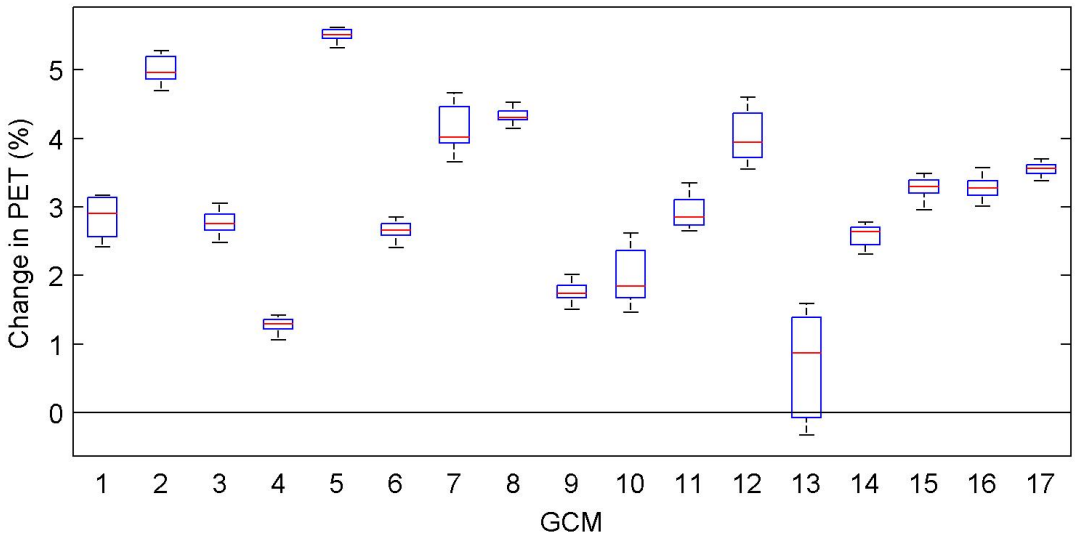

Figure 2.12. Boxplots (one per GCM) summarising change in mean annual PET across the 14 grid cells in the Upper Narmada Basin.

2.4.3. Scenario discharge

Projected changes in discharge under the RCP4.5 scenario, 2031–2060 time slice, are assessed relative to simulated discharges for the baseline period of 1971–2000. The boxplots in Figure 2.13 summarise the variability in absolute and percentage changes in mean, Q10 and Q90 discharges across the 17 GCMs for each gauging station. Percentage changes in mean discharge are broadly similar at each of the five stations, with the majority of GCMs projecting increases in mean discharge and the median change ranging between +19.5% (Station a - Dindori) and +24.7% (Station c - Barmanghat). For stations a and b (Manot), the inter-GCM range in percentage change is around 60–70%, with changes varying from around -15% to +50%. For stations c–e, the inter-GCM range in percentage change is slightly higher at 75–80%, with changes ranging from around -10% to +70%. The interquartile range in percentage change is fairly consistent across all stations, varying between 27.2% and 30.7%, with the middle 50% of changes falling between +3.6% and +38.7%. Although the distribution of percentage changes in mean discharge show similarities across the stations, it is worth noting that projected changes in absolute terms are much smaller at the upstream stations, a, b and d (Dindori, Manot and Gadarwara, respectively) (maximum change of +54 m^3s^{-1}), compared to stations c (Barmanghat) and e (Hoshangabad) (maximum changes of 295 m^3s^{-1} and 544 m^3s^{-1}, respectively).

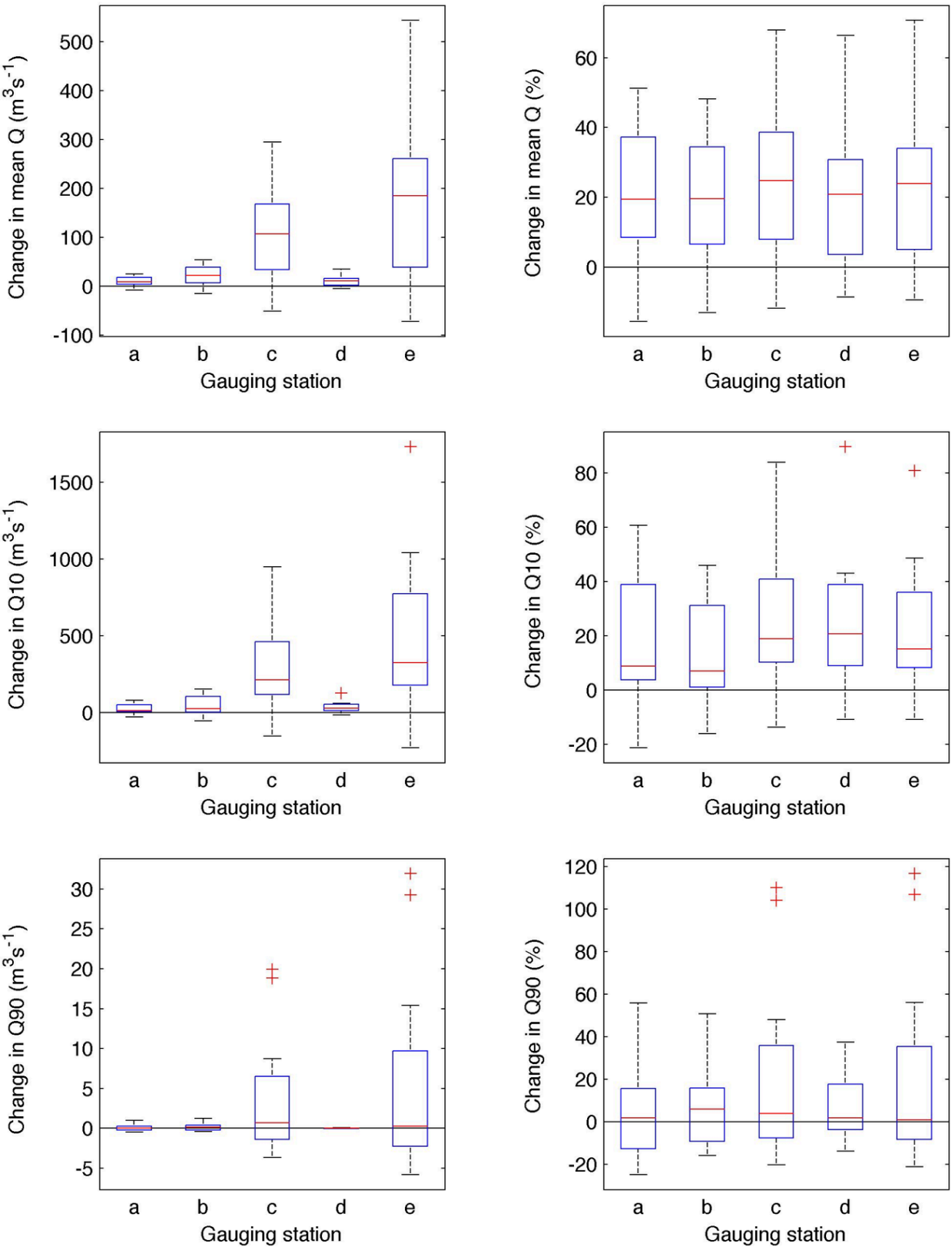

Figure 2.13. Boxplots of absolute (left) and percentage (right) changes in mean, Q10 and Q90 discharges across the 17 GCMs for each gauging station. The boxplots show the median, 25th and 75th quartiles, and range of the data. Any value that lies more than 1.5 times the interquartile range below the 25th quartile or above the 75th quartile is plotted as an outlier (+). See Table 2.7 for gauging station names.

Changes in high flows (Q10) show a similar pattern of variability across the GCMs to changes in mean discharge, with increases projected by the majority (>75%) of GCMs and the middle

50% of percentage changes at each station falling somewhere between 0% and 40%. Low flows (Q90) show only negligible (<±2 m^3s^{-1}) absolute changes at station a, b and d. Projected changes are also very minor at stations c (Barmanghat) and e (Hoshangabad), with 15 of the GCMs projecting changes of between -6 m^3s^{-1} and +16 m^3s^{-1}, and two outlier GCMs displaying small increases of around 20 m^3s^{-1} and 30 m^3s^{-1} at stations c and e, respectively. Unlike changes in mean discharge and Q10, changes in Q90 show more of an even split between GCMs that project increases or decreases at each station.

Although Figure 2.13 provides a useful summary of the variability in projected discharges, it does not allow the results of individual GCMs to be discerned. Percentage changes in mean discharge for each station and each GCM are therefore shown in Figure 2.14, with a separate subplot for each GCM group.

In terms of the spatial pattern in the magnitude of changes in mean discharge, most GCMs show a relatively consistent magnitude of change across the five stations. Differences between GCMs can predominantly be explained by projected changes in precipitation. For example, Figure 2.14 demonstrates that only two GCMs, GCM 8: GFDL-ESM2M and GCM 11: MIROC5, project reductions in mean discharge. In the case of the former, changes are consistently very small (no more that -3.5%). MIROC5 displays larger reductions of between -8.5% and -15.5%. These are the only two GCMs that project reductions in annual precipitation across the majority of grid cells within the catchment (Figure 2.10), with MIROC5 showing larger reductions for a greater number of grid cells. The GCM that produces the largest increases in discharge (~+50% to ~+70%) is IPSL-CM5A-LR, which displayed the largest increases in annual precipitation (between +20% and +46%, Figure 2.10).

Within some of the groups that contain multiple GCMs, there are sometimes clear similarities between models in terms of the magnitude and spatial pattern of changes. In many cases however, there are often relatively notable differences between GCMs within the same group. For example, in Group 7, whilst MIROC5 and MIROC5-ESM-CHEM display very similar results at all stations, with increases in mean discharge of >27% at all stations and the largest increase at Station a (Dindori), MIROC-ESM in the same group projects reductions at all stations (maximum change: -15.5%, Station a).

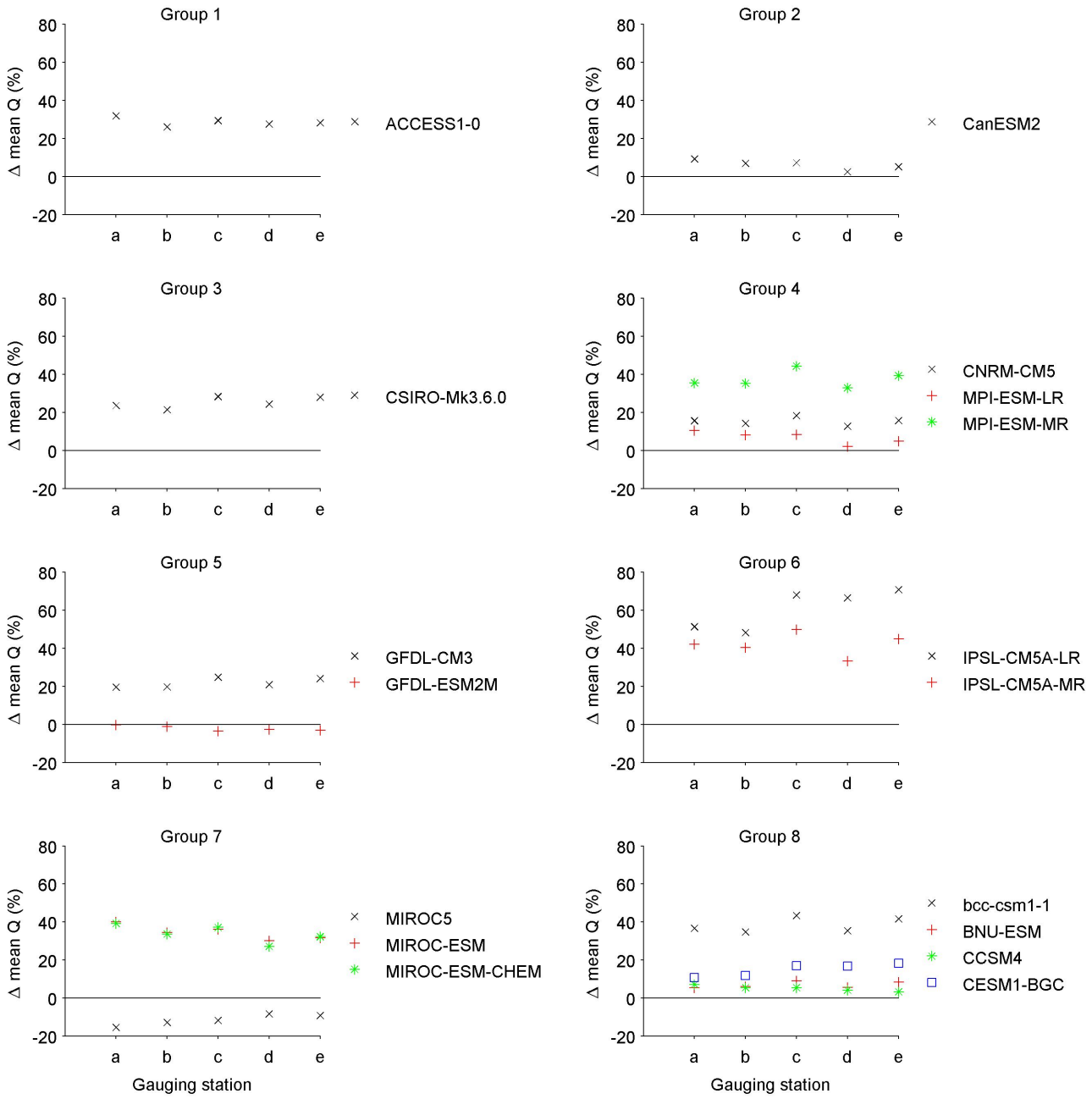

Figure 2.14. Projected percentage change in mean discharge across the 5 gauging stations (a–e). Individual subplots for each GCM group. See Table 7 for gauging station names.

Figure 2.15 displays simulated river regimes (mean monthly discharges) for the scenario period for each GCM and the ensemble mean, as well as the baseline. As previously indicated by changes in Q90 (Figure 2.13), all GCMs project very little change, in absolute terms, in dry season flows throughout November–May (<20 m^3s^{-1} at stations a (Dindori), b (Manot) and d (Gadarwara), <55 m^3s^{-1} at stations c (Barmanghat) and e (Hoshangabad)). In June–July, the majority of GCMs project increases in discharge, with only four to seven GCMs projecting reductions in discharge, depending on the station and month. In August to October, the number of GCMs projecting a reduction decreases to between four and zero. This is when the

ensemble mean shows the largest absolute changes in discharge, with the largest increases occurring in August at all stations (e.g. station a: +43 m^3s^{-1}, station e: +987 m^3s^{-1}). Dependent on station, either August or September displays the largest spread in simulated discharges from the different GCMs, meaning that these are the months with the greatest uncertainty in the magnitude of change.

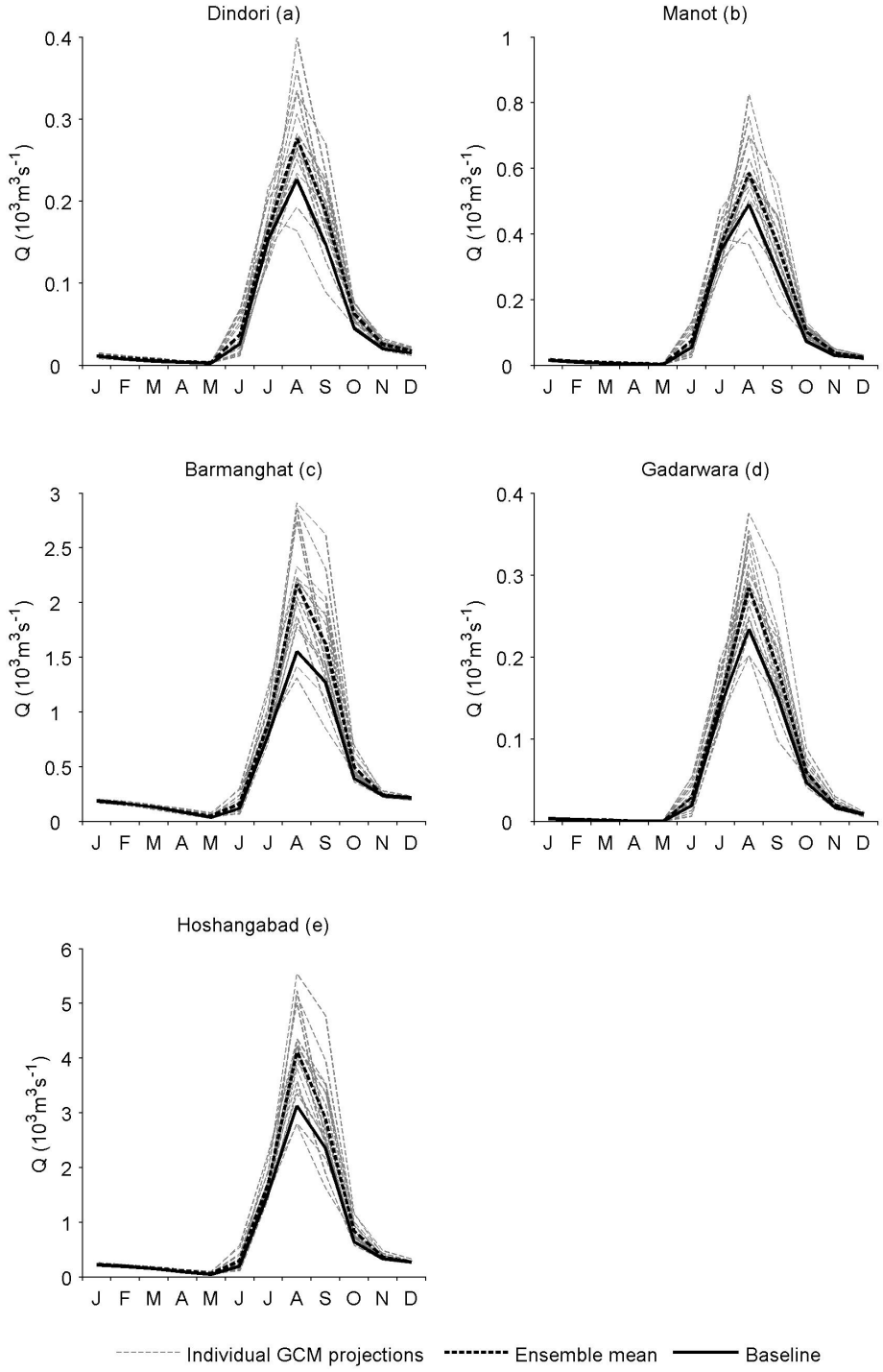

Figure 2.15. Simulated river regimes for the five gauging stations for the baseline, each GCM and the ensemble mean. (Note different y-axis scales.)

2.5. The GWAVA water resources model

The Global Water AVailability Assessment model (GWAVA) was developed by the Centre for Ecology & Hydrology (CEH) and the British Geological Survey (BGS) in order to provide an improved methodology for the assessment of water resources at the regional to global scale (Meigh *et al.*, 1999). It is a gridded, semi-distributed model, incorporating the PDM rainfall-runoff model structure (Moore, 2007), along with key elements of river infrastructure and water demands relevant for the assessment of water resources. These include artificial water transfers and the routing of flows through lakes, reservoirs and wetlands. The model allows for water use from various sectors, including that of domestic consumption, industrial and agricultural demands and water use for energy. GWAVA is run at a daily time-step, and both daily and monthly outputs produced to give a comprehensive assessment of water scarcity across the study domain. Runoff and recharge are generated via inputs of precipitation and evapotranspiration through the PDM rainfall-runoff model. An additional model accounts for rainfall that is intercepted by a forest canopy. Runoff is then generated from the input of effective precipitation and routed through each model cell via surface and subsurface storages (Moore, 2007).

The model provides a comparison of surface water availability and demand at the scale of the grid cell for a comprehensive assessment of spatial and temporal variability of water resources across a user-defined basin or region. Model outputs include simulated daily to monthly flows, water scarcity indices and environmental flow risk maps, all on a model cell-by-cell basis.

2.6. Development/Improvement of the GWAVA model of the Upper Narmada Basin

The model was developed for the assessment of water scarcity over large domains, and as such has been previously applied at spatial resolutions of between $0.5^{o} \times 0.5^{o}$ to 7km × 9km (Meigh *et al.*, 1999; Dumont *et al.*, 2012). The choice of grid size is a compromise between the need to represent spatial variability, and critically, the availability of suitable data. For the application of GWAVA to the Upper Narmada Basin, a spatial resolution of 0.125^{o} latitude × 0.125^{o} longitude was selected. This resolution enables a detailed analysis and understanding of the spatial variability of the water availability in the Upper Narmada at a scale that allows for the meaningful use of available data (Fung *et al.*, 2006).

One of the largest water consumers within the Narmada is the agricultural sector, with crop irrigation a vital influence on the hydrological regime within the basin. GWAVA has been developed to represent the individual water needs of up to eight crops in any one cell via the use of FAO cropping coefficient values (Kc), varying the demand by month according to the stage of the growing cycle (Allen *et al.*, 1998). Irrigation demands were updated from the original GWAVA application, encompassing the two main command areas in the Upper Narmada from the Bargi and Barna dams. The Rabi and Kharif growing seasons were represented on an annual basis, with crop rotation based on information gathered by NIH. Detailed water transfers out of the basin were also added to the original application, including that transfers from the Tawa Dam to the adjacent Ganges Basin, which is undertaken to help meet the water requirements of the city of Bhopal, state capital of Madhya Pradesh.

The data used for GWAVA model configuration are listed in *Table 2.8*. These include data that were used as part of the MIKE SHE model, along with information on the artificial influences datasets used to configure the water demands component of the GWAVA model. IMD (India Meteorological Department) / NCC (National Climate Centre) gridded climate data were used to drive the GWAVA model, as with the MIKE SHE model (see Section 2.2). PET was calculated for each grid cell using the Hargreaves method. Note that no lapse rates were applied to precipitation for the GWAVA application to the Upper Narmada.

2.7. GWAVA model calibration and validation

Using the PDM structure, GWAVA calibrates four parameters for each sub-catchment specified, allowing the user to manually set a further three parameters. The calibrated parameters include the PDM parameter of the power law probability distribution (b), describing the spatial variations in soil moisture storage capacity; the surface runoff routing parameter (S_{rout}) and the groundwater routing parameter (G_{rout}), representing the lag in water being transported via overland flow and baseflow respectively; and a multiplying factor (fact) to adjust vegetation rooting depths, wilting points and soil column depths.

The previous application of the GWAVA model to the Upper Narmada Basin did not facilitate the use of the inbuilt automatic calibration routine, and was configured using global default settings. The calibration of the GWAVA model for the updated application was conducted via

an automated iterative process, based on observed discharge data for the period 1990–2000. This time period was selected as the construction of the Bargi was not completed until 1988, with the model configured to include all three of the major dams in the upper part of the basin. This time period also allowed for a sufficient validation period, which was chosen as 2002–2010. Again, this period includes the major anthropogenic influences known to be affecting flows within the basin. The year 2001 was excluded from the validation period due to a number of outlier values in the observed flow records at two of the gauging stations selected for calibration / validation (Mohgaon and Belkheri). After statistical analysis of the data at these stations, it was decided that in the interests of consistency the validation period for all stations should commence in 2002.

Table 2.8. Summary of set-up of updated GWAVA model of the Upper Narmada Model

Model component	**Key inputs**	**Data sources/ derivation**
Model domain	Catchment extent – the basin area upstream of Hoshangabad	ESRI polygon shapefile provided by NIH
Topography	Topography	Extracted from SRTM (Shuttle Radar Topography Mission) DEM (digital elevation model).
Land use/ vegetation	Land use distribution	USGS LULC map (USGS, 2015) - Reclassified to six land cover types: Forest, Shrub, Water bodies, Wetlands, Bare soil and Grass/cropland.
Unsaturated zone: modelled via PDM rainfall-runoff model	Root depths	Implicit to model, taken from Vorosmarty et al. (1989)
	Soil classes	The spatial distribution of six soil classes was specified using a 1 km × 1 km grid based on a georectified and digitised version of a Government of India Survey of India soil map, provided by NIH.
	Soil hydraulic properties	Values for the different soil classes derived from the literature (Vorosmarty et al., 1989; Saxton & Rawls, 2006)
Catchment meteorology: Precipitation and evapo-transpiration modules.	Precipitation	0.25° × 0.25° gridded daily precipitation obtained from the IMD (India Meteorological Department) / NCC (National Climate Centre) High Spatial Resolution (0.25° × 0.25°) Long Period (1901–2013) Daily Gridded Rainfall Data Set Over India (Pai *et al.*, 2014).
	Potential evapotranspiration (PET)	Calculated using Hargreaves method and IMD gridded daily temperature (Srivastava *et al.*, 2009).
Artificial influences	Reservoir & lake abstraction, water body dimensions	National Institute of Hydrology (1997); Goel et al. (2009)
	Population & Domestic consumption	Indian Population Census (GOI, 2011), provided by NIH; AQUASTAT (FAO, 2016)
	Irrigated crops	Portmann (2011); additional information from NIH
	Water transfers	Goel *et al.* (2009); additional information from NIH
	Cattle, sheep and goat populations	Indian Livestock Census (GOI, 2007), from NIH

In total, discharge records for five sub-catchment gauging stations in the Upper Narmada were selected for calibration / validation. This selection was based on the completeness of their records and the stations location in the basin (see *Figure 2.16* for station locations, note that some stations differed from those used in the MIKE SHE model which were dictated by the distribution of the linear reservoir-based saturated zone model). GWAVA calibration includes basic dam operations, along with all known abstractions and demands from the agricultural and domestic sectors. As with the MIKE SHE model, model performance at each station was assessed for both the calibration and validation periods via a number of model performance statistics. The indicators used were the Nash–Sutcliffe coefficient (NSE; Nash and Sutcliffe, 1970), the Pearson correlation coefficient (r) and the percentage deviation in simulated mean flow from the observed mean flow (Dv; Henriksen *et al.*, 2003; see Section 2.2 for details of each criterion).

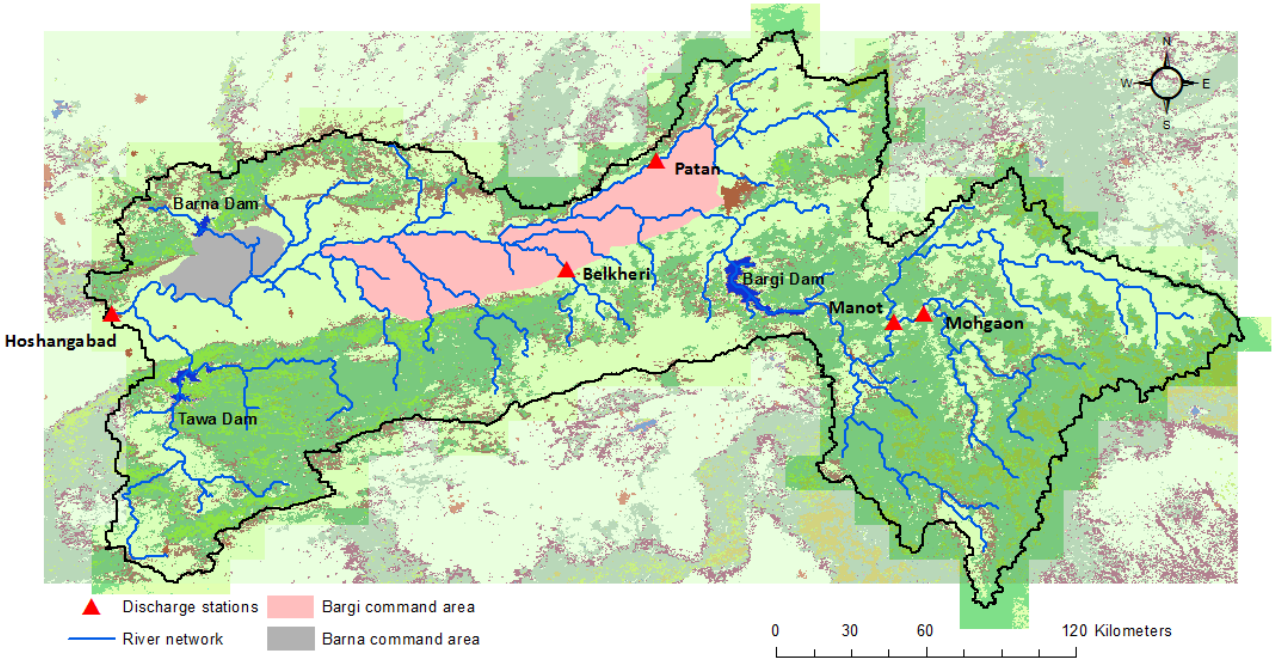

Figure 2.16. River discharge gauging station locations for the GWAVA Upper Narmada model

In summary, the following improvements were made to the GWAVA model to the Upper Narmada as part of the current project:

- Updated land use data via USGS.
- Improved flow direction via the SRTM DEM.
- Incorporation of two cropping seasons, additional crop types and irrigation practices, as directed by NIH.
- The use of the Hargreaves equation for PET input, replacing the Thornthwaite methodology.

- The inclusion of the Bargi, Barna and Tawa reservoirs with basic operations, to allow for a more realistic routing of water through the upper basin.
- Monthly abstractions from the Tawa Reservoir
- The division of the basin in to 5 sub-catchments, enabling a more representative and heterogeneous parameter set
- Automatically derived PDM parameters via the GWAVA model calibration routine

2.8. Simulation of climate change

The baseline period used to drive the GWAVA model was the same as for the calibration period (i.e. 1990–2010). The decision to select this period was made as any validation prior to 1988 would need to take in to account alterations in anthropogenic influences throughout the Upper Narmada, including the absence of the Bargi reservoir. It was therefore felt that the time slice used for calibration would provide a more realistic baseline from which to assess any changes as a result of future climate alone. Data for the climate change simulations were taken from the bias-corrected CMIP5 ensemble described in Section 2.3, and listed in Table 2.5. These were run for the period 2028-2060, and the output metrics standardised to enable comparison with the baseline period.

2.9. Results

2.9.1. Model calibration and validation

Table 2.9 summarises the optimised values of the GWAVA calibration. All manual parameters were kept at their default global values. Model performance statistics for the calibration and validation periods are shown in *Table 2.10*. These include performance metrics for both daily and monthly flow regimes. The model performs well during the calibration period at a monthly temporal resolution, displaying 'very good' to 'excellent' NSE metrics, along with r values ranging from 0.85–0.97. It can be seen from *Figure 2.17* and *Figure 2.18* that the timing of the annual monsoon is captured reasonably well at all sites. Dv is classed as 'very good' to 'excellent' at three sites, but is weaker at Mohgaon and Belkheri, the latter being classed as 'very poor'. This can be seen in *Figure 2.17*, where flow is significantly overestimated throughout the annual regime.

Model performance at a daily resolution (Figure 2.19) is weaker than at the monthly time step for all sites. The NSE metrics for the calibration period range from 'fair' to 'excellent', with r values from 0.75-0.93 (*Table 2.10*). Flows during the dry season at Hoshangabad are also underestimated throughout, as reflected by a Dv metric of -7.7.

Table 2.9. Final calibration parameters for GWAVA's application to the Upper Narmada

Sub-catchment number	**1**	**2**	**3**	**4**	**5**
Sub-catchment name	**Manot**	**Mohgaon**	**Patan**	**Belkheri**	**Hoshangabad**
b	0.69	0.54	0.69	0.39	0.29
fact	0.66	0.38	2.84	0.43	2.31
S_{rout}	0.84	0.76	0.43	0.97	0.35
G_{rout}	7.45	0.90	2.49	0.40	10.38

Table 2.10. Model performance statistics for the calibration and validation periods (validation shaded). Calibration period: 1990–2000 Validation period: 2002–2010 for all stations. Performance indicators from Henriksen et al. (2008).

Station	**Dv**		**Daily NSE**		**Daily r**	**Monthly NSE**		**Monthly r**
Manot (1)	-0.6	*****	0.74	****	0.86	0.94	*****	0.97
	-3.2	*****	0.68	****	0.82	0.95	****	0.97
Mohgaon (2)	13.5	***	0.55	***	0.75	0.70	****	0.85
	-10.4	***	0.58	***	0.79	0.81	****	0.92
Patan (3)	0.00	*****	0.87	*****	0.93	0.95	*****	0.98
	-0.8	*****	0.81	****	0.9	0.93	*****	0.97
Belkheri (4)	40.5	*	0.65	****	0.81	0.84	****	0.95
	54.4	*	0.69	****	0.84	0.79	****	0.94
Hoshangabad (5)	-7.7	****	0.77	****	0.88	0.93	*****	0.97
	-14.2	***	0.64	***	0.8	0.89	*****	0.96

Performance indicator	**Excellent** *****	**Very good** ****	**Fair** ***	**Poor** **	**Very poor** *
Dv	< 5%	5–10%	10–20%	20–40%	>40%
NSE	>0.85	0.65–0.85	0.50–0.65	0.20–0.50	<0.20

Monthly NSE metrics for the validation period range from 0.92-0.97, again indicating a good model fit to the observed data. Dv metrics are classed as 'excellent' through to 'very poor' across the five gauging station. As demonstrated in *Figure 2.20*, the model tends to underestimate discharge in the monsoon season at Mohgaon, and overestimate discharge throughout the year at Belkheri. As was the case for the calibration period, model performance during the validation period at a daily time step is weaker than it is for the

monthly resolution. NSE values decrease from the calibration period at three of the five gauging stations. It can be seen in Figure 2.19 and *Figure 2.20* that the model struggles to simulate flows at Hoshangabad during the dry season. The underestimation of discharge at Hoshangabad is highlighted by the Dv of -14.2. However, the timing and magnitude of the annual peak are more aligned with the observations, especially at a monthly resolution.

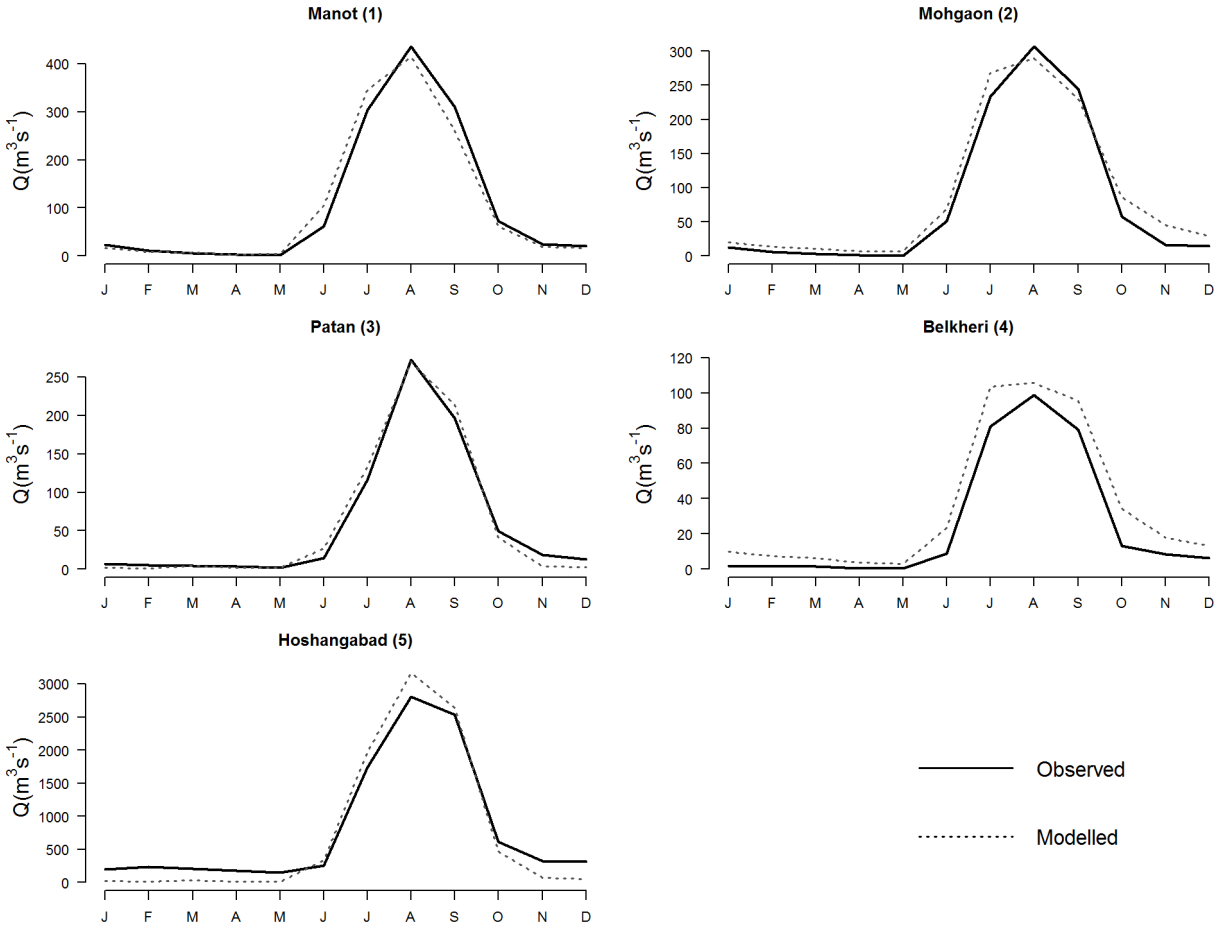

Figure 2.17. Observed and simulated flow regimes for the calibration period (1990–2000)

The relatively poorer model performance at all gauging stations at the daily time step is likely the result of a combination of factors, both within the model and the input data. The overestimation of flows at Belkheri is a trend that was also noted by Thomas (2017) when using SWAT for hydrological modelling of the Upper Narmada. It may be the case that the routing of water through this catchment is subject to processes not currently being captured by the model, along with possible inaccuracies in the climate data and observed flow data.

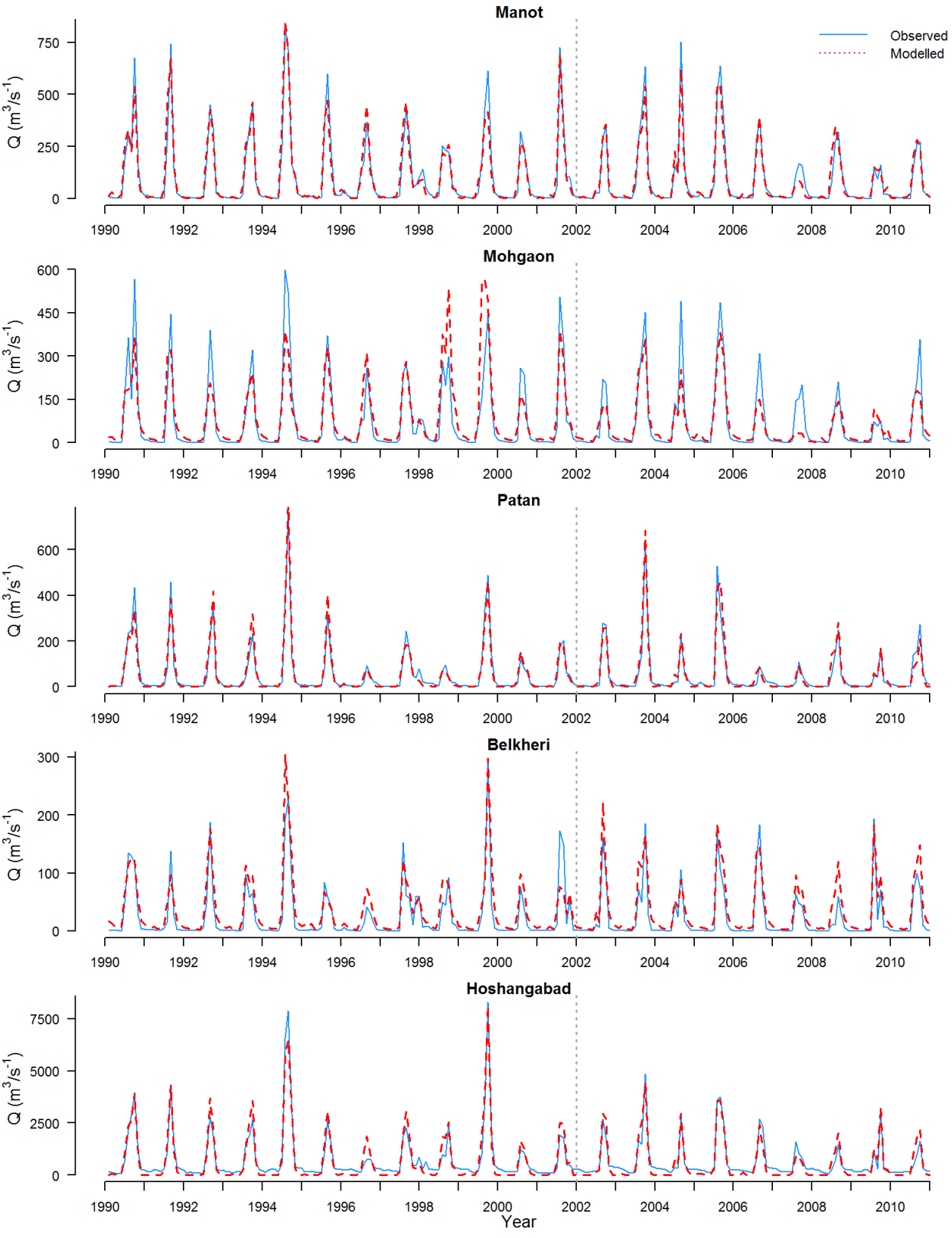

Figure 2.18. Observed and simulated monthly mean discharge for the calibration and validation periods (separated by dashed line).

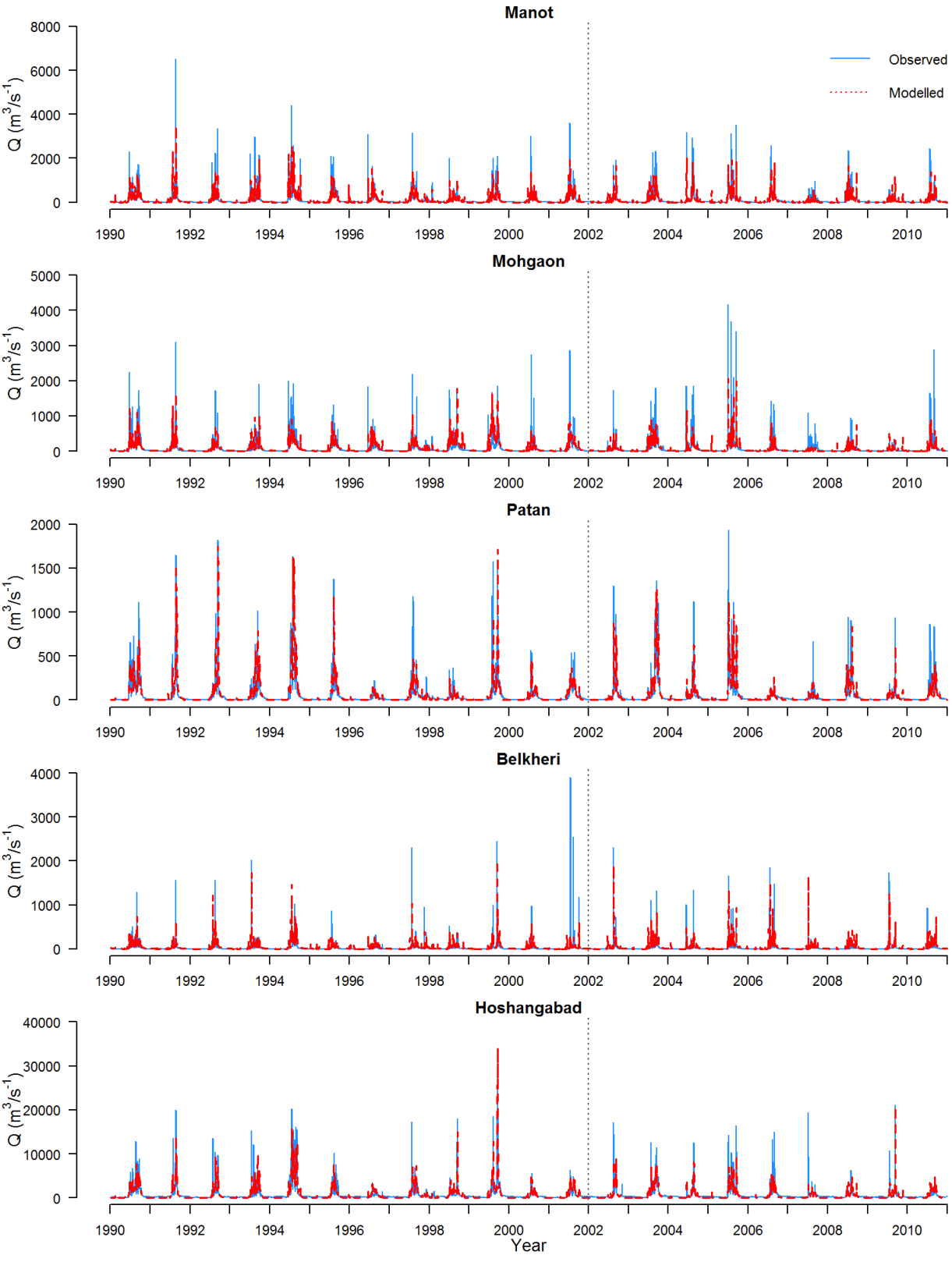

Figure 2.19. Observed and simulated daily discharge for the calibration and validation periods (separated by dashed line).

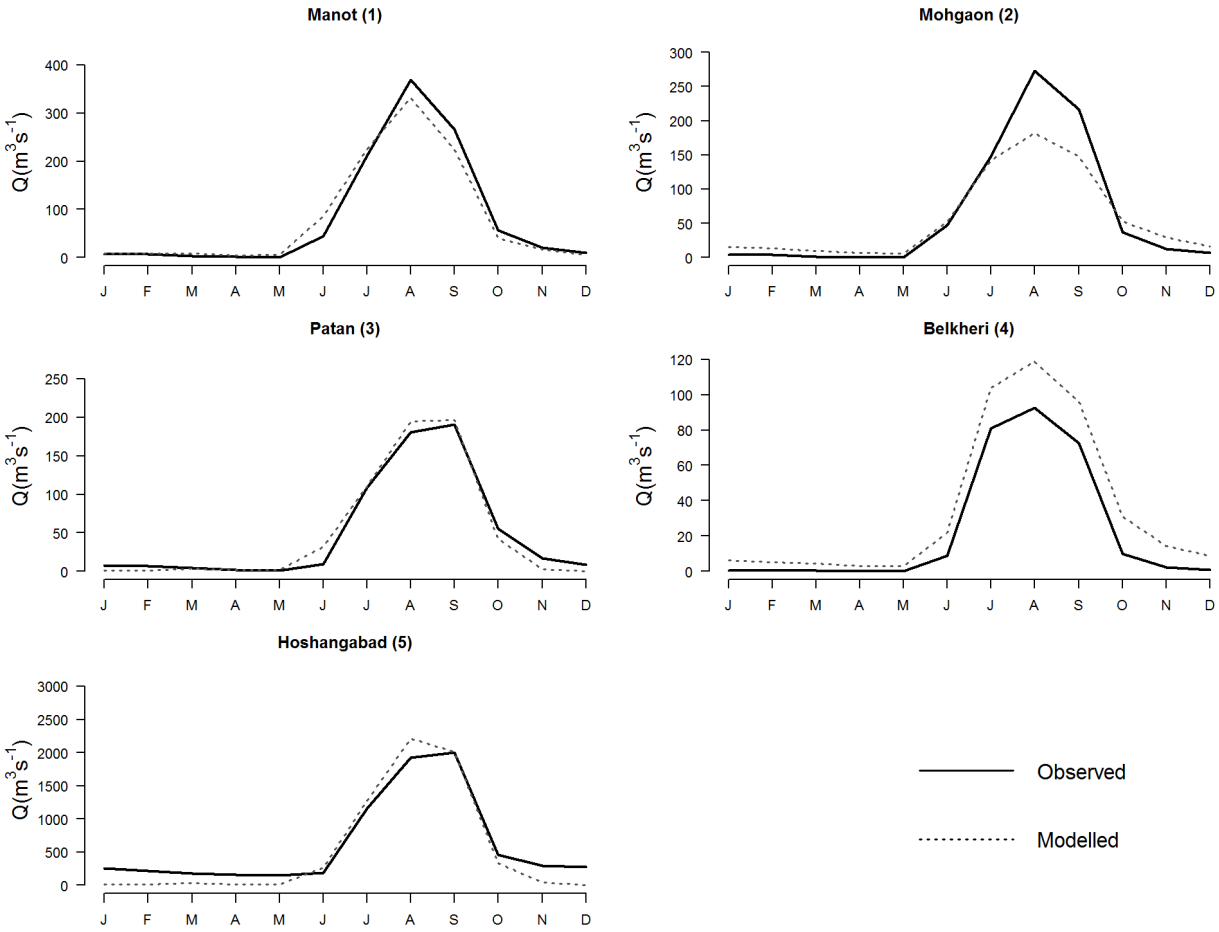

Figure 2.20. Observed and simulated flow regimes for the validation period (2002–2010)

The simulated low flows during the dry season at Hoshangabad tend to be lower than the observed flow, with the model struggling to maintain sufficient flows from around Q70. One possible reason for this may be the operational rules of the three major reservoirs in the basin. Detailed information regarding operational rules and release thresholds were not available for this study, and so it may be the case that GWAVA is storing too much water during the dry season. Future improvements for the GWAVA application to the Upper Narmada should include a sensitivity analysis around the release of water from all three reservoirs, to help better represent low flows at the most downstream point of the basin.

Despite the areas of less-satisfactory performance described above, the model overall can be seen to do well in capturing and representing the key events of the hydrological regime. As such, the model is considered to be appropriate for use when assessing future impacts of climate change within the Upper Narmada on river flow and water resources.

2.9.2. Scenario discharge

As with the MIKE SHE model, all projected changes in discharge under the RCP4.5 scenario are assessed relative to the baseline period, in this case 1990–2010. *Figure 2.21* displays boxplots summarising the variability in absolute and percentage changes for the mean, Q10 and Q90 flows across the 17 GCMs for each of the five guaging stations. The percentage change in mean discharge increases in the majority of GCMs, reflected in the median of the mean flow at all sites, ranging from 21% at Manot (Site 1) through to 31.5% at Belkheri (Site 4). The largest range in predicted mean flows is at Patan (Site 3), where the inter-GCM range is -19%- to + 79%. The interquartile range across all sites is between 21% and 29.4%, with the middle 50% between 6.5% and 45.4%.

As would be expected, the absolute changes in discharge are less pronounced at the upstream gauging stations, with a maximum of 62.0 m^3s^{-1} at Manot, a 65.21% increase from the baseline mean. The interquartile ranges at Manot, Mohgaon, Patan and Belkheri are also relatively small. The downstream site of Hoshangabad displays a maximum absolute change of 353.8 m^3s^{-1}, which represents a 53% increase from the mean baseline discharge.

Changes in Q10 at each of the gauging stations again show a general trend of predicted increases in flow, as highlighted by the median values. At stations 1-4, >75% of the 17 GCMs show an increase from the baseline, with Belkheri displaying an outlier value of >80%. Decreases in Q10 are predicted by 5 of the 17 GCMs at Hoshangabad, ranging from -5.7% to -45.8%. Interquartile metrics for percentage changes are relatively similar between the five gauging stations, ranging from 15.5% at Hoshangabad up to 25.9% at Manot.

The boxplot displaying percentage changes in Q90 indicates an increase in mean Q90 discharges at Manot, Mohgaon and Belkheri. The variability in the range between stations is more noticeable at low flows than for mean and Q10 discharges, with the median change at stations 1,2 and 4 being 43.8%, 19.6% and 2.32% respectively. Percentage changes in Q90 discharges for Patan and Hoshangabad are not displayed, as flow values were simulated at 0 m^3s^{-1} in the baseline and across all 17 GCM scenarios. This is likely the result of in accuracies in the reservoir operations within the model, and highlights the underestimation of flows during the dry season noted in Section 2.9.1.

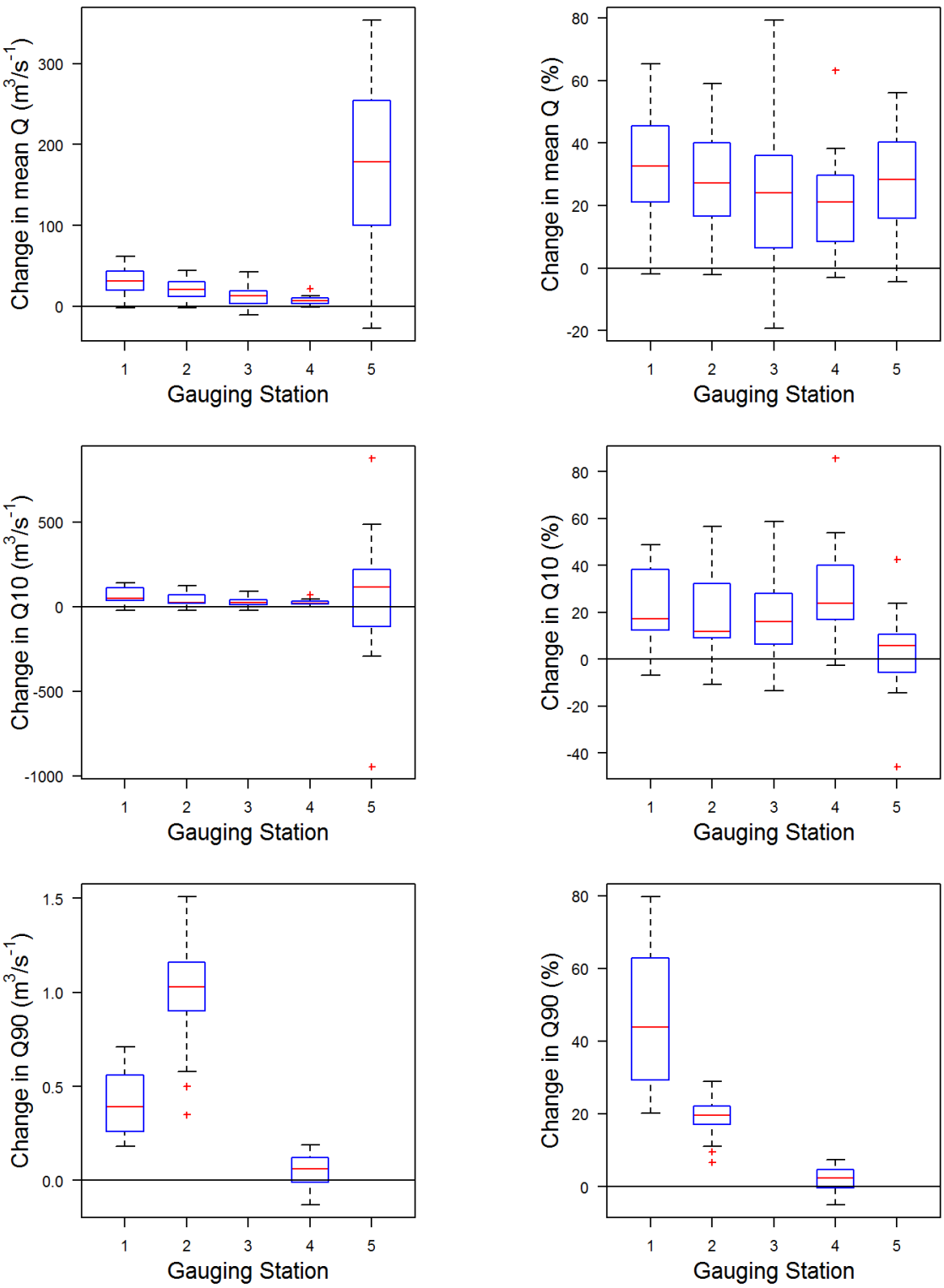

Figure 2.21. Boxplots of absolute (left) and percentage (right) changes in mean, Q10 and Q90 discharges across the 17 GCMs for each gauging station. The boxplots show the median, 25th and 75th quartiles, and range of the data. Any value that lies more than 1.5 times the interquartile range below the 25th quartile or above the 75th quartile is plotted as an outlier (+). See Table 2.10 for gauging station names

Figure 2.22 displays projected percentage change in mean discharge at the five gauging stations for each of the 17 GCMs. In a similar way to the results of the MIKE SHE model, differences between the GCMs can be largely explained by predicted changes in precipitation.

GFDL-ESM2M indicates reductions in mean discharge at stations 3, 4 and 5, whilst MIROC5 suggests decreases in flows at all stations, ranging from -1.9% at Manot to -19.3% at Patan. As noted previously (Section 2.4.2), these GCMs are the only two within the ensemble that display reductions in precipitation across the majority of grid cells. The largest percentage increases in mean flow across gauging stations 1-4 are produced by the IPSL-CM5A-LR GCM, with increases of 65.2%, 58.9%, 79.2% and 63.1% respectively. The largest percentage increase at Hoshangabad is 56% and is associated with MPI-ESM-MR GCM in Group 4.

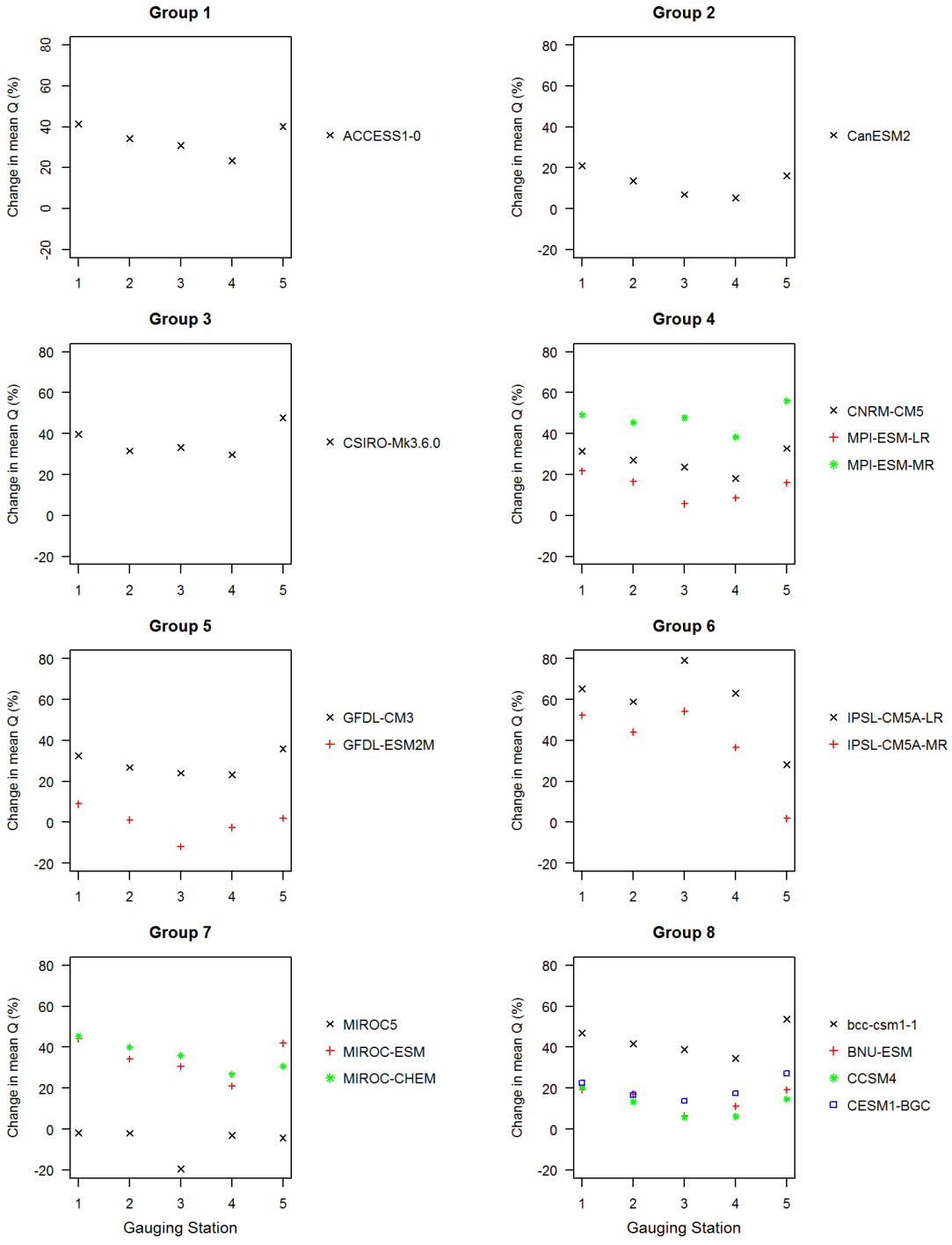

Figure 2.22. Projected percentage change in mean discharge across the 5 gauging stations (1–5). Individual subplots for each GCM group. (+). See Table 2.10 for gauging station names.

The relative direction and magnitude of change is in general very consistent within the groups containing multiple GCMs, with the exception of Group 7. This was also noted in the results for the MIKE SHE model when driven by the same set of climate change scenarios (Section 2.4.3). Within Group 7, the MIROC5 GCM projects much lower percentage changes in discharge than either of the other two GCMs in the same group, these being MIROC-ESM and MIROC-CHEM. The relative direction of change between the gauging stations is also different for MIROC5, displaying opposite trends at Belkheri and Hoshangabad when compared to the other GCMs in Group 7.

Figure 2.23 shows the mean monthly discharge at the five gauging stations for each of the 17 GCMs, along with those for the baseline period. Ensemble means at each of the stations predict higher flows during the rainy season (June–October) when compared with the baseline, with peak flows in August at Manot and Patan more than doubling for some GCMs, increasing by maximums of 435.16 $m^3s^{-1}$and 245.52 m^3s^{-1} respectively. The largest absolute changes in discharge across all five stations are projected in August. The magnitude of these changes varies from 56.84 m^3s^{-1} at Belkheri, up to 1460.46 m^3s^{-1} at Hoshangabad. The dry season of November–May sees less change across the 17 GCMs. Manot, Mohgaon, Patan and Belkheri display differences within the range of <15 $m^3s^{-1}$and > -3 m^3s^{-1}, whilst changes in dry season flows at Hoshangabad are in the range of <33.46 m^3s^{-1} and > -24.01 m^3s^{-1}.

2.9.3. GWAVA water resources output

As part of GWAVA's functionality, one of its key outputs is that of indices for water resources/scarcity across the region of interest. This index is found by calculating the 90% reliable flow for the driest month of the year and then abstracting from this the demands for this month until they are met, or until cell runoff is no longer able to sustainably meet these demands. This is then converted to a ratio ranging from -1 (negligible water availability to meet demand) through to 1 (available water greater than demand). This index therefore reflects the critical point in the year with regards to water availability, and distinguishes areas where there may be a shortfall of water relative to demand on a cell-by-cell basis. (Meigh *et al.*, 1999).

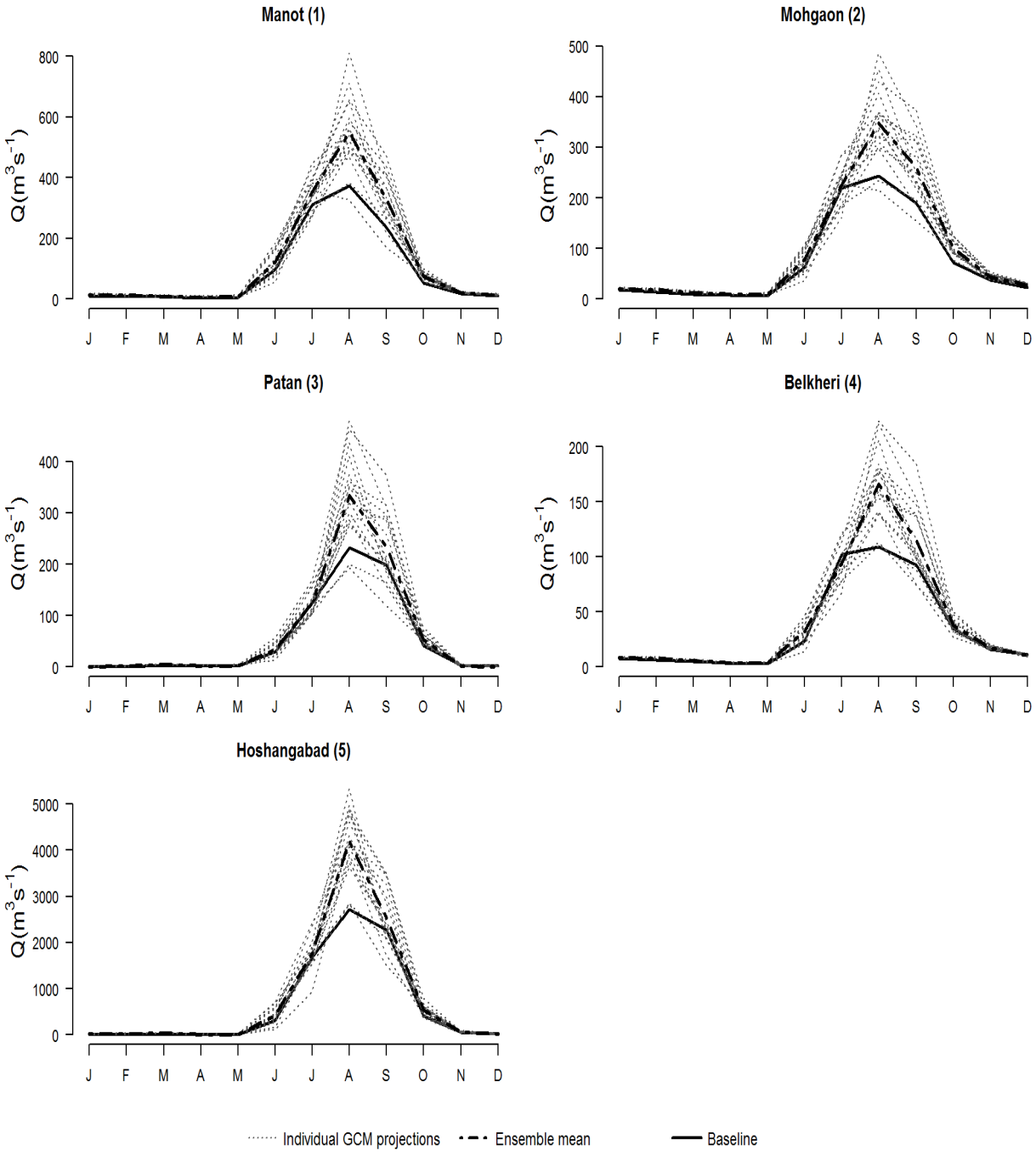

Figure 2.23. Projected Simulated river regimes for the five gauging stations for the baseline, each GCM and the ensemble mean. (Note different y-axis scales).

Figure 2.24 and *Figure 2.25* display examples of water availability across the Upper Narmada Basin for the baseline climate and the ACCESS1-0 GCM climate change scenario, respectively. It can be seen that the main regions of water scarcity within the baslin for both climate periods are that of the command areas for the Bargi and Barna reservoirs. The future climate scenario appears to reduce the water stress placed upon these areas in comparison to the baseline period, possibly due to an increase in precipitation throughout the year, allowing the

reservoirs supplying the command areas to fill, ready for irrigation in the dry season. Such outputs, with the inclusion of the full CMIP5 ensemble, will allow for a future comprehensive analysis of the key drivers of the potential future state of water resources within the Upper Narmada Basin.

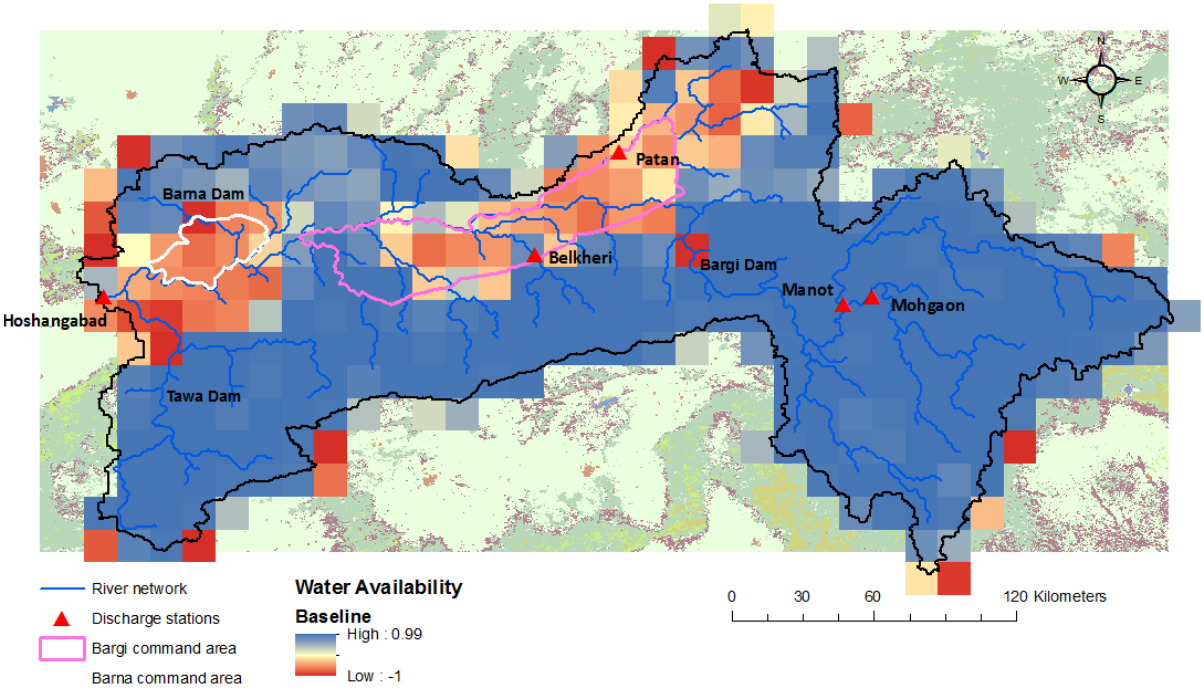

Figure 2.24. GWAVA water resources output for the Upper Narmada Basin for the baseline period (1990–2010)

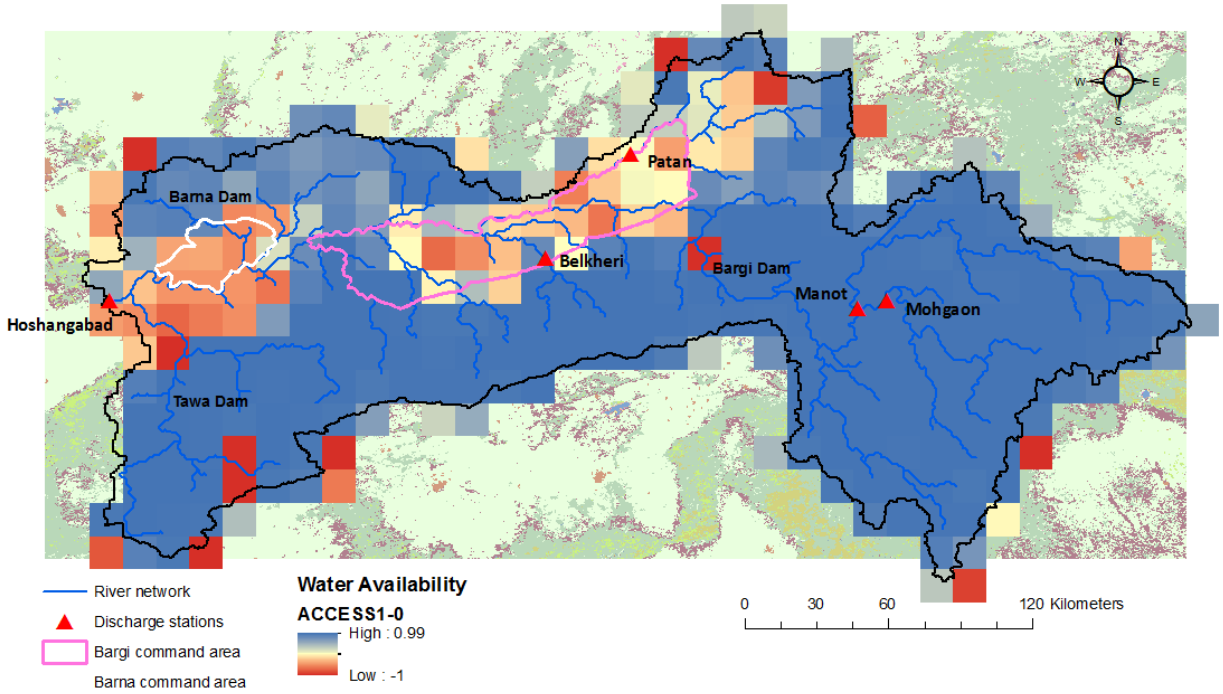

Figure 2.25. GWAVA water resources output for the Upper Narmada Basin for the ACCESS1-0 GCM climate change scenario (2028–2060)

2.10. MIKE SHE / GWAVA comparison

This project has further enhanced two existing hydrological models of the Upper Narmada each developed using a different modelling system; MIKE SHE/MIKE 11 and GWAVA. This in principle enables a comparison of the each model's ability to simulate historical river discharges as well as an assessment of any hydrological-model related uncertainty in future projections due to climate change. However, any such comparison should, in this case, be undertaken with a number of caveats.

In the case of the models' performance in simulating observed discharges, the approaches used to spatially distribute processes and the historical development of the existing models restricts common gauging stations to two; Manot in the upstream, eastern part of the basin and Hoshangabad, the lowest point on the Upper Narmada. Additionally, the use of alternative calibration and validation periods (which was largely related to overall data availability and in the case MIKE SHE meant that simulated discharges at Manot were not validated) prevents a direct side-by-side comparison of observed and simulated river discharges for the same period. Notwithstanding these issues, it is still possible to review the relative values of the common statistical measures of model performance used in the calibration and validation of the two models (*Table 2.11*) and to identify any commonalities / differences in simulated discharges using, in this case, the river regime (*Figure 2.26*).

Table 2.11. Model performance statistics for the calibration and validation for the two common gauging stations simulated by MIKE SHE and GWAVA

Station	Model	Period*	Dv	Daily NSE	Daily r	Monthly NSE	Monthly r
Manot	SHE	Cal	-4.4 *****	0.53 ***	0.73	0.94 *****	0.97
	GWAVA	Cal	-0.6 *****	0.74 ****	0.86	0.94 *****	0.97
		Val	-3.2 *****	0.68 ****	0.82	0.95 ****	0.97
Hoshangabad	SHE	Cal	-3.8 *****	0.76 ****	0.87	0.93 *****	0.97
		Val	14.2 ***	0.77 ****	0.88	0.89 *****	0.96
	GWAVA	Cal	-7.7 ****	0.77 ****	0.88	0.93 *****	0.97
		Val	-14.2 ***	0.64 ***	0.80	0.89 *****	0.96

Performance indicator	Excellent *****	Very good ****	Fair ***	Poor **	Very poor *
Dv	< 5%	5–10%	10–20%	20–40%	>40%
NSE	>0.85	0.65–0.85	0.50–0.65	0.20–0.50	<0.20

* *Calibration: MIKE SHE 2002-2008 / GWAVA 1990-2000; Validation: MIKE SHE 2009-2013 / GWAVA 2000-2010*

The statistics in *Table 2.11* point to similar performance for the two models albeit. as discussed, for different periods. At Manot, the DV for the calibration periods used by the two models are both classified as excellent although MIKE SHE does tend to underestimate discharges by a larger amount than GWAVA. *Figure 2.26* shows that the August peak is underestimated by 8.8% for MIKE SHE compared to 4.4% for GWAVA. The largest percentage differences between observed and simulated discharges occur, however, at the very end of the dry season although, of course, absolute differences are very low at this time.

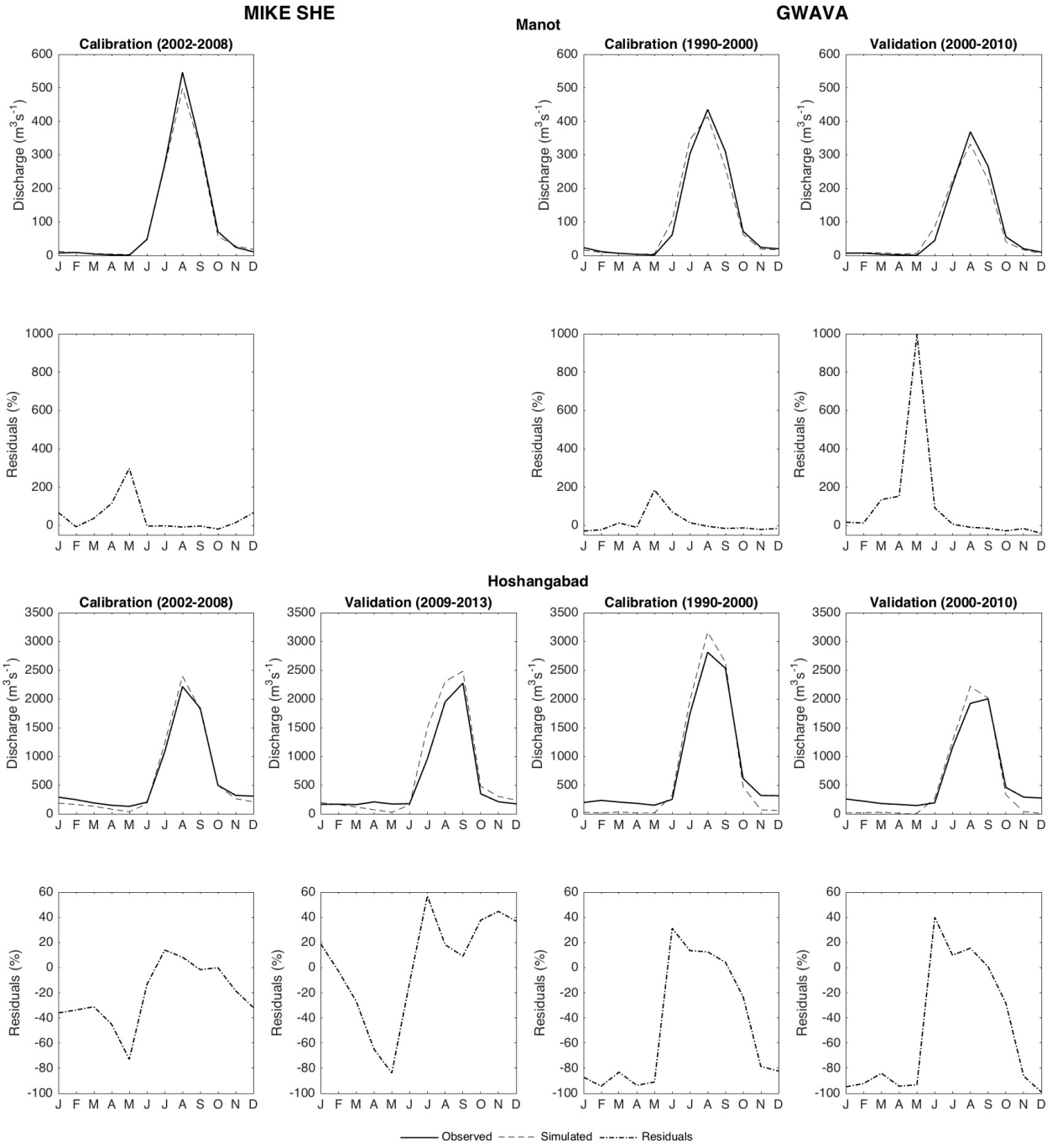

Figure 2.26. Observed and simulated river regimes for Manot and Hoshangabad for the calibration and validation periods employed by the MIKE SHE and GWAVA models.

Results for GWAVA tend to suggest an earlier rise in the annual flood at Manot during the calibration period compared to both the observations and results for MIKE SHE. GWAVA simulated discharges also lead the observed for this model's validation period. At a monthly resolution, MIKE SHE and GWAVA produce identical NSE and r values with the former being classified as excellent. This statistic is on the boundary between excellent and very good for the validation period for GWAVA. At a daily resolution the NSE and r values suggest better performance by GWAVA compared to MIKE SHE. It is, however, worth noting that at this shorter temporal resolution inter-model differences in the values of these model performance statistics will be more influenced by the different meteorological conditions experienced during the different calibration periods and, in turn, their impact upon river flows.

The values of Dv for Hoshangabad in the calibration periods point to better performance by MIKE SHE (excellent) compared to GWAVA (very good). *Figure 2.26* shows that whilst both models overestimate the calibration periods' peak of the river regime (in August by on average 8.2% and 12.5%, respectively), discharges are underestimated during the longer dry period leading to the overall negative Dv values. This underestimation is more evident in results from GWAVA. Overestimation of peaks and underestimation of dry season flows could result from incomplete representation of the impacts of the dams on the Upper Narmada that, in particular, impact discharges at Hoshangabad. Indeed prior to the incorporation of dams within the MIKE SHE model, this differential model performance was more extreme (Robinson *et al.*, 2016). As discussed above, (Section 2.2) detailed information on the operation of the dams was limited necessitating the representation of dam operation using the limited data that were available. Notwithstanding this issue, the statistical performance of the two models for their respective calibration periods as indicated by NSE and r are almost identical. In both cases NSE is classified as very good at a daily resolution and excellent at a monthly resolution. Results for the two models' validation period are similar. Again, the annual peak at Hoshangabad is overestimated (by 9.1% in September for MIKE SHE and whilst the discharge simulated for GWAVA in this month is within 1% of the observed, the model simulates a mean peak one month earlier and 15.4% higher than the observed). Dry season discharges again tend to be underestimated, and again most clearly for GWAVA which simulates very low flows between November and May. In contrast, whilst MIKE SHE underestimates the lowest discharges (March–May), flows at the start–middle of the dry season are overestimated. These differences result in bias (Dv values) of equal value but opposite sign with the performance being classified in both cases as fair. Again, the different

calibration periods should be noted and these values are not, therefore, directly comparable. Whilst performance as indicated by NSE and r at a daily time step for the validation periods is better for MIKE SHE, the former statistic is still classified as very good. At a monthly resolution the values of these two statistics are identical for MIKE SHE and GWAVA with NSE being, as for the calibration periods, classified as excellent.

Comparing results for the climate change scenarios between the two hydrological models should be done with even more caution. Whilst approximately the same scenario period was employed (MIKE SHE: 2031–2060; GWAVA 2028–2060), the baseline period differed (MIKE SHE: 1971–2000; GWAVA: 1990–2010). This was linked in the case of GWAVA to the restriction of the period to after the construction of the Bargi Dam whilst all dams were simulated as being in operation for MIKE SHE (to isolate the impacts of the climate change scenarios). *Figure 2.27* shows that at both Manot and Hoshangabad, the scenario river regimes are, in most cases, associated with increased discharges, especially during the wet season (as discussed for each model in Sections 2.4.3 and 2.9.2). As a result, the ensemble mean scenario as simulated by both hydrological models is associated with increases in mean monthly discharge for all 12 months at Manot and every month except December at Hoshangabad. The magnitude of the increase in the seasonal peak for the ensemble mean scenarios tends to be larger for GWAVA compared to MIKE SHE (e.g. at Manot it is 46.6% for GWAVA compared to 19.7% for MIKE SHE with the corresponding figures for Hoshangabad being 53.7% and 31.6%, respectively).

A notable difference between the results of the two models is in the projected changes in dry season discharges, especially at the beginning of the year and in particular at Hoshangabad. In percentage terms the changes for an individual scenario tend to be relatively constant for MIKE SHE although whilst they are all relatively small at Hoshangabad, they are more variable at Manot. Given the low baseline discharges, in absolute terms the differences between scenario discharges are low. This is also the case for GWAVA, but in percentage terms scenario changes show large month-on-month variations, especially at Hoshangabad where, as discussed above, the model tends to underestimate dry season discharges compared to observations. Therefore whilst, *Figure 2.27* demonstrates near zero baseline discharges at this station during the dry season, relatively small absolute changes in flow at this time of year translate into large percentage changes and the wider inter-GCM spread of changes in river flow.

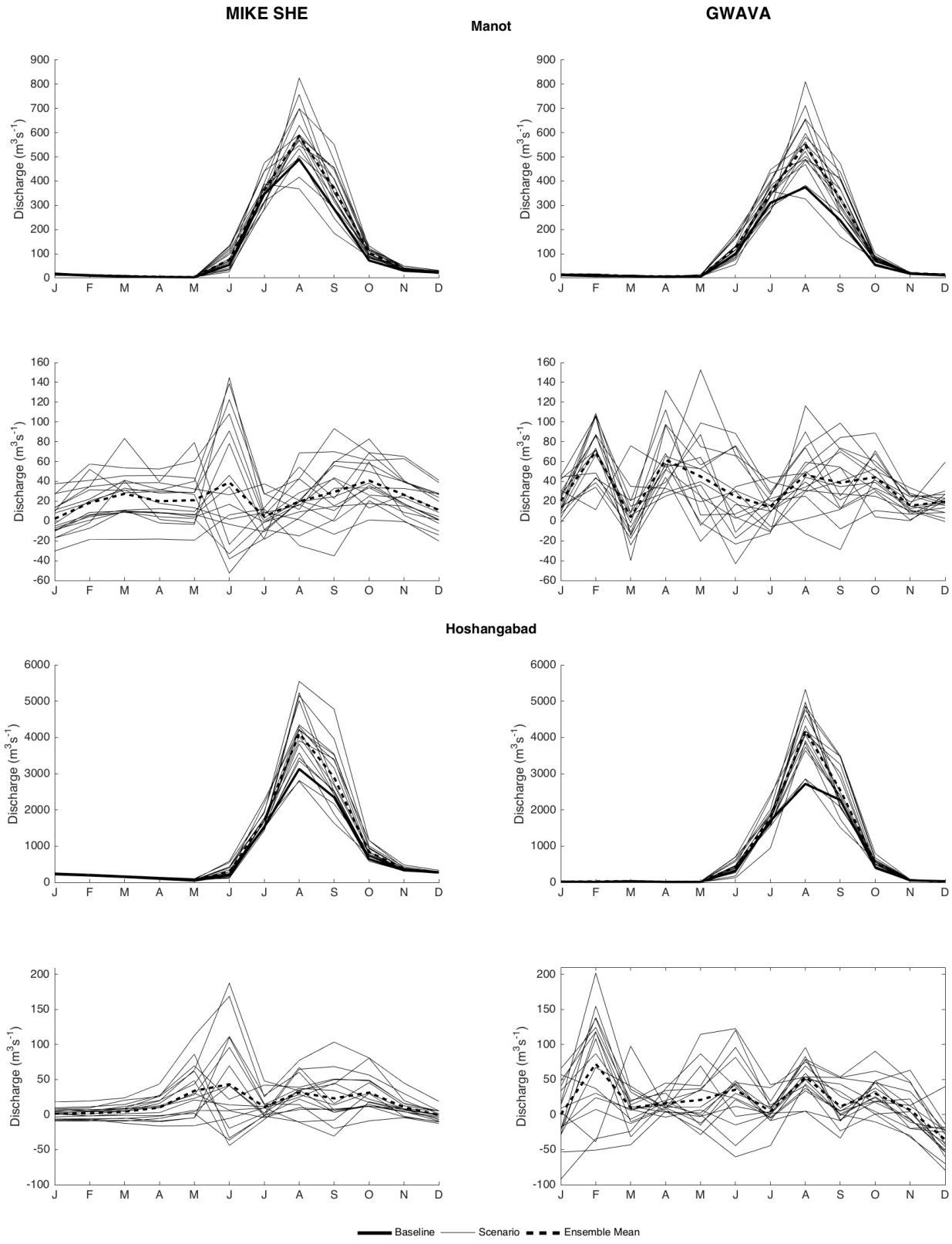

Figure 2.27. River regimes at Manot and Hoshangabad simulated by MIKE SHE and GWAVA for the baseline, each GCM and the ensemble mean

An initial assessment of the consistency or otherwise in changes simulated for the different scenarios by the two hydrological models is presented in *Figure 2.28*. It demonstrates a general lack of consistency in the magnitude of change in mean discharges for the same

scenario when simulated by the different models. However, at this stage this is considered the limit to which such an inter-model comparison could be taken given the different baseline periods. An extension of this work is intended through the modification of the GWAVA model's baseline period to map on to the earlier and longer period used in MIKE SHE. This will, necessitate the inclusion of the Bargi Dam throughout the GWAVA model's simulation period.

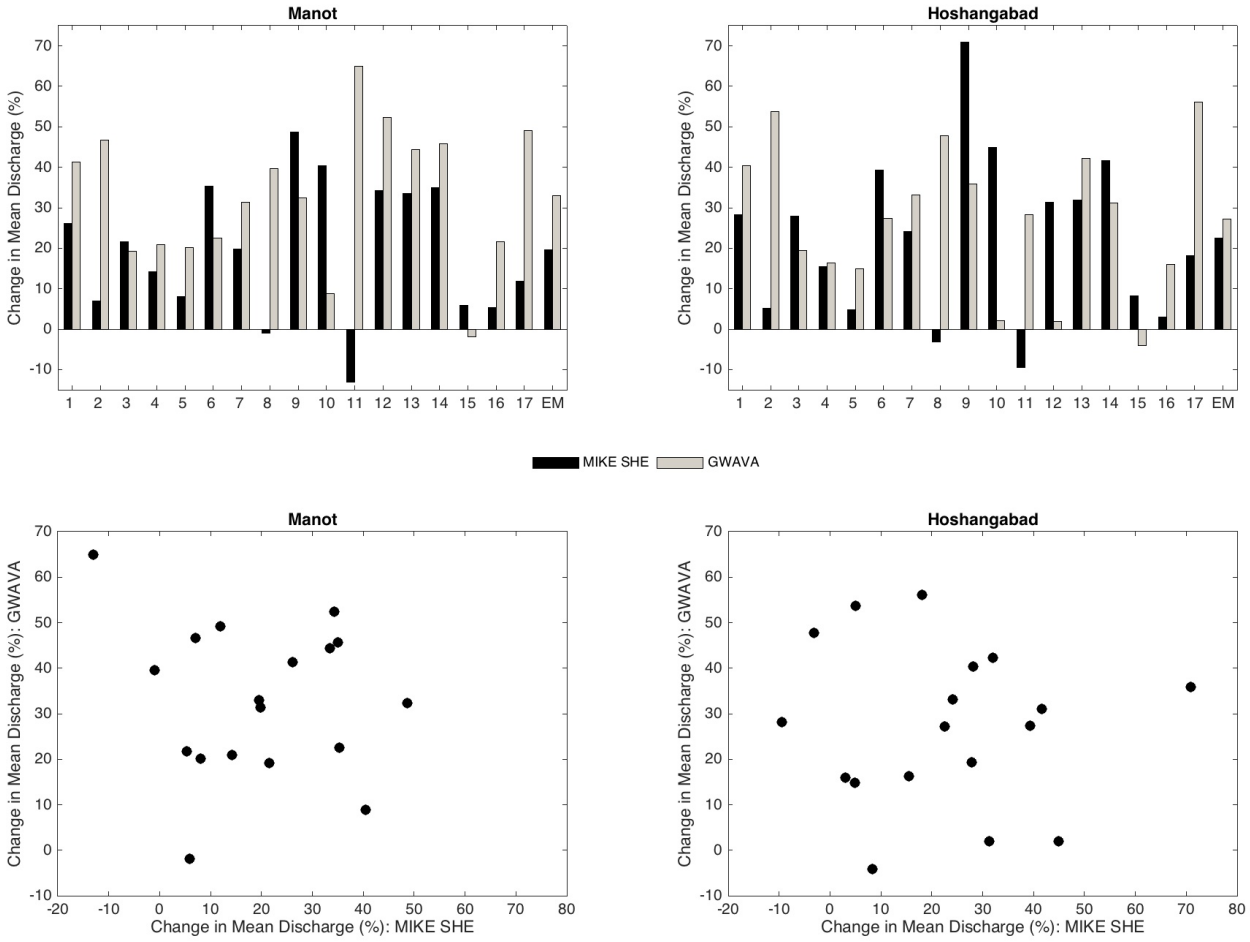

Figure 2.28. Comparison of changes in mean discharge at Manot and Hoshangabad as simulated for each scenario by MIKE SHE and GWAVA

3. Environmental flow assessments for climate change scenarios of the Narmada

J.R. Thompson, C.L.R. Laizé, M.C. Acreman

3.1. Environmental flows

The hydrological characteristics of a river exert critical controls on aquatic ecosystems. This is implicit within the natural flow paradigm (Poff *et al.*, 1997) that recognises that a river's regime, comprising components that characterise the variability, magnitude, frequency, duration, timing and rate of change of discharge, is central to sustaining aquatic biodiversity and ecosystem integrity. All elements of the flow regime influence some aspect of riverine ecosystems. For example, the variability in discharge drives the structure of fish communities both directly, by influencing life history processes including migration, spawning and recruitment, and indirectly by impacting habitat availability and diversity (Nestler *et al.*, 2012). The latter includes connections between a river, its floodplain and riparian wetlands that in turn support numerous wetland ecosystem services. Modifications to river regimes can produce modified, hybrid and novel riverine ecosystems and impact ecosystem service delivery (Acreman *et al.*, 2014).

The science of environmental flows has developed as a result of the requirement to determine flow regimes necessary to maintain economically, socially and ecologically important ecosystem services (e.g. Dyson *et al*., 2003; Horne *et al.,* 2017). There are a range of methods that can be employed to assess environmental flow requirements and potential impacts of hydrological change (e.g. Acreman and Dunbar 2004). Many are based on the natural flow paradigm and are designed to define the responses of freshwater ecosystems to change, including defining thresholds where ecological change may be significant (Poff *et al.*, 2010). Examples include the Range of Variability Approach (RVA) that uses Indicators of Hydrological Alteration (IHA), a statistical technique for comparing natural and altered flow regimes (e.g. Richter *et al*., 1996). The RVA method assumes that some organism or community will have exploited all niches created by the complexity of a river's hydrograph and its interaction with the landscape. If a river ecosystem is adapted to the baseline hydrological regime, departures from these conditions are likely to lead to ecosystem modifications. The likelihood of such modifications will increase as the hydrological regime departs further from the baseline. In turn, the risk of ecological change will progress from none through low and medium to high as more flow alteration thresholds are exceeded. These

thresholds are associated with important flow regime characteristics that can be indexed by IHAs that describe key flow regime properties.

3.2. Application of ERFA to the Narmada

The potential environmental flow impacts of each of the 17 climate change scenarios simulated using the MIKE SHE and GWAVA models of the Narmada (see Section 2) were assessed using a modified version of the Ecological Risk due to Flow Alteration (ERFA) screening method (Laizé *et al.,* 2014). ERFA is itself based upon the RVA/IHA technique (Richter *et al*., 1996). Modification of ERFA follows the approach employed by Thompson *et al.* (2014b) in a climate change assessment for the Mekong River Basin, southeast Asia and Thompson *et al.* (2017b) who applied the same approach to projections of climate change impacts on river flow in West Africa's Upper Niger Basin as well as flood extent within the extensive floodplains of the Inner Niger Delta. The latter application of ERFA included the development of approaches for summarising environmental flow assessments for large numbers of different scenarios.

In common with RVA/IHA, ERFA uses a number of indicators that together describe the river flow regime under baseline and scenario conditions. However, unlike RVA/IHA, which employs daily flow variables, the modified ERFA method uses monthly variables (termed Monthly Flow Regime Indicators; MFRIs). There are many potential indices that can characterise a river's hydrological regime. For example, Olden and Poff (2003) identified 171 hydrological indices although they subsequently categorised them into nine distinct components of the flow regime. They further suggested that the most appropriate indices for a given situation depends upon the type of flow regime. Here we used the same MFRIs as those employed by Thompson *et al.* (2014b; 2017b). This is consistent with Olden and Poff's (2003) strategy given the dominant influence of highly seasonal rains upon river regimes in the Narmada and both the Mekong and Upper Niger that were the focus of these earlier ERFA studies. ERFA first calculates hydrological variables for each year of the period under consideration. These are then used to derive MFRIs that capture the magnitude and variability of each variable as a single value for the complete period. Magnitude is described by the median (50^{th} percentile) and variability by the interquartile range (IQR, i.e. the difference between 25^{th} and 75^{th} percentiles) of the annual variables. Indicators associated with the timing of peak and low flows differ since they are defined by the month in which the largest

and lowest flows are simulated (i.e. they have integer values of between 1 and 12). Consequently, they are more appropriately summarised by their mode. Eight MFRIs were derived based on five hydrological variables (*Table 3.1*): three medians, three IQRs, and two modes. The first three indicators (MFRI 1–3) are associated with high flows and the remaining five (MFRI 4–8) with low flows.

Table 3.1. Monthly Flow Regime Indicators (MFRIs).

Hydrological variables (one per year)	**MFRI[c] (one per period)**	**Flow type**	**Regime characteristics**
Number of months above threshold[a]	Median (1) IQR[d] (2)	High	Magnitude; Frequency
Month of maximum flow / flooding (1-12)	Mode (3)	High	Timing
Number of months below threshold[b]	Median (4) IQR (5)	Low	Magnitude; Frequency
Month of minimum flow / flooding (1-12)	Mode (6)	Low	Timing
Number of periods of at least two months duration with flow / flooding below threshold[b]	Median (7) IQR (8)	Low	Magnitude; Frequency; Duration

a. Threshold: Q5 (95th percentile) from the 1971-2000 baseline period.
b. Threshold: Q95 (5th percentile) from the 1971-2000 baseline period.
c. Indicator identification number between brackets.
d. Inter-Quartile Range.

MFRIs are first calculated for a baseline and each scenario. Absolute differences between MFRIs for each scenario and the baseline are subsequently calculated. MFRIs based on the median and the IQR are considered to depart significantly from the baseline if the difference is more than 30%. Substantial changes in the mode-based MFRIs are assumed when differences are larger than one month. These thresholds are the default values employed in the application of ERFA to the Mekong and Upper Niger (Thompson *et al.*, 2014b; 2017b). They can, in principle, be varied and on-going NERC funded research[2] is developing approaches through which local ecological expert knowledge can be used to fine-tune ERFA for specific situations. ERFA results are then aggregated for each scenario using a risk of ecological change classification based on how many of the MFRIs differ from the baseline by more than

[2] *Translation of Environmental Flow Research in Cambodia* (*TEFRIC*) is funded under the NERC Innovation Follow-on call with a project lifetime of 2017–2019. It is led by UCL (J.R. Thompson) in collaboration with CEH (C.L.R. Laizé), Institute of Technology of Cambodia and the Tonle Sap Authority. The project is developing a user-friendly interface for ERFA as well as trialing ERFA using a series of Cambodia-specific scenarios and fine-tuning the ERFA thresholds for the Cambodian situation using local expert ecological knowledge.

the defined thresholds (Laizé *et al.* 2014). Risks of ecological change are evaluated in this way for both high and low flows using the coding scheme of Thompson *et al.* (2014b; 2017b) which reflects the different number of MFRIs for high and low flows. For high flows the no risk, low risk, medium risk and high risk classes are defined when the number of indicators differing from the baseline is 0, 1, 2, or 3, respectively. In contrast, for low flows the corresponding number of differences in MFRIs is 0 (no risk), 1 (low), 2–3 (medium) and 4–5 (high). The low risk category is intentionally set to one MFRI differing from the baseline in both cases.

In the case of the ERFA application to the Upper Narmada, assessments were made for the five gauging stations used in the calibration and validation of the MIKE SHE model and for which baseline and scenario discharges were simulated. The selection of these gauging stations was largely dictated by the division of the Upper Narmada into a reasonable number of evenly distributed sub-catchments for use within the linear reservoir saturated zone module (see Section 2.2). Whilst, the GWAVA model employs some alternative gauging stations for calibration and validation (and subsequently for the assessment of climate change), two (Manot and Hoshangabad) are common. In order expand the potential for comparing the environmental flow results from the two alternative hydrological models, simulated discharges for the baseline and each climate change scenario were abstracted from the GWAVA cells in which the other three gauging stations (Dindori, Barmanghat and Gadarwara) are located. However, it is appropriate to provide some important caveats to the resulting comparison. Firstly, the GWAVA model was not explicitly calibrated for these three stations. Secondly, and as discussed in Section 2.10, alternative baseline periods were employed for the two hydrological models (MIKE SHE: 1971–2000; GWAVA: 1990–2010) with some minor differences in the scenario period (MIKE SHE: 2031–2060; GWAVA: 2028-2060). For this reason, ERFA results from the two hydrological models are initially treated separately before being only briefly compared.

3.3. ERFA results

ERFA results based on the MIKE SHE model simulated discharges are presented using the approach developed by Thompson et al. (2017b). *Figure 3.1* shows individual subplots for the five gauging stations within the Upper Narmada Basin that indicate whether each of the eight MFRIs exceed the thresholds associated with assumed significant change. MFRIs associated

with high and low flows are grouped together and results are shown for each of the 17 GCMs. The risk of ecological change for high and low flows is also shown using a "traffic-light" colour-coded classification that replicates the earlier approach employed by Laizé *et al.* (2014) and Thompson *et al.* (2014b).

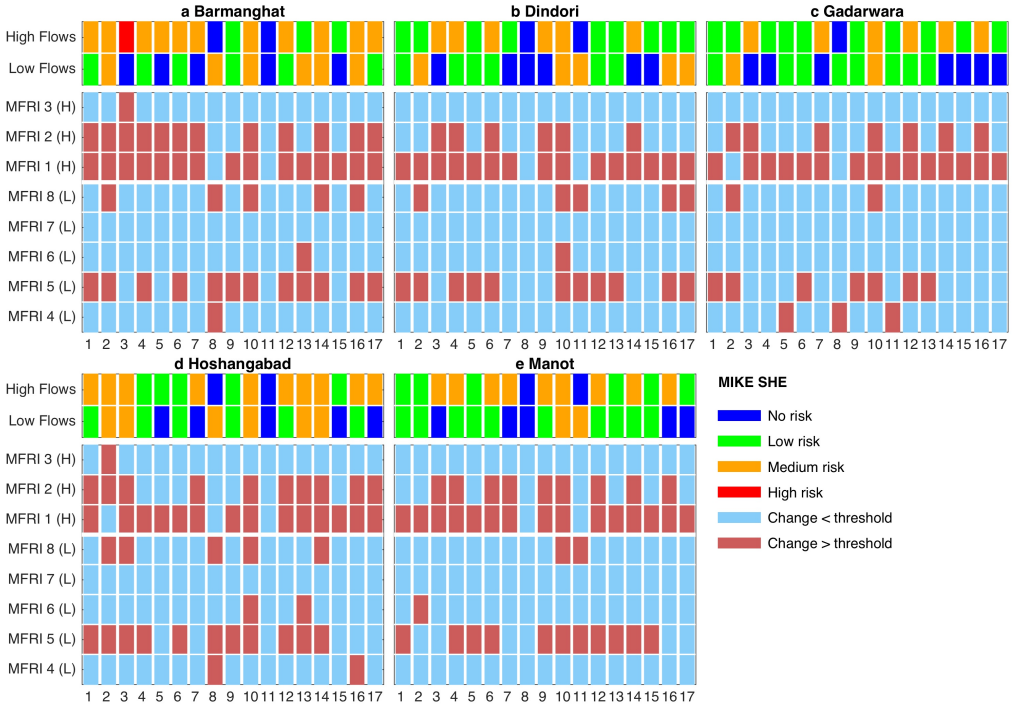

Figure 3.1. ERFA results for five gauging stations in the Upper Narmada for each of the 17 climate change scenarios as simulated by MIKE SHE. The lower part of each subplot identifies whether individual high (H) and low (L) flow MFRIs are above the thresholds associated with assumed significant change. The top part of each subplot presents the traffic light colour coded classification of risks of ecological change for high and low flows.

The ERFA results for MIKE SHE demonstrate broadly similar patterns for each individual GCM at the five different gauging stations within the Upper Narmada Basin although there are some differences. Most GCMs result in at least some degree of overall risk of change in either low or high flows (or both). With the exception of Gadarwara, only one GCM (GCM8 - GFDL-ESM2M for Dindori and Manot; GCM11 - MIROC5 for Barmanghat and Hoshangabad) is associated with no significant changes in all eight MFRI (and consequently no over all risk of change in both flow extremes). At Gadarwara all GCMs project a significant change in at least one MFRI. At the other extreme of risk of overall change, no GCMs project a high risk of change in both low and high flows at any gauging station. Indeed of the 85 gauging station-GCM combinations (i.e. 5 gauging stations × 17 GCMs) only one is associated with a high risk of change for high flows (GCM3 - CSIRO-Mk3.6.0 at Barmanghat). No GCMs project high risk of change in low flows at any of the five gauging stations.

Across the five gauging stations there is some variability in the most frequent overall risk class, especially for low flows. At both Barmanghat and Hoshangabad the low and medium risk of change in low flows classes are equally common (six GCMs closely followed by no risk for the remaining five GCMs). For Dindori, six GCMs each project no and low risk with the remaining five projecting medium risk. Low risk of change in low flows is most frequent at Gadarwara (eight GCMs) and, especially, Manot (ten GCMs). Medium risk is less common (two GCMs in both cases with the remaining GCMs projecting no risk). For high flows, following the high risk class, no risk is least common (either one or two GCMs). Low risk of change in high flows dominates at two gauging stations (nine and ten GCMs for Dindori and Gadarwara, respectively) with medium risk dominating at the other three stations (between nine and 11 GCMs). Consistency in the risk of change class for both low and high flows for an individual GCM are in the minority at all gauging stations. For example, the number of GCMs projecting low risk of change in both flow extremes varies between one and six (Barmanghat and Gadawara, respectively). The corresponding range for medium risk is 1–5 (Dindori and Hoshangabad, respectively).

There is some consistency in the individual MFRIs that are most / least commonly projected to experience an assumed significant change. For low flows, changes in MFRI5 are assumed to be significant for the majority of GCMs (11–12) at all gauging stations apart from Gadarwara (seven GCMs). In contrast, no GCMs project a significant change in MFRI7 with few (no more than three or two, respectively) projecting such changes in MFRI1 or MFRI3. The vast majority of GCMs (15 at all but Hoshangabad where this figure is 14) project significant change in the high flow MFRI1. Significant changes in MFRI2 are relatively common (between six and 12 GCMs at individual gauging stations) whereas such changes for MFRI3 are restricted to a single GCM at just two stations (GCM3 – Barmanghat; GCM 2 – Hoshangabad).

The ERFA results derived using the GWAVA simulated discharges at the same five gauging stations are shown in *Figure 3.2*. These are presented in an identical form to those for the MIKE SHE-derived results in *Figure 3.1*. It is evident that changes in the metrics associated with high flows, and so the resulting assessments of the overall risk of change in these flows, show broadly similar results for the five different gauging stations whereas there is much larger variability for low flows. Across the five stations no GCM is associated with no significant changes in all eight MFRIs. Consequentially, no GCM projects no overall risk of change in both high and low flows (contrasting with one GCM, either GCM8 or GCM11, for four

of the stations for MIKE SHE). At the other extreme, and in common with the MIKE SHE results, no GCMs project high risk of change in both low and high flows at any gauging station. Also in common with MIKE SHE, none of the 85 gauging station-GCM combinations is associated with high risk of change in low flows and whilst for MIKE SHE one GCM projects high risk of change in high flows at one station, for GWAVA not a single GCM projects this high risk of change at any station.

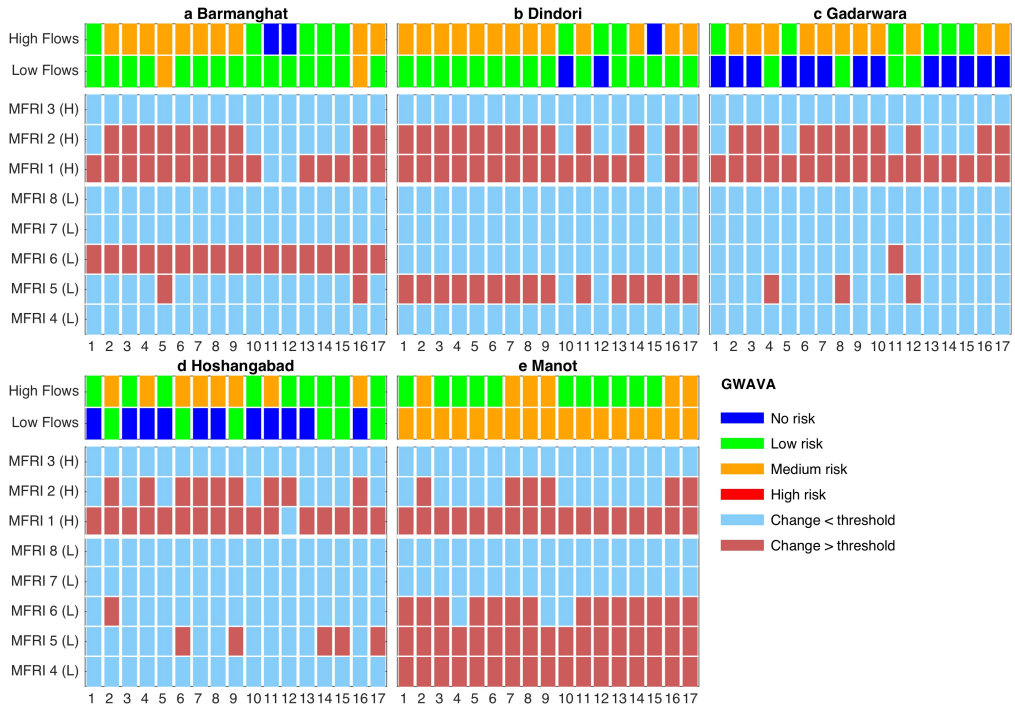

Figure 3.2. ERFA results for five gauging stations in the Upper Narmada for each of the 17 climate change scenarios as simulated by GWAVA. The lower part of each subplot identifies whether individual high (H) and low (L) flow MFRIs are above the thresholds associated with assumed significant change. The top part of each subplot presents the traffic light colour coded classification of risks of ecological change for high and low flows

As for MIKE SHE, there is some variability in the most frequent overall risk class, especially for low flows. At Barmanghat and Dindori low risk of change in low flows predominates with this level of risk being projected in both cases by 13 GCMs. The remaining two GCMs project either no (Dindori) or medium risk (Barmanghat). No risk of change in low flows is predominant at Gadarwara (13 GCMs) and Hoshangabad (11 GCMs) with, in both cases, the remaining GCMs projecting low risk of change. ERFA risks of change in low flows at Manot are very different to those for the other four gauging stations with either three (14 GCMs) or two (3 GCMs) of the low flow MRFIs showing significant changes. As a result, all 17 GCMs project medium risk of change in low flows.

As for the MIKE SHE ERFA results, following the high risk class, no risk is least common at all five gauging stations (either none, one or two GCMs). Whilst in common with the MIKE SHE results, low risk of change in high flows is dominant at two gauging stations, these stations differ; Hoshangabad (9 GCMs) and Manot (11 GCMs) compared to Dindori and Gadarwara for MIKE SHE. Consequently, and as for MIKE SHE, medium risk dominates at three stations (10, 11 or 13 GCMs) but again, these stations, with the exception of Barmanghat, differ between the different hydrological models. In a similar way to MIKE SHE, consistency in the risk of change class projected by GWAVA for both low and high flows for an individual GCM are in the minority at all of the gauging stations. The number of GCMs projecting low risk of change in both flow extremes varies between one and five (Gadarwara and Barmanghat, respectively). The corresponding range for medium risk is 2–6 (Barmanghat and Manot, respectively).

There is again, some consistency in the individual MFRIs that are most / least commonly projected to undergo a significant change. This is especially the case for the high flow MFRIs. For example, the vast majority, and in some cases all of the GCMs (range 15–17), project a significant change in MFRI1. With the exception of Manot (6 GCMs), the majority (9–13) of GCMs project significant changes in MRFI2 whilst no GCMs produce a significant change in MRFI3. In common with the MIKE SHE results, no GCMs at any gauging station project a significant change in the MFRI7 low flow indicator. This is repeated for MFRI8 at all stations and MRFI4 at all stations except Manot (which, as previously noted, is characterised by very different risks of changes in low flows). Whilst at three gauging stations (excluding Manot), changes in MRFI5 are most common, the number of GCMs projecting such changes vary dramatically from only three (Gadarwara) to 15 (Dindori). At the remaining station (Barmanghat) only two GCMs project a change in this indicator whilst all 17 GCM project a significant change in MRFI6 that is very uncommon (absent in the case of Dindori) at the other gauging stations.

In summary, the application of the ERFA environmental flow methodology to projections of future river flow derived from two alternative hydrological models of the Upper Narmada demonstrate both consistencies and differences in potential risks of change. In comparing ERFA results from these two models, the important caveats described in Section 3.2 should be borne in mind. Future work should seek to harmonise as much as possible approaches used in the two models including the gauging stations used for calibration, validation and scenario analysis as well as simulation periods. Notwithstanding these issues, inter-model consistency

in ERFA results tends to be greater for high flows compared to low flows (which are characterised by very low flows compared to the high flow period during the monsoon). It is possible that these differences are strongly impacted by the alternative representations of the existing hydraulic infrastructure within the Upper Narmada by the two different hydrological models. Whilst in absolute terms, discharges at this time of year that are simulated by the different models may differ by relatively small amounts, relative differences may be large both under baseline and scenario climate. Given the potential for dams to impact low flows according to patterns of releases and the absence of detailed information on dam operating regimes that necessitated relatively simple and temporally consistent approaches to be used within the MIKE SHE and GWAVA models, this represents a considerable source of uncertainty. Future development of this work would require the acquisition (if available) of more detailed information on current operating regimes for dams within the Upper Narmada. Additionally, how these might vary given the projected changes in river flow and water demands under climate change (which represents another source of uncertainty – e.g. Van Dijk *et al.*, 2008; Thompson *et al.*, 2016, 2017a) would need to be considered. Project partners will consider the potential for these developments through future collaborative research.

4. Applying statistical flood frequency estimation methods in the Godavari and Krishna river basins: pilot study

A. Griffin, L. Stewart, G. Formetta, C. Kalai, A. Mondal

4.1. Summary

Monsoon-related extreme flood events are experienced regularly in the Indian state of Maharashtra causing costly damage and disruption to local communities. Being able to estimate the likely magnitude of the 1-in-30 year flood, say, would allow hydrological practitioners to design new structures to prevent such damage or at least withstand it. To this end, this pilot study investigated the feasibility of developing spatially consistent flood frequency estimates using an index flood approach. Catchment descriptor equations and distribution choices were made for the region using stepwise regression and Hosking-Wallis distribution tests. Along with this, a web application was developed to showcase how stakeholders and practitioners in the region could use the work.

4.2. Aims

This part of the project was undertaken to assess the feasibility of developing spatially consistent flood frequency estimates for relatively long return period floods at ungauged sites within the Indian state of Maharashtra. Rivers in Maharashtra have a wide range of hydrological behaviours. In particular, around Mumbai and within the Wainganga Basin, there are regular extreme flood events due to monsoon-related heavy rainfall. Although prediction on a short timescale (flood warning systems) is a key focus in these locations, estimation of the frequency of large, destructive flood events is less well documented in the current literature. This work is aimed at providing an addition to the toolkit of civil engineers and planners, as well as developing academic collaboration with Indian parties, such as IIT Bombay.

The key objectives of this part of the project were to use open-source or freely available data to develop preliminary examples of tools such as catchment descriptor equations, growth curves and web applications to assess whether a more comprehensive follow-on study including the use of more data and enhanced stakeholder engagement would be fruitful.

This part of the project applied similar methods to those used in the Flood Estimation Handbook (FEH; Institute of Hydrology, 1999) alongside a comprehensive survey of the available data for use within the study and future studies. In conjunction with the development of flood frequency estimation methods, a prototype web application was developed for use by practitioners in river management, civil engineering and agriculture, as well as by the general public for their own information. This application includes summary outputs of relevant data including flood estimates at ungauged sites using a point-and-click interface similar to the FEH web service or StreamStats (USGS).

4.3. Background and current research

4.3.1. Extreme flood events in peninsular India

The summer monsoons experienced in peninsular India lead to regular, significant flooding. With rapid expansion of cities like Mumbai exerting further pressures on river and drainage networks, more disastrous flooding has occurred in recent years. Water storage problems also arise during these periods of intense rainfall, forcing the release of large volumes of water from some dams and reservoirs, thereby further enhancing flood problems. Table 4.1 provides examples of some of the worst floods that have impacted the region this century.

Table 4.1. Examples of extreme 21st Century flood events in Peninsular India

Date	Location	Notes
29th August 2017	Mumbai	Over 200mm of rain in 5 hours
July 2017	Gujarat	Over 550mm of rain in the month (over 165% of average) and leading to over 220 deaths.
9th November 2015	Neyveili	483mm rain over 2 days. More than 1000 people evacuated.
27th July 2015	Gujarat	An additional 7000 m^3s^{-1} of water released from Dharoi dam, affecting up to 4 million people.
10th August 2008	Kolhapur/ Andra Pradesh	"1266mm of rain overnight" in Kolhapur 53 deaths over the week.
July 26th 2005	Mumbai	994mm of rain fell in 24 hours, leading to over 1000 deaths.
23rd June 2005	Gujarat State	Over 505mm of rain in a week with floods affecting 250,000 people.

Most of the research into extreme events and monsoon behaviour is focused on short-term extreme event prediction and rainfall estimation methods. eSWIS (Central Water Commission) is an example of such a project giving up-to date predictions and warnings.

4.3.2. Areas of interest: Godavari and Krishna river basins

The Godavari and Krishna river basins were chosen for this pilot study. This was to allow focus on complete river basins (rather than administrative regions in which only part of a river basin might be contained) as well as allowing the use of data from a large number of river gauging stations (Figure 4.1).

The Godavari River has the largest basin in peninsular India (India-WRIS Project Team, 2014a), with a total extent of over 300,000 km^2, and a main channel length of over 1400 km (Central Water Commission, 1980; 1986). The Godavari Basin starts in Maharashtra and flows east towards the Bay of Bengal. The basin contains (as of 2014) 921 dams, which contribute towards 292 irrigation projects within the basin, and eight hydroelectric power stations. In terms of land cover, agricultural land accounts for approximately 60% of the basin, and forest a further 30%. Urban areas are small (around 1.7% of the basin). The majority of the rainfall (mean annual rainfall is 1093 mm) arrives as part of the southwest monsoon season in June-September. In the winter, rainfall for January and February ranges from 55 mm to 0.5 mm.

The Krishna River is the fourth largest river basin in India (India-WRIS Project Team 2014b), and the main channel, which flows south of the Godavari, runs for almost 1300 km with a total basin area of over 250 000 km^2 (Central Water Commission, 2000). Spread between the states of Maharashtra, Andhra Pradesh and Karnataka, the basin is bounded by the Eastern and Western Ghats, and flows eastwards into the Bay of Bengal. Like the Godavari, the majority of rainfall arrives during the southwest monsoon season. Average annual rainfall for the basin (1969–2004) is 859 mm, more than 70% of which falls between July and September. However, 30 districts within the basin are drought-prone, receiving an annual rainfall of less than 500 mm. The largest land covers by area are agriculture (75%), forest (10%), barren (7.6%) and urban (2.3%).

4.3.3. Previous work

This section outlines governmental and academic research into flood frequency estimation in the region, with a focus on catchment descriptor equations. A brief outline of FEH methods is also provided.

4.3.3.1. CWC (Central Water Commission) Subzone Reports 1980-2004

These reports for the various hydrological subzones within India have been conducted over the last 40 years to develop design storm methods for flood frequency estimation. The focus has been on long return period flood events, and methods rely predominantly on rainfall data, and a depth-duration-frequency relationship.

Upper Godavari Subzone 3(e) Report (1986)

- Focus on unit hydrograph method for estimation Q25, Q50, and Q100.
  - $Q_{25} = 2.967\ AREA^{0.868}\ SLOPE^{0.167} {R_{TD-25}}^{0.760} LEN^{-0.431}$
  - $Q_{50} = 3.317\ AREA^{0.871}\ SLOPE^{0.162} {R_{TD-50}}^{0.718} LEN^{-0.426}$
  - $Q_{100} = 3.569\ AREA^{0.876}\ SLOPE^{0.158} {R_{TD-100}}^{0.717} LEN^{-0.443}$
- AREA (km^2), LEN, longest stream in subzone (km), SLOPE = slope of longest stream (m/km), $R_{TD\text{-}N}$ design storm point rainfall with duration TD given by $TD = 0.799\ (SLOPE^{-0.5} LEN)^{0.59}$ rounded up to nearest hour.
- Computed by generalised multiple regression, giving correlation coefficient r>0.99.
- Unit hydrograph given using time-to-peak, from which the other hydrograph characteristics can be obtained using descriptors obtained from generalised linear regression.
- Data used were hourly river level, daily discharge data and hourly rainfall data for 5-11 years of monsoon season.

Lower Godavari Subzone 3(f) Report (1980)

- Data used were hourly river level, daily discharge data and hourly rainfall data for 3-10 years of monsoon season from 22 catchments with areas in the range 35-824 km^2.
- Unit hydrograph methods applied similarly to above through estimation of time-to-peak, but no derivations of Q_T given.

Krishna and Pennar Subzone Report (2000)

- Data used were from approximately 30 stations with 2-17 years' worth of hourly river level and rainfall data with daily discharge data.
- Focus on unit hydrograph methods for Q25, Q50 and Q100. Some work on catchment descriptor equations, no formula for QMED or QBAR.
  - $Q_{25} = 0.4285\ AREA^{0.733} LEN^{-0.272} LENC^{0.264} R_{25}^{1.426}$
  - $Q_{50} = 1.69432\ AREA^{0.753} LEN^{-0.338} LENC^{0.304} R_{50}^{0.934}$

- $Q_{100} = 8.33458\, AREA^{0.794} LEN^{-0.422} LENC^{0.313} R_{100}^{0.416}$
- LEN is longest main channel length in km, LENC is longest path from outlet to opposite point of catchment (across diameter through centroid) in km, R_N is the 24-hour N-year return period (in years) rainfall depth in mm.

- Synthetic Unit Hydrograph methods were shown to provide similar estimates to catchment descriptor equations above.
- The analyses were based on catchments of up to 1500 km^2, at the efficacy for larger catchments is unclear.

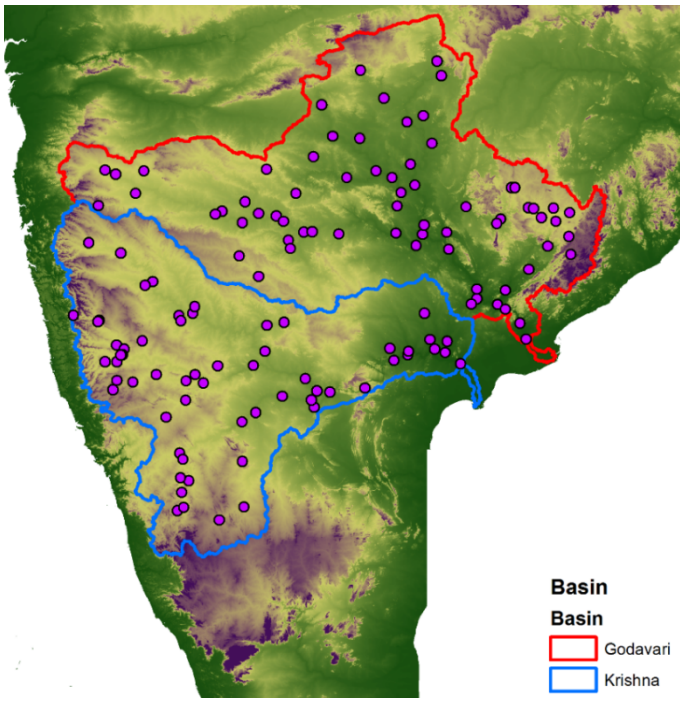

Figure 4.1. Location of basins and hydro-observation stations

4.3.3.2. Academic Papers - Garde and Kothyari (1990), Swamee et al. (1995), Bhunya et al. (2010); Singh et al. (2010).

These studies use various methods of dimensional analysis to generate non-dimensional descriptors that are combined to generate estimates of QMED and QT/QMED. They mostly use area, river length, rainfall depth (for given frequency and duration) and forest cover. Singh *et al.* (2010) made use of machine-learning methods to obtain "tree-like" models for QMED estimation in terms of area, slope and forest cover.

- Garde and Kothyari (1990)

$$Q_{2.33} = C\, R^{1.103} AREA^{0.74} SLOPE^{0.28} FOR^{-0.30}$$

- R = R(D,T) rainfall: D,T depend on ratio of area/slope.
- FOR = proportion of forest cover

- Swamee *et al.* (1995)

$$QBAR = 1.74\frac{AREA^{0.8925}p(D,T)^{0.92}}{D^{0.24}T^{0.17}}\left(\frac{SLOPE + 0.012}{FOR + 0.049}\right)^{0.55}$$

  - p(D,T) = estimated rainfall with duration D and return period T.
- Bhunya *et al*. (2010)

$$\frac{Q_T}{QBAR} = 0.8732\left(1 + \frac{\pi_6}{\pi_2}\right)^{0.45501}\left(1 + \frac{\pi_4}{\pi_5}\right)^{1.2211}\pi_5^{0.8983}\pi_2^{0.1092}\left(\frac{((1-\pi_1)^{0.35497})}{\pi_1}\right)$$

  - π_1 = Probability of exceedance = 1/T.
  - $\pi_2 = AREA/Length^2$
  - π_4 = L-CV
  - π_5 = L-skew
  - π_6 = L-kurtosis
  - Generated by trial-and-error through various functional forms.
  - QBAR estimated by $QBAR = 127.82\log(AREA) - 310.12$ from CWC reports.

4.3.3.3. FEH (Flood Estimation Handbook) Methods (1999, 2008).

In order to estimate QMED, we take a similar approach to that employed in the FEH (Institute of Hydrology, 1999) by using catchment descriptors and performing generalised linear regression on log(*QMED*) for a number of gauged sites within the two basins. To account for geographical correlation, we include a model error and sampling error as developed in Kjeldsen *et al*. (2008). This looks at geographical correlations, incorporating the selected distribution for the annual maxima series.

4.4. Data, methods and results

4.4.1. Data acquired

4.4.1.1. River discharge data

The CWC and Indian Meteorological Department (IMD) have over 900 hydro-observation stations that measure river stage, discharge, water quality and sediment content, although most stations only measure a subset of these parameters (Central Water Commission, 2016). Within the Godavari and Krishna basins, 129 stations have been identified as measuring river

discharge. Daily gauge data are available from the India-WRIS web portal for periods of between 2 and 40 years, from which we can determine annual maxima, and hence the median annual maximum, *QMED*. Some stations only measure stage/discharge for some parts of the year, namely around the monsoon season. Of these stations only 106 had sufficient discharge and rainfall data to allow an estimate of *QMED*.

Most of the discharge data is computed using an area-velocity method using autographic water level recorders, except in very high flow when slope-area methods are applied to estimate discharge. In some periods, missing observations are filled with estimates that match the general day-on-day trend of the discharge.

4.4.1.2. Elevation and flow direction data

Although several sources were investigated, this work ultimately made use of the HydroSHEDS (Lehner and Grill, 2013) and HydroBASINS (Lehner *et al*., 2008) datasets, maintained by the WWF. The datasets rely mostly on Shuttle Radar Topography Missions outputs and topographic maps. This included "hydrologically corrected" elevation data at a 3 arcsecond resolution (which equates to ≈90m at the equator), along with flow direction and accumulation data at a 15 arcsecond resolution.

4.4.1.3. Land use and land cover data

The Harmonised World Soil Database, maintained by the UN (Fischer *et al.,* 2008) provides a 30 arcsecond gridded dataset of land-use/cover combined from a series of existing regional and national soil datasets which described grid-square percentage cover of cultivated land (and specifically rain-fed land), forested land, built-up/urbanised land, and barren/sparsely vegetated land. In this study, we also use *SQ4*: "Oxygen availability to roots" as a proxy for drainage and permeability of soil, based on methods used by the Food and Agriculture Organisation of the United Nations. This takes into account the soil type, texture, soil phases and terrain slope.

HydroLAKES (Messager *et al.,* 2016) describes the inland waterbodies across much of the world's surface. Drawing data from the Global Lakes and Wetlands Database, as well as the Global Reservoir and Dam database, this includes the position and shape of waterbodies, along with a wide range of relevant information including lake pour point (point to which the

water drains), surface area, drainage area, volume and perimeter. All water bodies with a surface area of at least 0.1 km^2 were included, subject to shoreline smoothing and removal of small within-lake islands.

4.4.1.4. Meteorological data

Although we do not currently have access to systematic daily rain gauge data, some datasets are available which describe the weather and climate patterns of the two basins. The CFSR (Fuka *et al.,* 2014) has constructed a global weather model output dataset (1979–2014) on an approximately 38km grid-square with hourly resolution which records rainfall, wind, relative humidity and solar energy. This has been interpolated and downscaled, in the absence of other data, to determine average annual rainfall and peak rainfall for each catchment of interest.

Table 4.2 summarises the complete range of catchment descriptors derived from the datasets outlined above which were subsequently used in the flood estimation analyses described below.

Table 4.2. List of catchment descriptors

Descriptor	**Unit**	**Definition**
AREA	km^2	catchment area
Latitude	degree	latitude North
Longitude	degree	longitude East
ALTBAR	m	mean altitude
ASPBAR(VAR)	radian	mean aspect (clockwise from north)
DPLBAR(VAR)	km	average drainage distance
DPSBAR(VAR)	m/km	average drainage slope
RCBAR	km	mean channel length
RSBAR	m/km	mean channel slope
RABAR	radian	mean channel aspect (clockwise from north)
CDEN	km/km^2	channel density, length per unit area.
FARL	-	proportion of attenuation of flow due to lakes/reservoirs
AAR	mm	average annual rainfall
PET	mm/month	average potential evapo-transpiration
CULT	-	proportion of cultivated land
CULT-RF	-	proportion of rainfed cultivated land
FOREST	-	proportion of forested land
URBAN	-	proportion of urbanised land
NVG	-	proportion of barren (no vegetation) land
SQ4	-	permeability of soil (integer scale 1,2,3,…)

4.4.2. Regression methods

Beginning with a model including all the transformed covariates, the first step was to identify likely candidates for the model using a stepwise regression method, where covariates were added or removed to optimise the model. Following on from Meigh *et al*. (1997) and Kjeldsen, *et al*. (2008), certain unbounded descriptors such as *AREA* were transformed to log(AREA) to improve fit. The stepwise regression method outlined log(*AREA*), 1000/*AAR*, log(*PET*), log(*DPSBAR*), log(*FARL*), *SQ4*, and *ASPBAR* as the factors which gave rise to the best model in terms of AIC, a measure of information content which is optimal when low (most negative). The stepwise procedure starting from a single covariate is outlined in *Table 4.3*.

Table 4.3. Summary of stepwise regression results.
Final model with fse = 1.74, adjusted R^2 = 0.832

Covariates	AIC
log(AREA)	-28.2
log(AREA), 1000/AAR	-71.71
log(AREA), 1000/AAR, log(PET)	-85.25
log(AREA), 1000/AAR, log(PET), log(DPSBAR)	-94.93
log(AREA), 1000/AAR, log(PET), log(DPSBAR), log(FARL)	-105.57
log(AREA), 1000/AAR, log(PET), log(DPSBAR), log(FARL), SQ4	-109.09
log(AREA), 1000/AAR, log(PET), log(DPSBAR), log(FARL), SQ4, ASPBAR	-112.62

The correlation graph for these variables alongside QMED is shown in Figure 4.2. Fitting the variables showed they were all significant at the 95% level, and all but ASPBAR at the 99% level. The fitted model was (after taking the exponential of both sides):

$$QMED = (1.71\times10^{-10})AREA^{0.765}\ 0.0920^{\frac{1000}{AAR}}\ PET^{3.903}\ DPSBAR^{0.711}$$
$$\times FARL^{6.904}1.627^{SQ4}0.903^{ASPBAR}$$

A more comprehensive, systematic investigation was made into all models that consisted of a subset of the variables selected above; no better model was found in terms of AIC or adjusted R^2. An inspection of the residuals (difference between observed and fitted QMED) showed that there was some correlation in the variance of log(AREA) compared to the residuals, and some correlation remained in the residuals compared against log(QMED). This is due to some unexplained behaviour by some aspect of the basins not yet documented. One possibility is the influence of dams, levees and reservoirs on the flow of the network, since the QMED model described above implicitly assumes naturalised river flow. None of the other variables showed correlation with the residuals.

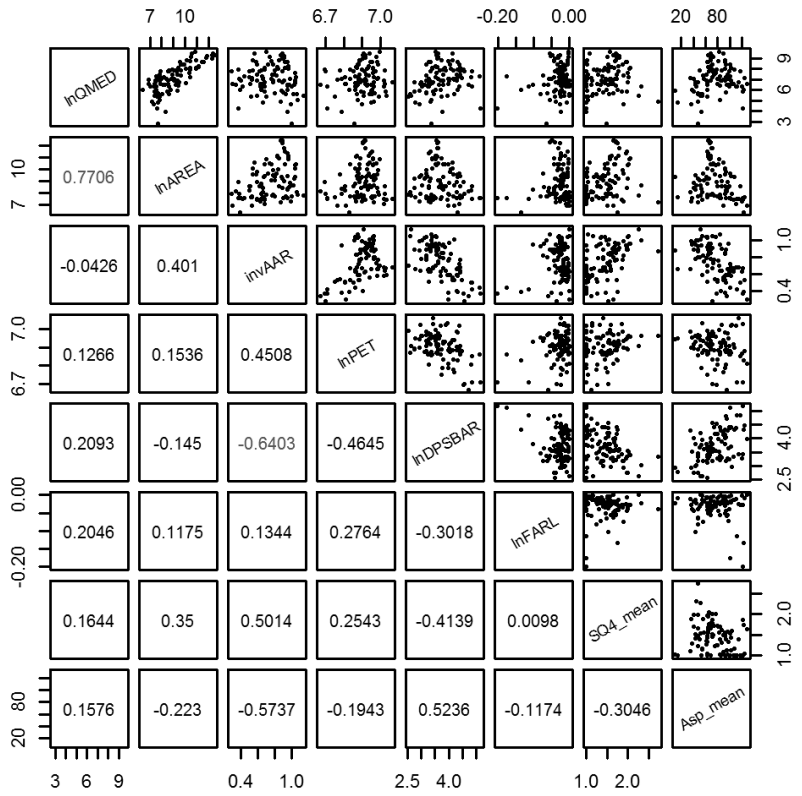

Figure 4.2. Pairwise correlation plot of variables used in QMED equation.

4.4.3. Statistical distribution for flood growth curve

A similar method to that described in Kjeldsen *et al.* (2008) was applied to determine appropriate distributions for use across the basins using the Hosking-Wallis test. This computes the L-moment ratios (L-CV, L-skew, L-kurtosis) for the AMAX series at each station in order to assess acceptability of distribution, and choose the distribution with the most success. The proposed distributions are: Generalised Extreme Value (GEV), Generalised Pareto (GPA), Generalised Logistic (GLO), Generalised Log-normal (GLN) and Pearson type-3 distribution (PE3).

An initial assessment of distribution choice was performed using the L-moment ratios and the Z_{dist}-statistic as described in Kjeldsen *et al.* (2008) on the whole dataset using the lmomRFA package from R (Hosking, 2017). Any distribution with a value of $|Z_{dist}| < 1.64$ is deemed to be potentially acceptable for that station. The distribution with the smallest value is also recorded. *Table 4.4* shows that although the Generalised Pareto is most often the best distribution, it is not the most frequently accepted; instead, the Pearson Type III is. Figure 4.3 shows that there is no obvious spatial correlation to the choice of distribution; these patterns do not match the major river channels.

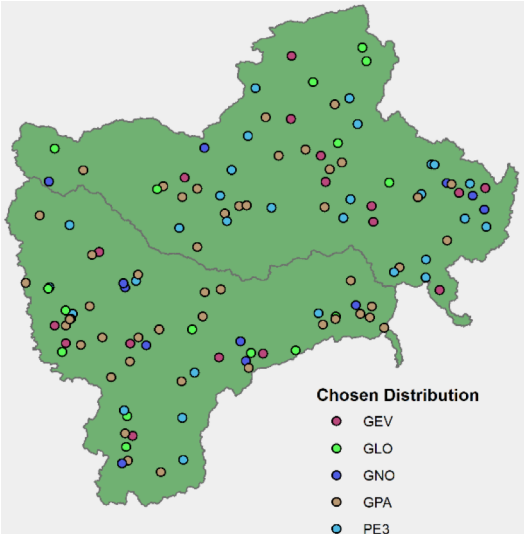

Figure 4.3. Locations of chosen distributions showing no clear geographical correlation.

Table 4.4. Distribution test results over whole region of study

	GLO	GEV	GLN	PE3	GPA
Accepted	67	91	95	101	92
Chosen	17	17	12	29	47

4.5. Use within web application

A web application was constructed in the `R` programming language (R Core Team, 2016) using the `shiny` package (Chang *et al.,* 2017). The purpose of the application (screen shot provided in Figure 4.4) was to allow users to select a location by point-and-click or entering latitude/longitude, and the catchment which pools into that point would be highlighted. The estimate for QMED, along with relevant catchment descriptors (subject to data licensing) would be presented along with either a growth curve, or further estimates of other return periods (30, 50, 100-year). In this pilot study, the selectable points were restricted to the hydro-observation stations in the current dataset. The next step will be to either perform real-time catchment computation, or to pre-calculate results for a large set of catchments which cover the whole region and also encompass a wide range of sizes of catchment. Both will require additional rainfall and evapotranspiration data.

From preliminary discussions with stakeholders and practitioners, a number of additional inclusions to the web application have been noted as possibilities. These include a more explicit inclusion of more return periods in the display, rather than only showing them in the context of a growth curve. Additionally the web tool could eventually be extended to include

flood frequency estimates derived from continuous rainfall-runoff modelling, but this would have to be done carefully to avoid confusion between "real-time" updating flood predictions and long-term flood frequency estimation in an assumed stationary system. It will also be important to highlight the differences between this web application and the already existing WRIS and eSWIS.

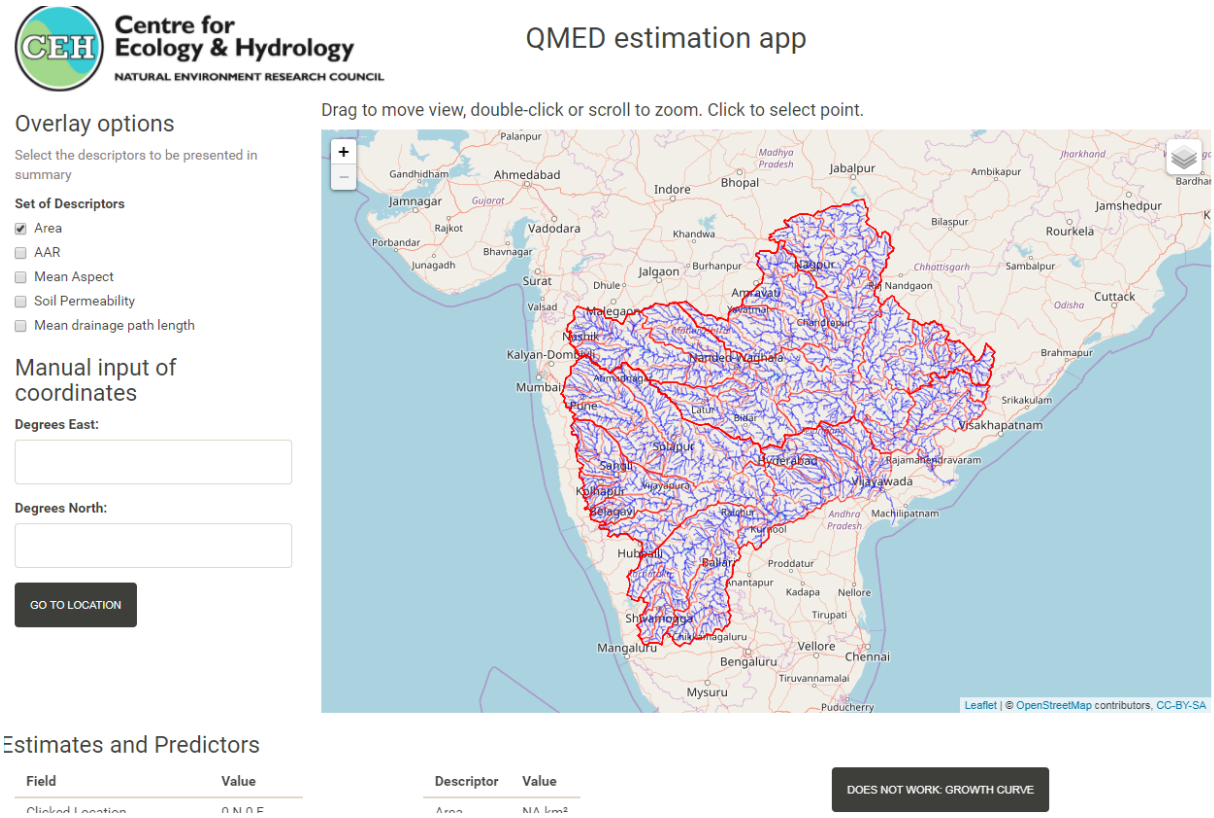

Figure 4.4. Screenshot of application demonstrating layout and function

4.6. Next steps

The next steps will be to improve the statistical models and the web application, conditional on the availability of higher resolution rainfall and evapotranspiration data. These improvements are outlined in the previous section. In addition to this, there is interest in performing more regional analysis to identify hydrological regions in Maharashtra for which the flood estimation can be tuned. The Wainganga Basin has been identified as a specific case study on which this optimisation should be performed. This regionalisation may be done in conjunction with a catchment classification project with IIT Bombay. Hopefully this will allow the project to refocus on Maharashtra rather than the Godavari and Krishna basins.

If more data are acquired, then the analysis in Section 4 can be rerun. This may lead to different descriptors being chosen or different coefficients being obtained, and the web

application in Section 4.5 can be updated to include more accurate output. Additionally, these additional data would allow a better quantification of uncertainty, and also allow the project to investigate other regional flood frequency estimation methods, such as pooling groups that use sets of hydrologically similar catchments to improve the estimates at ungauged locations.

References

Acreman, M. and Dunbar, M.J. (2004) 'Defining environmental river flow requirements – a review', *Hydrology and Earth System Sciences*, 8, 861–876.

Acreman, M.C., Arthington, A.H., Colloff, M.J., Couch, C., Crossman, N., Dyer, F., Overton, I., Pollino, C., Stewardson, M. and Young, W. (2014) 'Environmental flows - natural, hybrid and novel riverine ecosystems', *Frontiers in Ecology and Environment*, 12, 466–473.

Allen, R.G., Pereira, L.S., Raes, D. and Smith, M. (1998) *Crop evapotranspiration - Guidelines for computing crop water requirements - FAO Irrigation and drainage paper 56,* Rome: FAO.

Andersen, J., Refsgaard, J.C. and Jensen, K.H. (2001) 'Distributed hydrological modelling of the Senegal River Basin – model construction and validation', *Journal of Hydrology*, 247, 200–214.

Bhunya, P.K., Panigrahy, N., Kumar, R. and Berndtsson, R. (2010) 'Development of a Regional Non-Dimensional Return Period Flood Model', *Water Resources Management*, 24(7), 1425–1439.

Central Water Commission (1980) *Flood Estimation Report for Lower Godavari Subzone 3(f)*, New Delhi: Central Water Commission.

Central Water Commission (1986) *Flood Estimation Report for Upper Godavari Subzone 3(e)*, New Delhi: Central Water Commission.

Central Water Commission (2000) *Flood Estimation Repor for Krishna and Pennar Subzone 3(h)*, New Delhi: Central Water Commission.

Central Water Commission (2016) *India-WRIS Wiki*. [Online] Available from: http://india-wris.nrsc.gov.in/wrpinfo/index.php?title=Main_Page.

Chang, W., Cheng, J., Allaire, J.J., Xie, Y. and McPherson, J. (2017) *Shiny: Web Application Framework for R*. https://cran.r-project.org/web/packages/shiny/index.html.

Chow, V.T. (1959) *Open Channel Hydraulics*, New York: McGraw-Hill.

Clapp, R.B. and Hornberger, G.M. (1978) 'Empirical equations for some soil hydraulic properties', *Water Resources Research*, 14, 601–604.

DHI (2009) *MIKE SHE Technical Reference,* Hørsholm: DHI Water and Environment.

DHI-WE (2009) *MIKE SHE User Manual. Volume 2: Reference Guide,* Hørsholm: DHI Water and Environment.

Dyson, M., Bergkamp, G. and Scanlon, J. (Eds.) (2003) *Flow - the essentials of environmental flows*. Gland, Switzerland and Cambridge, UK: IUCN.

Food and Agricultural Organization (FAO) (2016). *AQUASTAT* [Online] Available from http://www.fao.org/nr/water/aquastat/main/index.stm

Fischer, G., Nachtergaele, F.O., Prieler, S., Teixeira, E., Tóth, G., van Velthuizen H., Verelst, L. and Wiberg, D. (2008) *Global Agro-Ecological Zones (GAEZ ver 3.0.) Model* Documentation, IIASA, Laxenburg, Austria and FAO, Rome, Italy.

Frei, C. and Schär, C. (1998) 'A precipitation climatology of the Alps from high-resolution rain-gauge observations', *International Journal of Climatology*, 18, 873–900.

Frei, C., Christensen, J.H., Déqué, M., Jacob, D., Jones, R.G. and Vidale, P.L. (2003) 'Daily precipitation statistics in regional climate models: Evaluation and intercomparison for the European Alps', *Journal of Geophysical Research*, 108(D3), 4124.

Fuka, D.R., Walter, M.T., MacAlister, C., Degaetano, A.T., Steenhuis, T.S. and Easton, Z.M. (2014) 'Using the Climate Forecast System Reanalysis as Weather Input Data for Watershed Models', *Hydrological Processes,* 28(22), 5613–5623.

Fung, C.F., Farquharson, F. and Chowdhury, J., (2006). Exploring the impacts of climate change on water resources-regional impacts at a regional scale: Bangladesh. *IAHS Publication 308*, 389.

Garde, R.J. and Kothyari, U.C. (1990) 'Flood Estimation in Indian Catchments', *Journal of Hydrology*, 113, 135–146.

Goel, M.K., Jain, S.K. and Agarwal, K. (2000) *Reservoir Sedimentation Study of Bargi Dam using Satellitte Data,* Roorkee: National Institute of Hydrology.

Government of India (GOI) (2007). Indian Livestock Census. Supplied by National Institue of Hydrology, India.

Government of India (GOI) (2011). Indian Population Census. Supplied by National Institue of Hydrology, India.

Government of India Ministry of Water Resources (2014) *Narmada Basin* [Online] Water Resources Information System of India Available from: http://www.india-wris.nrsc.gov.in/wris.html [Accessed 23 February 2016].

Graham, D.N. and Butts, M.B. (2005) 'Flexible integrated watershed modeling with MIKE SHE', In: Singh, V.P. and Frevert, D.K. (eds.) *Watershed Models*, Boca Raton: CRC Press, 245–272.

Havnø, K., Madsen, M.N. and Dørge, J. (1995) 'MIKE 11 – A generalized river modelling package', In: Singh, V.P. (ed.) *Computer Models of Watershed Hydrology*, Highlands Ranch, Colorado: Water Resources Publications, 733–782.

Henriksen, H.J., Troldborg, L., Højberg, A.L. and Refsgaard, J.C. (2008) 'Assessment of exploitable groundwater resources of Denmark by use of ensemble resource indicators and a numerical groundwater–surface water model', *Journal of Hydrology*, 348, 224–240.

Henriksen, H.J., Troldborg, L., Nyegaard, P., Sonnenborg, T.O., Refsgaard, J.C. and Madsen, B. (2003) 'Methodology for construction, calibration and validation of a national hydrological model for Denmark', *Journal of Hydrology*, 280, 52–71.

Horne, A.C., Webb, J.A., O'Donnell, E., Arthington, A.H., McClain, M., Bond, N., Acreman, M., Hart, B., Stewardson, M.J., Richter. B. and Poff, N.L. (2017) 'Research priorities to improve future environmental water outcomes', *Frontiers in Environmental Science*, 5, 1–11.

Hosking, J.R.M. (2017) *Regional Frequency Analysis Using L-Moments*. https://cran.r-project.org/package=lmomRFA.

Immerzeel, W.W., Beek, L.P.H., Konz, M., Shrestha, A.B. and Bierkens, M.F.P. (2012a) 'Hydrological response to climate change in a glacierized catchment in the Himalayas', *Climatic Change*, 110, 721–736.

Immerzeel, W.W., Pellicciotti, F. and Shrestha, A.B. (2012b) 'Glaciers as a Proxy to Quantify the Spatial Distribution of Precipitation in the Hunza Basin', *Mountain Research and Development*, 32, 30–38.

India-WRIS (2013a) *Bargi (Rani Avanti Bai Lodhi Sagar) Major Irrigation Project JI00740* [Online] Available from: http://india-wris.nrsc.gov.in/wrpinfo/index.php?title=Bargi(Rani_Avanti_Bai_Lodhi_Sagar)Major_Irrigation_Project_JI00740 [Accessed 23 February 2016].

India-WRIS (2013b) *Barna Major Irrigation Project JI00745* [Online] Available from: http://india-wris.nrsc.gov.in/wrpinfo/index.php?title=Barna_Major_Irrigation_Project_JI00745 [Accessed 23 February 2016].

India-WRIS (2015) *Narmada* [Online] Available from: http://india-wris.nrsc.gov.in/wrpinfo/index.php?title=Narmada [Accessed 23 February 2016].

India-WRIS Project Team (2014a) *Godavari Basin Report*. New Delhi.

India-WRIS Project Team (2014b) *Krishna Basin Report*. New Delhi.

Institute of Hydrology (1999) *Flood Estimation Handbook*. Wallingford: Institute of Hydrology.

Jain, S.K., Storm, B., Bathurst, J.C., Refsgaard, J.C. and Singh, R.D. (1992) 'Application of the SHE to catchments in India Part 2. Field experiments and simulation studies with the SHE on the Kolar subcatchment of the Narmada River', *Journal of Hydrology*, 140, 25–47.

Kite, G. (2001) 'Modelling the Mekong: hydrological simulation for environmental impact studies', *Journal of Hydrology*, 253, 1–13.

Kjeldsen, T.R., Jones, D.A. and Bayliss, A.C. (2008) *Improving the FEH Statistical Procedures for Flood Frequency Estimation*, Bristol: Environment Agency.

Laizé, C.L.R., Acreman, M., Schneider, C., Dunbar, M.J., Houghton-Carr, H.A., Flörke, M. and Hannah, D.M. (2014) 'Projected flow alteration and ecological risk for pan-European rivers', *River Research and Applications*, 30, 299–314.

Lehner, B. and Grill, G. (2013) 'Global River Hydrography and Network Routing: Baseline Data and New Approaches to Study the World's Large River Systems', *Hydrological Processes,* 27(15), 2171–2186.

Lehner, B., Verdin, K. and Jarvis, A. (2008) 'New Global Hydrography Derived from Spaceborne Elevation Data', *Eos,* 89(10), 93–94.

Li, Y., Thompson, J. and Li, H. (2016) 'Impacts of Spatial Climatic Representation on Hydrological Model Calibration and Prediction Uncertainty: A Mountainous Catchment of Three Gorges Reservoir Region, China', *Water*, 8, 73.

Meigh, J.R., Farquharson, F.A.K. and Sutcliffe, J.V. (1997) 'A Worldwide Comparison of Regional Flood Estimation Methods and Climate', *Hydrological Sciences Journal*, 42(2), 225–244.

Meigh, J.R., McKenzie, A.A. and Sene, K.J. (1999). A grid-based approach to water scarcity estimates for eastern and southern Africa. *Water Resources Management*, *13*(2), 85–115.

Messager, M.L., Lehner, B., Grill, G., Nedeva, I. and Schmitt, O. (2016) 'Estimating the Volume and Age of Water Stored in Global Lakes Using a Geo-Statistical Approach', *Nature Communications*, 7, 13603.

Mondal, A. and Mujumdar, P.P. (2015) 'Modeling Non-Stationarity in Intensity, Duration and Frequency of Extreme Rainfall over India', *Journal of Hydrology*, 521, 217–231.

Moore, R.J. (2007). The PDM rainfall-runoff model. *Hydrology and Earth System Sciences*, 11, 483–499.

Nash, I.E. and Sutcliffe, I.V. (1970) 'River flow forecasting through conceptual models', *Journal of Hydrology*, 10, 282–290.

National Institute of Hydrology (1997) *Development of Operation Policy for Tawa Dam,* Roorkee: National Institute of Hydrology.

Nestler, J.M., Pompeu, P.S., Goodwin, R.A., Smith D.L., Silva, L.G.M, Baigun, C.R.M. and Oldani, N.O. (2012) 'The River Machine: A template for fish movement and habitat, fluvial geomorphology, fluid dynamics and biogeochemical cycling', *River Research and Applications*, 28, 490–503.

Norman, D.W. and Dixon, J. (1995) *Sustainable dryland cropping in relation to soil productivity - FAO Soils Bulletin 72,* Rome: Food and Agriculture Organization of the United Nations.

Olden, J.D. and Poff, N.L. (2003) 'Redundancy and the choice of hydrologic indices for characterizing streamflow regimes', *River Research and Applications*, 19, 101–121.

Pai, D., Sridhar, L., Rajeevan, M., Sreejith, O.P., Satbhai, N.S. and Mukhopadhyay, B. (2014) 'Development of a new high spatial resolution (0.25° × 0.25°) long period (1901-2010) daily gridded rainfall data set over India and its comparison with existing data sets over the region', *Mausam*, 65, 1–18.

Patel, J., Patel, H. and Bhatt, C. (2014) 'ECALTOOL: fuzzy logic based computer program to calibrate the Hargreaves equation for accurate estimation of evapotranspiration', *Agricultural Engineering International: CIGR Journal*, 16, 245–250.

Payasi, Y.K. (2015) 'Diversity and Distribution of Phytoplankton in the River Hiran', *Global Journal for Research Analysis*, 4.

Poff N.L., Richter, B., Arthington, A.H., Bunn, S.E., Naiman, R.J., Kendy, E., Acreman, M.C., Apse, C., Bledsoe, B.P., Freeman, M., Henriksen, J., Jacobson, R.B., Kennen, J., Merritt, D.M., O'Keeffe, J., Olden, J.D., Rogers, K., Tharme R.E. and Warner, A. (2010) 'The Ecological Limits of Hydrologic Alteration (ELOHA): a new framework for developing regional environmental flow standards', *Freshwater Biology*, 55, 147–170.

Poff, N.L., Allan, J.D., Bain, M.B., Karr, J.R., Prestegaard, K.L., Richter, B., Sparks, R. and Stromberg, J. (1997) 'The Natural Flow Regime: a new paradigm for riverine conservation and restoration', *BioScience*, 47, 769–784.

Portmann, F.T. (2011). Global estimation of monthly irrigated and rainfed crop areas on a 5 arc-minute grid. *Frankfurt Hydrology Paper* 09, Institute of Physical Geography, University of Frankfurt, Frankfurt am Main, Germany.

R Core Team (2016) *R: A Language and Environment for Statistical Computing*. https://www.r-project.org/.

Rahman, M.M. (2016) *Modelling climate change impacts on the water regimes of the river-wetland systems in the data-scarce transboundary Upper Meghna River Basin (Bangladesh and India)*, Doctoral thesis, University College London, London.

Rajaguru, S.N., Gupta, A., Kale, V.S., Mishra, S., Ganjoo, R.K., Ely, L.L., Enzel, Y. and Baker, V.R. (1995) 'Channel form and processes of the flood-dominated Narmada River, India', *Earth Surface Processes and Landforms*, 20, 407–421.

Refsgaard, J.C., Storm, B. and Clausen, T. (2010) 'Système Hydrologique Europeén (SHE): review and perspectives after 30 years development in distributed physically-based hydrological modelling', *Hydrology Research*, 41, 355–377.

Richter, B.D., Baumgartner, J.V., Powell, J. and Braun, D.P. (1996) 'A method for assessing hydrologic alteration within ecosystems', *Conservation Biology*, 10, 1163–1174.

Richter, B.D., Baumgartner, J.V., Wigington, R. and Braun, D.P. (1997) 'How much water does a river need?', *Freshwater Biology*, 37, 231–249.

Robinson, A.J., Thompson, J.R., Acreman, M.C., Lehmann, K., Dumon, E.L., Rickards, N.J., Thomas, T., Nema, M., Mishra, P., Gaur, S., Agarwal, P., Singh, Y., Jain, S. (2016). *Building joint India-UK capacity, capability, research and innovation in the environment: Final report*. Report to NERC. London: UCL Department of Geography, Wallingford: Centre for Ecology and Hydrology, Roorkee: National Institute of Hydrology.

Singh, K.K., Pal, M. and Singh, V.P. (2010) 'Estimation of Mean Annual Flood in Indian Catchments Using Backpropagation Neural Network and M5 Model Tree', *Water Resources Management*, 24(10), 2007–2019.

Srivastava, A.K., Rajeevan, M. and Kshirsagar, S.R. (2009) 'Development of a high resolution daily gridded temperature data set (1969-2005) for the Indian region', *Atmospheric Science Letters*, 10, 249–254.

Stisen, S., Jensen, K.H., Sandholt, I. and Grimes, D.I.F. (2008) 'A remote sensing driven distributed hydrological model of the Senegal River basin', *Journal of Hydrology*, 354, 131–148.

Swamee, P.K., Ojha, C.S.P. and Abbas, A. (1995) 'Mean Annual Flood Estimation', *Journal of Water Resources Planning and Management*, 121(6), 403–407.

Taylor, K.E., Stouffer, R.J. and Meehl, G.A. (2012) 'An Overview of CMIP5 and the Experiment Design', *Bulletin of the American Meteorological Society*, 93, 485–498.

Thomas, T. (2017), *Optimal Water Resources Management in Narmada Basin as a Climate Change Adaptation Tool*, PhD Thesis, IIT Madras.

Thompson, J.R., Crawley, A. and Kingston, D.G. (2016). 'GCM-related uncertainty for river flows and inundation under climate change: The Inner Niger Delta', *Hydrological Sciences Journal*, 61, 2325–2347.

Thompson, J.R., Crawley, A. and Kingston, D.G. (2017a). 'Future river flows and flood extent in the Upper Niger and Inner Niger Delta: GCM-related uncertainty using the CMIP5 ensemble', *Hydrological Sciences Journal*, 62, 2239–2265.

Thompson, J.R., Green, A.J. and Kingston, D.G. (2014a) 'Potential evapotranspiration-related uncertainty in climate change impacts on river flow: An assessment for the Mekong River basin', *Journal of Hydrology*, 510, 259–279.

Thompson, J.R., Green, A.J., Kingston, D.G. and Gosling, S.N. (2013) 'Assessment of uncertainty in river flow projections for the Mekong River using multiple GCMs and hydrological models', *Journal of Hydrology*, 486, 1–30.

Thompson, J.R., Laize, C.L.R., Acreman, M.C., Crawley, A. and Kingston, D.G. (2017b) *GCM-related uncertainty in future environmental flows and flooding in the Upper Niger and Inner Niger Delta*, International Association of Hydrological Sciences 2017 Scientific Assembly, Port Elizabeth, South Africa, 10–14 July 2017.

Thompson, J.R., Laizé, C.L.R., Green, A.J., Acreman, M.C. and Kingston, D.G. (2014b) 'Climate change uncertainty in environmental flows for the Mekong River', *Hydrological Sciences Journal*, 59, 935–954.

Thompson, J.R., Laizé, C.L.R., Green, A.J., Acreman, M.C. and Kingston, D.G. (2014) 'Climate change uncertainty in environmental flows for the Mekong River', *Hydrological Sciences Journal*, 59, 259–279.

Thrasher, B., Maurer, E.P., McKellar, C. and Duffy, P.B. (2012) 'Technical Note: Bias correcting climate model simulated daily temperature extremes with quantile mapping', *Hydrology and Earth System Sciences*, 16, 3309–3314.

Thrasher, B., Xiong, J., Wang, W., Melton, F., Michaelis, A. and Nemani, R. (2013) 'Downscaled climate projections suitable for resource management', *Eos, Transactions, American Geophysical Union*, 94, 321–323.

Van Dijk, A.I.J.M., Kirby, M., Paydar, Z., Podger, G., Mainuddin, Md., Marvanek, S. and Peña Arancibia, J. 2008. *Uncertainty in river modelling across the Murray-Darling Basin*. A report to the Australian Government from the CSIRO Murray-Darling Basin Sustainable Yields Project, Canberra: CSIRO.

Vázquez, R.F., Feyen, L., Feyen, J. and Refsgaard, J.C. (2002) 'Effect of grid size on effective parameters and model performance of the MIKE-SHE code', *Hydrological Processes*, 16, 355–372.

Vieux, B.E. (2004) *Distributed Hydrologic Modeling Using GIS*, Dordrecht: Kluwer Academic.

Wijesekara, G.N., Gupta, A., Valeo, C., Hasbani, J.G., Qiao, Y., Delaney, P. and Marceau, D.J. (2012) 'Assessing the impact of future land-use changes on hydrological processes in the Elbow River watershed in southern Alberta, Canada', *Journal of Hydrology*, 412-413, 220–232.

Appendix 1. Data requirements for extension of FEH methods

A1.1. Gridded and at-site rainfall and evapotranspiration data

Currently, rainfall data have been collected on a district level with monthly averages from 1901–2002 (example pictured), with some data for 2004–2010 in some districts, which were interpolated from coarse gridded global datasets. For UK methods, a daily total rainfall is typically used to determine an average annual rainfall within each catchment using rainfall stations within the catchment or close to it.

It would be of most use to obtain rain gauge records of *total rainfall on a daily time-step* for locations throughout Maharashtra, but particularly in regions with river gauging stations. This is particularly important in regions that are strongly affected by flooding in the state, as well as for urban areas such as Mumbai. To aid with estimates within the state, it would also be of use to obtain rainfall data for hydrologically similar regions within the Tapi, Godavari and Krishna river basins but outside the state. In addition, to investigate seasonality of such floods, significant dates associated with the monsoons (start date, end date, extreme rainfall events) would be of use. *A finer gridded rainfall dataset* may be useful within the hydrological modelling methods.

In addition to the rainfall data, *gridded potential evapotranspiration* (PET) data would be useful in both the catchment descriptor equation for QMED and the continuous modelling approach. As an alternative, thermal energy data could be used along with a recommended method of computing PET or actual evapotranspiration.

A1.2. Locations and information of major anthropogenic impacts

In order to account for man-made structures and water abstraction and storage in the river network, it would be useful to have access to precise geographical locations of these installations, as well as how they affect stream flow (e.g. storage, level of abstraction). Currently the National Registry of Large Dams, compiled by CWC is known but is not in a form that can be readily applied to our analysis.

More recent land use maps, including information on the extent of agricultural and urbanised land at a high spatial resolution would allow for more accurate application in the catchment descriptor equations.

Appendix 2. Flood estimation in Maharashtra State: Stakeholder engagement

The main motivation for research in flood frequency estimation is improved prediction of extreme flood events leading to more effective flood risk management. Throughout the flood estimation part of the project, CEH has engaged with a number of stakeholders within the state of Maharashtra to discuss the state of the art and research gaps to ensure that future research is clearly targeted. Areas explored have included data resources, key research needs and possible ways to collaborate and exchange ideas and data. The stakeholders include academic institutions such as Indian Institute of Technology (IIT) Bombay, industrial partners such as the Maharashtra Engineering Research Institute (MERI), and government departments such as the India Meteorological Department (IMD).

Early in the project, links were made with Professor Arpita Mondal from IIT Bombay who has a research interest in extreme hydrological events and non-stationarity. CEH staff made two visits to Maharashtra to discuss data and progress and also hosted the visit of a PhD student from IIT Bombay. An outline of the discussions and outcomes of the meetings is provided below.

A2.1. Visit of PhD student - Chingka Kalai (June 2017)

CEH hosted a PhD student, Chingka Kalai, for two weeks to work with us on this part of the project, offering useful insights into local freely-available data. In particular, Kalai was able to assist the team with the acquisition of freely available river discharge and catchment descriptor data and to help evaluate data quality. Kalai presented his work to CEH in a seminar during his stay, and helped the group find several new sources of data for evaluation. This working relationship has been of great benefit to the project, both in UK and in India.

A2.2. Visit to Maharashtra (August 2017)

Lisa Stewart (CEH team leader for the flood estimation part of the project) and Harry Dixon visited Mumbai and Pune in August 2017. Discussions were held with Arpita Mondal and her team at IIT Bombay to consider the scope of the work possible in the relatively short pilot project. Common areas of research included extreme value distribution fitting, flood and rainfall frequency estimation using non-stationary methods and the use of spatial data as covariates. It was agreed that informal collaboration between CEH and IITB would continue with the latter assisting with the acquisition of data from government sources in Maharashtra State and India generally.

Representatives from Maharashtra Engineering Research Institute (MERI) in Nashik visited IITB to learn about the project and to discuss existing needs for generalised flood frequency

estimates in the state of Maharashtra. It was agreed that a point of contact would be confirmed and that MERI would release data to CEH via IITB.

CEH staff also travelled to the India Meteorological Department (IMD), Pune to discuss project scope and possible collaboration, particularly through the provision and analysis of rainfall, temperature and potential evapotranspiration data. Again, a project representative was appointed.

A2.3. Visit to Maharashtra (February 2018)

A second visit of CEH staff to Maharashtra took place in February 2018 with the aim of discussing the outcomes of the pilot project with the project partners. The group included Lisa Stewart (CEH team leader), Gwyn Rees and Adam Griffin. A number of meetings were held as discussed below.

A2.4. IIT Bombay, Mumbai (21 February 2018) - Prof T. Eldho, Prof Arpita Mondal, Prof Riddhi Singh, Prof Basudev Biswal, Prof Subimal Ghosh

In this meeting CEH presented the work from the pilot study, focusing on the statistical methods used in flood frequency estimation. Outcomes of the previous trips by CEH and by Chingka Kalai were discussed, with positive feelings about the work done so far. Following this, the current challenges in the work, particularly data acquisition problems, were discussed. Prof Singh spoke of current catchment characterisation methods that her group is researching, and possible collaborations to this end were discussed. Current flood estimation methods in India were discussed, and how they could be improved.

Recommendations were made to ask the Indian Central Water Commission (CWC) about further gauging stations in the state, and about current flood estimation practice. Chingka Kalai accompanied the CEH team to the rest of the meetings in Maharashtra during this trip.

A2.5. MERI, Nashik (23 February 2018) - Mr Rajendra Pawar, Director General; D.R. Joshi, Chief Engineer; Dr. Mahendra Nakil; others

In this meeting, CEH presented its wider work as an organisation, including a summary of the work done in water resources research. Following this, the work done in the pilot study was presented, and the web application was demonstrated. The priorities of the Water Resources Department were discussed: flood estimation in Wainganga, water resources assessment in Krishna and water quality of the Nag at Nagpur; MERI want to investigate all of them. The next steps will focus primarily on the flood estimation with emphasis on the Waingana Basin, although it is possible that other projects at CEH might explore the other two branches of

work. Mr Pawar showed interest in MOUs with CEH, and recommended keeping Mr Joshi as a primary correspondee.

A2.6. IMD, Pune (26 February 2018) - Dr AK Sahai; Dr Pulak Guhathakurta, Climate Data Management & Services; Dr G Krishnakumar, National Data Centre; Dr Shivana Pai, Climate Prediction; Dr Somenath Dutta, Climate Application & Users' Interface; Dr N Chattopadhyay, Deputy Director General of Meteorology)

As at MERI, CEH presented the findings from the pilot study as well as an introduction to the wider work CEH undertakes within water resources research and hydro-climatic risks. This led to interesting discussions on the work, and how it fits in with the current work IMD is doing; their focus is primarily on rainfall and evapotranspiration modelling and drought monitoring (HydroSOS). IMD explained the extent of their monitoring network including 144 stations with daily evapotranspiration readings and 25km gridded data.

There was a lot of interest in CEH's Hydrological Outlooks programme, and in collaborating with IMD to share rainfall and evapotranspiration data, conditional on more concrete outlines for the next steps in the project. Dr Guhathakurta remains the main contact for CEH within this area of work.

A2.7. National Water Academy, Pune (26 February 2018) - Sunil Kumar, Director; Dattakumar Chaskar, Director; Aditya Sharma, Director-in-Charge)

The National Water Academy is a training centre and is overseen by the Central Water Commission. Following previous meetings between Gwyn Rees and Sunil Kumar, the pilot study was presented as a current project of interest. It was recommended that to pursue this work further more active stakeholder engagement was key. NWA was positive about assisting with developing this area and any capacity building or training that is run following future research and development; this will be specified in future correspondence with NWA. This would probably be aided through an MOU.

The exchange of training programmes was discussed with regard to the project at hand, as well as other opportunities for training by CEH.